Acta
Technica
Jaurinensis

Vol. 7., No.1., pp. 1-10, 2014
DOI: 10.14513/actatechjaur.v7.n1.219
Available online at acta.sze.hu

The Effect of Technological Parameters on the Foaming of Injection Moulded Recycled PET

B. Molnár

Budapest University of Technology and Economics
Department of Polymer Engineering
H-1111 Budapest, Műegyetem rkp. 3., Hungary
E-mail: frederik.moriente@gmail.com

Abstract: The foaming of regranulate made from recycled PET bottles was examined, varying two important technological parameters: holding pressure, and the amount of material injected into the mould cavity, which was controlled with the switchover point. It was shown with optical and density tests that these parameters have a significant effect on the foam structure, which greatly influences mechanical properties.

Keywords: recycled PET, injection moulding, foaming

1. Introduction

One of the largest branches of polymer industry is the packaging industry, and within this the use and recycling of PET bottles is gaining more and more prominence. In 2010, 97.1% of PET was used for packaging in Hungary, while the share of PET in all packaging was 20.6%. These bottles have a short life cycle, and are mostly used only once so they generate a massive amount of waste. This waste can be recycled in several ways: most commonly as a clothes industry raw material or in the form of plastic strips or sheets, but its use for plastic bottles is also more and more widespread [1, 2].

Another possibility is reuse as engineering plastic. PET is an excellent engineering plastic (hard, rigid, highly wear-proof, good dimensional stability, physiologically neutral, resistant to weak acids and alkalis, little water absorption). Although its characteristics degrade during recycling, it can still serve as a good alternative to various polymers, and with the proper preparation it can be used for the original purpose (e.g. manufacturing bottles from bottles). In addition various “value-adding” processes can be applied, such as foaming, using special additives, or making the plastic flame retardant [3, 4].

Foaming is a common procedure in the plastic industry. It can be a separate technology (e.g. manufacturing EPS foam), or part of another manufacturing process (e.g. injection moulding, extrusion). There are also various classifications (according to foam structure, density or manufacturing procedure). The procedures can be classified into three groups according to manufacturing process:

- mechanical: the gas is mixed with the plastic mechanically;
- physical: two types are possible
  - gas is blown into the melt or
  - a foaming agent of low boiling point is added, which creates the foaming gas through a change of state;
- chemical: the foaming gas is produced with a chemical reaction [5, 6].

There are more and more articles about the foaming of PET in the literature. These describe various methods (physical/chemical extrusion foaming, creating a sandwich structure, injection moulding, hot forming, etc.). Most extrusion and injection moulding experiments use physical foaming, which produces a more uniform foam structure and lower density (down to 0.2-0.5 g/cm^3) can be achieved than with chemical foaming, but separate equipment is needed for the introduction of the high-pressure gas. Chemical foaming on the other hand can be done on a normal extruder/injection moulding machine without additional equipment. I used chemical foaming in my experiments [7].

In the foam injection moulding of recycled PET the viscosity of the polymer is important. This is determined not only by processing parameters but also by molecular structure. In secondary materials molecule length decreases considerably, which can be attributed to multiple processing. This leads to a decrease in the intrinsic viscosity of the melt, and the processability of the material is decreased. This can be dramatically improved by adding chain extenders. These materials connect to the ends of several polymer chains, this way increasing their length and the number of branches, thus increasing intrinsic viscosity of the material, giving it better processability [8-11].

The goal of the experiment is to produce an engineering plastic part from recycled PET using foam injection moulding, and to reveal the connection between the holding pressure and switchover point, and the physical and mechanical properties of the product.

2. Description of the equipment, raw materials and technology

The regranulate used to manufacture the product were made from recycled and ground PET. Before processing the granules were dried at 50 degrees Celsius for 6 hours in each case. CESA Extend chain extender (Clariant) was added, its proportion was 2%. The foaming agent was Safoam RPC-40 (Reedy International). Injection moulding was done with an Arburg Allrounder Advance 370S 700-290 injection moulding machine. The polymer was ground and recycled PET, turned into granules. In the injection moulding cycle I used a 0.1 mm mould opening after holding pressure, as a result of which the surface of the product did not get into contact with the mould and so no external pressure was exerted on it, which could have inhibited foaming. This led to better foaming. The samples were manufactured with three different holding pressure profiles. Table 1 contains the main settings and technological parameters used during manufacturing, Table 2. contains the holding pressure profiles and Table 3. contains the switchover point values.

Table 1. Main technological parameters and holding pressure profiles

Holding pressure profile		High	Medium	Low
Raw material		RPET regranulate		
Foaming agent		4% Safoam RPC-40		
Chain extender		2% CESA Extend		
Drying temperature/time	[°C]/[h]	50/4		
Clamp force	[kN]	175		
Mould opening	[mm]	0,1		
Delay (residual cooling time)	[s]	20		
Nozzle temperature	[°C]	275		
Mould temperature	[°C]	50		

Table 2. Used holding pressure profiles

Holding pressure profile		High	medium	Low
Switchover point	[cm^3]	14		
Holding pressure profile (p_1-t_1-p_2-t_2-p_3)	[bar]-[s]-[bar]--[s]-[bar]	600-6-400--2-50	600-3-400--1-50	400-2-200--1-50

Table 3. Used switchover points

Holding pressure [bar]/[s]/[bar]/[s]/[bar]	400/2/200/1/50			
Shot volume [cm^3]	40			
Switchover point [cm^3]	14	18	22	26

The foam structure of samples was examined with an Olympus optical microscope. Different settings resulted in various foam structures in the samples. The longitudinal section of the parts provides information about the foamed layer in their centre, while the cross section shows the cell size. Using the microscope images I estimated the average cell size by looking at 50-50 cells. I made an estimate for all cells using the volume of the foamed part and the cell size (taking into consideration of the density of the raw material and the foaming gas).

Mechanical properties were determined with a three-point bending test with a Zwick Z020 universal testing machine. Testing was performed at room temperature with the following technological parameters: supporting pin distance: L=28mm, loading speed: v=10mm/min.

3. Results

3.1. Foam structure

Table 4. contains the main characteristics of the foamed layer and the cells, and Fig.1. shows the various microscope images at various holding pressures.

Table 4. Foam layer properties at different holding pressures

Holding pressure profile	High	Medium	Low
Average cell size [µm]	301	237	222
No. of all cells (estimated)	3837	17013	24807
Volume ratio of foamed layer [%]	49	62	66
Average mass of samples [g]	15,33	15,19	14,9

Using high holding pressure the volume ratio of the foamed layer is 50%, and few large cells were produced (300 µm/4000), at medium holding pressure the foamed layer is 62% and more (17000) smaller cells (240 µm) were produced, while at small holding pressure the ratio of foamed layer was largest (66%) and also this produced the smallest size and largest number of cells (220 µm/25000). This can be attributed to the amount of material injected into the mould: using higher holding pressure more melt enters the mould cavity, a higher internal pressure is created and this inhibits the growing of foamed layer more. Also, the forming cells can spread less so the little cavities connect and form larger cavities, which results in fewer but larger cells inside the product.

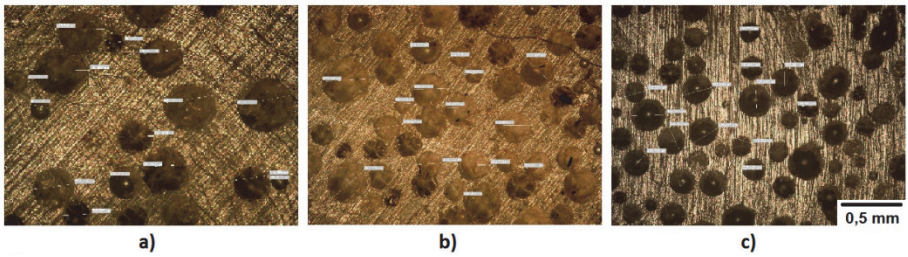

Figure 1. Cell structure forming at high (a), medium (b), and low (c) holding pressure

Table 5. includes the properties of the foam structure, and Fig. 2. shows the microscope images at various switchover points.

Table 5. The properties of the foam layer at various switchover points

Switchover point [cm^3]	14	18	22	26
Average size [µm]	231	225	263	295
No. of all cells (estimated)	16307	18146	11912	7734
Volume ratio of foamed layer [%]	66	61	64	62
Average mass of samples [g]	14,95	14,94	14,94	14,97

Changing the switchover point has the same effect like changing holding pressure: higher values mean less melt in the cavity. The switchover point is normally at the end of the fill phase, but at foam injection moulding it can be before the end of fill. In this case the foaming process causes the melt filling the cavity (and the holding pressure).

When the switchover point was increased, the average size of the cells did not change significantly, the range is about 15%. There is no regularity in the volume ratio of the foamed layer but the change of values within a range of 5%, as opposed to the values in the case of the holding pressure, when the range was much wider, namely 17%.

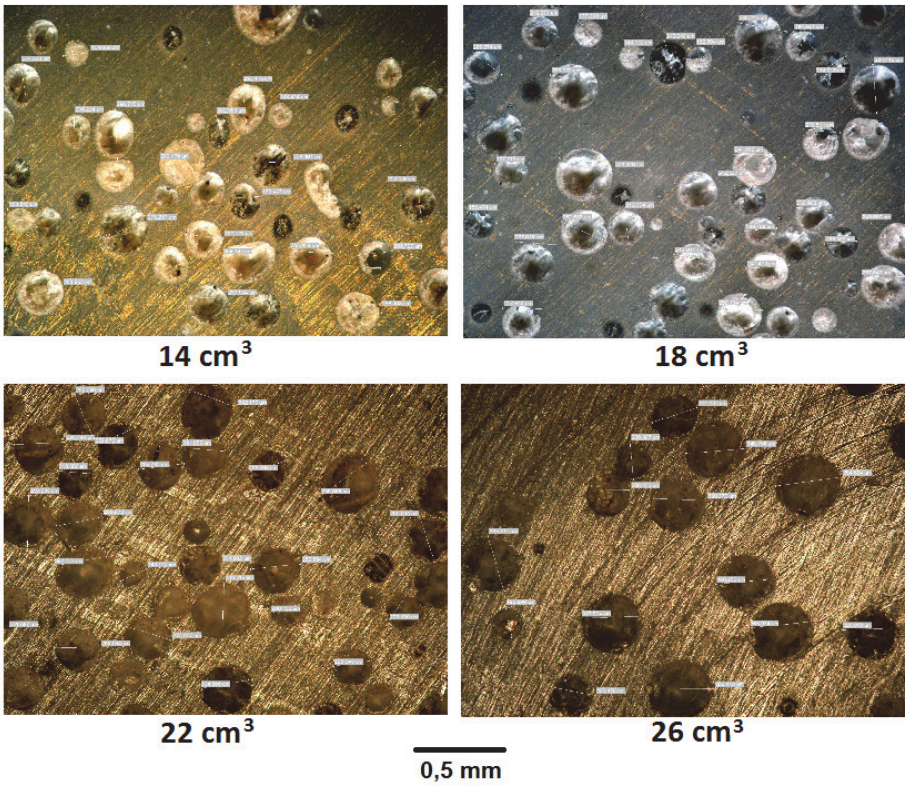

Figure 2. Cell structure forming at various switchover points

Fig. 3. shows images of the foam structure of samples made with different holding pressures whereas Fig. 4. shows the foam structures created with different switchover points.

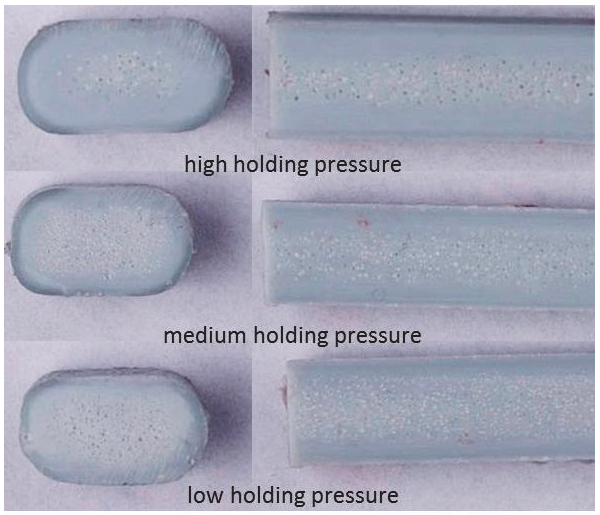

Figure 3. The longitudinal and cross-section of a sample made with different holding pressure

Figure 4. The longitudinal and cross-section of a sample made with different switchover point

4. Density

The densities of the samples at various holding pressure profiles can be seen in Fig. 5. When the holding pressure was high, medium and low, the density of the samples was 1,28 g/cm^3, 1,2 g/cm^3, and 1,17 g/cm^3, respectively. Since the volume of the samples is the same, the density is determined by the amount of material injected and the extent of foaming. The goal during foaming is that the appropriate product quality and surface quality is provided by foaming. This can be ensured by decreasing the holding pressure, which results in less material entering the mould, and the mass and consequently the density of the product decreases.

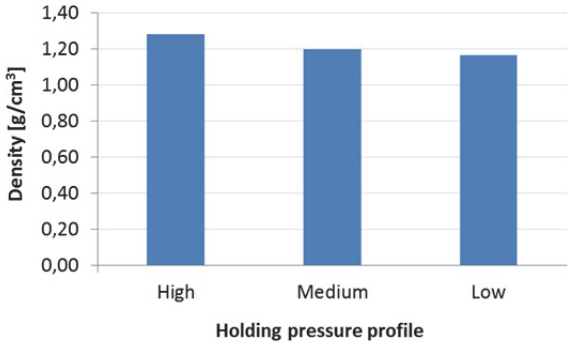

Figure 5. The effect of the holding pressure profile on the density

Fig 6. shows the densities of samples made with different switchover points. As the switchover point was increased, the density of the samples decreased very slightly, by only a few hundredths of g/cm^3. This change can be ignored compared to the effect of holding pressure.

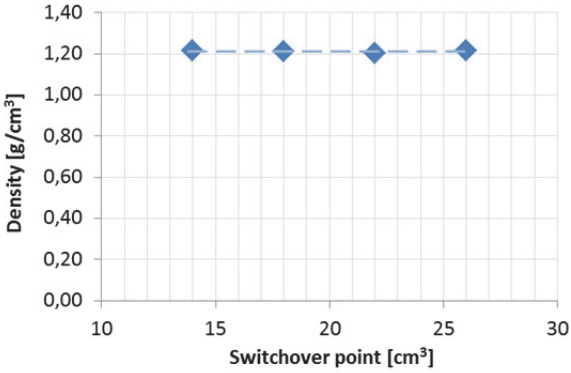

Figure 6. Density as a function of the switchover point

5. Mechanical properties

Fig. 7. shows specific flexural strengths, while Fig. 8. shows specific flexural modulus with three holding pressure profiles. In the case of high holding pressure 35 MPa/(g/cm^3) specific flexural strength was measured, while at medium and low holding pressure a nearly identical 25 MPa/(g/cm^3) was measured, which is close to 30% less. The results – compared to the foam structure – show that as the holding pressure decreases, the proportion of the foamed part increases and the average size of the cells, and the specific strength decrease. The same tendency can be observed in the case of modulus values, too. In the case of high holding pressure specific flexural modulus is 750 MPa/(g/cm^3), while with medium and low holding pressure specific flexural modulus is close to 400 MPa/(g/cm^3).

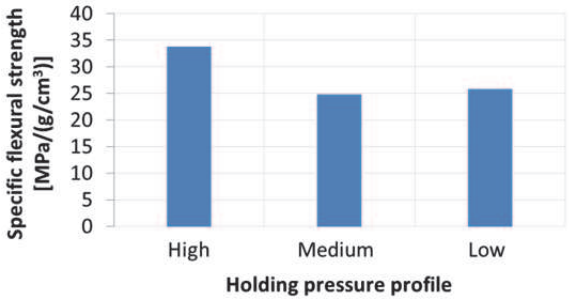

Figure 7. The effect of holding pressure profiles on specific flexural strength

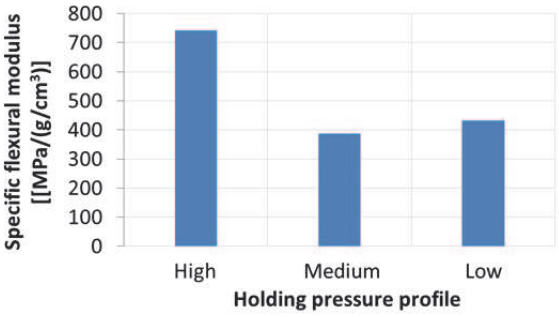

Figure 8. The effect of holding pressure profiles on specific flexural modulus

Fig. 9. shows the specific strength values of the samples, while Fig. 10. shows the specific modulus values of the samples manufactured with various switchover points. The results are similar to the values measured when holding pressure was varied: as the cells grew in the foam structure, the strength also increased: at higher switchover points strength and rigidity were higher. An explanation can be that larger but fewer cells break up the continuity of the structure less and the layer of material is thicker and thus stronger between cells so the part can withstand higher loads.

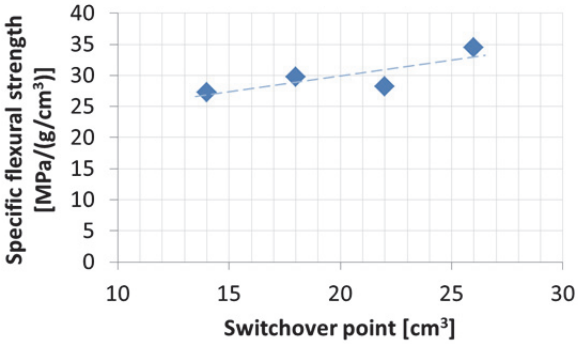

Figure 9. Flexural strength specificized for density as a function of switchover point

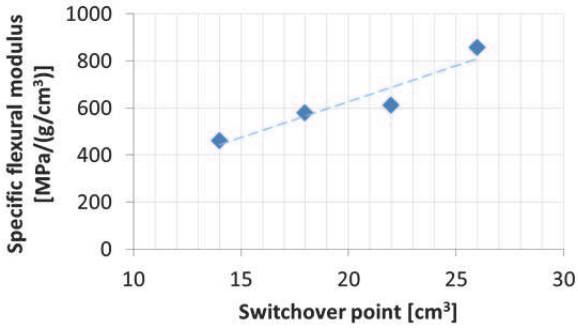

Figure 10. Flexural modulus specificized for density as a function of switchover point

6. Summary

The results obtained during the experiments showed that variation in the holding pressure and switchover point both influence the structure and properties of the foamed product considerably. When holding pressure was decreased, the volume ratio of the foamed part in the product increased, and cell size decreased, along with density and strength. When the switchover point was increased no correlation could be observed in the volume ratio of the foamed part but the average size of the cells increased. Density slightly decreased but it was negligible compared to the effect of holding pressure on density. Strength and modulus increased when thinner foamed layer were evolved with larger cells. Based on the results it can be said that density was greatly influenced by variations of holding pressure, while the foam structure was significantly influenced by variations in both holding pressure and switchover point. The mechanical properties can be explained with the foam structure: the thinner foamed layer with larger, but fewer cells break up the continuity of the structure less, the part can withstand higher loads.

Acknowledgement

The publishing of this paper was supported by the Hungarian Scientific Research Fund (OTKA K109224).

References

[1] Buzási, L.: *A műanyag csomagolóanyag gyártás helyzete Magyarországon 2010-ben (Status of polymer packaging manufacturing in Hungary in 2010, in Hungarian)*, Műanyag és Gumi, vol. 48, no. 11, pp. 405-411, 2011

[2] Welle, F.: *Twenty years of PET bottle to recycling – An overview,* Resources, Conservation and Recycling, vol. 55, no. 11, pp. 865-875, 2011 DOI:10.1016/j.resconrec.2011.04.009

[3] Dunai, A., Macskási L.: *Műanyagok fröccsöntése (Injection molding of polymers, in Hungarian),* Lexica Kft., Budapest, 2003

[4] Dogossy, G., Ronkay, F.: *Hulladék PET minőségnövelt újrahasznosítása (Value-added recycling of PET waste, in Hungarian),* A Jövő Járműve, vol. 8, no 1-2, pp. 47-49, 2013

[5] Schwarz, O., Ebeling, F.-W., Lüpke, G., Schelter, W.: *Műanyag-feldolgozás (Polymer processing, in Hungarian),* Műszaki Könyvkiadó, Budapest, 1987

[6] Chanda, M., Roy, S. K.: *Plastics Technology Handbook,* Taylor & Francis Group, LLC, 2006

[7] Japon, S., Letterrier, Y., Manson, J.-A. E.*: Recycling of Poly(Ethylene Terephthalate) Into Closed-Cell Foam,* Polymer Engineering and Science, vol. 40, no. 8, pp. 1942-1952, 2000 DOI: 10.1002/pen.11326

[8] Turfa, E., Dogossy, G., Ronkay, F.*: Reciklált PET tulajdonságainak javítása reaktív extrudióval (Improvement of properties of recycled PET with reactive extrusion, in Hungarian),* Anyagok világa, vol. 11, no. 2, pp. 50-58, 2013

[9] Dogossy, G., Ronkay, F.*: Reciklált PET habosítása (Foaming of recycled PET, in Hungarian)* In: Csibi-Venczel J: OGÉT 2013: XXI. 21st International Conference on Mechanical Engineering, Romania, Arad, pp. 97-100, 2013

[10] Coccorullo, I., Di Maio, L., Montesano, S., Incarnato, L.: *Theoretical and experimental study of foaming process with chain extended recycled PET*, Express Polymer Letters, vol. 3, no. 2, pp. 84-96, 2009 DOI: 10.3144/expresspolymlett.2009.12

[11] Di Maio, L., Coccorullo, I., Montesano, S., Incarnato, L.: *Chain extension and foaming of recycled PET in extrusion equipment*, Macromolecular Symposia, Special Issue: Times of Polymers, vol. 228, no. 1, pp. 185–200, 2005 DOI: 10.1002/masy.200551017

Acta
Technica
Jaurinensis

Vol. 7., No.1., pp. 11-20, 2014
DOI: 10.14513/actatechjaur.v7.n1.19
Available online at acta.sze.hu

Road Safety Study during Construction Work of an at Grade Intersection Converting it to a Flyover

A. Sala

Research Scholar

EU-Asia Road Safety Centre of Excellence (RoSCoE)
Prince of Songkla University, Hat Yai 90112, Songkla, Thailand
E-mail: s.weerajak@gmail.com

Abstract: A flyover was constructed for solving the traffic problems, to improve the traffic flow at an intersection, to reduce the delays and accidents. 25 traffic accidents occurred during the construction work. This study will point out the issues that might be the cause of all these accidents around the construction area and in the conclusion the data of road safety evaluation (accident costs) will be shown.

Keywords: road safety, flyover construction, accident cost

1. Introduction

To solve the traffic problems at intersections on bypass roads such as traffic volume, accidents (as shown in Figure 1) and delays etc., the flyover is one of the tools to solve these problems. Normally in Thailand, the flyover is constructed at junctions on bypass roads near big cities.

A flyover is the special bridge constructed above existing at-grade intersections. It allows for the free flow of traffic on different levels, with the main goal of for reducing traffic conflicts, whereas the intersection is still the same old signal controlled.

Hat Yai City is an important center of the transport sector and economic growth of the southern provinces, particularly, the transport of passengers and goods in the three borderland southern provinces and between Thailand and neighboring countries like Malaysia and Singapore. Definitely, the transport of passengers and goods are efficiently provided and facilitated by the transport sector; Songkhla has a total of 750.748 km. of route length, 22 train stations and Hat Yai International Airport (9 km from the downtown of Hat Yai city) can support 1,505,906 passengers in 2010.

In 2009 the Government hired the Department of Highway (DOH) to construct a flyover at Sanambinnai Intersection. It was constructed on a length 1+325.570 kilometers above the old intersection by an investment of 249,597,672.5 THB. There were about 12,500 vehicles per day (DOH, 2008) travelling as usual despite the construction and 25 accidents occurred (DOH, 2011) during construction work. This

study will point out the issues that might be the cause of all these accidents around the construction area and in the conclusion the data of road safety evaluation (accident costs) will be shown.

2. Study area details

The study area consists of Highway route number 43 and Highway route number 4135 in Songkhla province. The intersection was an at-grade one before a flyover was recently constructed at station 24+489.400 km (a schematic map of Hat Yai city is shown in Figure 2), and 967.00 meters of length of bridge and 540 days of construction time (increased to 929 days due to the natural disaster).

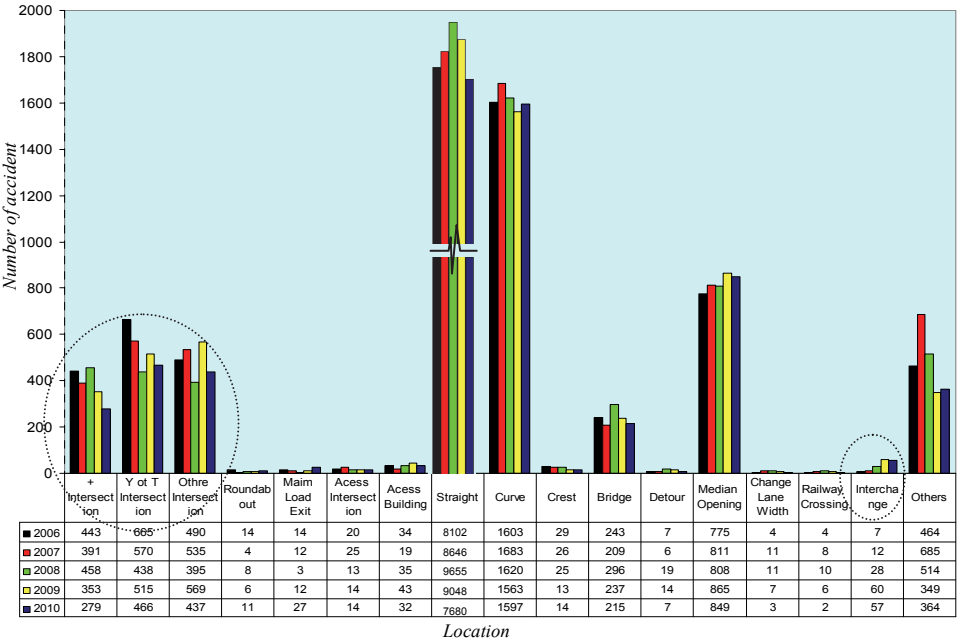

	+ Intersection	Y ot T Intersection	Othre Intersection	Roundabout	Maim Load Exit	Acess Intersection	Acess Building	Straight	Curve	Crest	Bridge	Detour	Median Opening	Change Lane Width	Railway Crossing	Interchange	Others
2006	443	665	490	14	14	20	34	8102	1603	29	243	7	775	4	4	7	464
2007	391	570	535	4	12	25	19	8646	1683	26	209	6	811	11	8	12	685
2008	458	438	395	8	3	13	35	9655	1620	25	296	19	808	11	10	28	514
2009	353	515	569	6	12	14	43	9048	1563	13	237	14	865	7	6	60	349
2010	279	466	437	11	27	14	32	7680	1597	14	215	7	849	3	2	57	364

Figure 1. Traffic accidents on highways by accident location in Thailand [4]

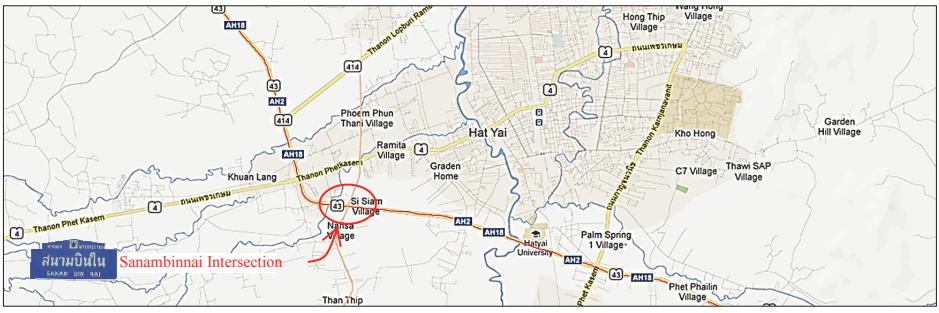

Figure 2. A schematic map of Hat Yai city with the study area marked

This intersection is situated at 6˚59'13.00" N latitude and 100˚25'42.93" E longitude and the physical data of the two important roads are;

Highway route number 43

- The distance is 104.268 km, link road from Phatthalung province along the road to Pattani province,
- AADT at station 8+317 km: 15,824 vehicles/ day and lane separated by an island, and
- 2 lanes/ direction, 3.5 meter/ lane, outer and inner shoulders of the road are 1.0 & 0.5 meter, respectively.

Highway route number 4135

- The distance is 9.965 km, link road from the Sanambinnok intersection along the road to Hat Yai International Airport.
- AADT at station 1+300 km: 18,323 vehicles/ day and lanes separated by yellow markings, and
- 2 lanes/ direction, 3.5 meter/ lane, outer and inner shoulders of the road are 1.0 & 0.5 meters respectively.

The signal control at the intersection was fixed time type, 4 phases, 2 programs a day; the first program has a cycle length of 244 seconds, it was operating from 06:00 am to 12:00 pm and the second program was flashing amber, it was used from 00:00 am to 06:00 am, the data as shown in Figure 3.

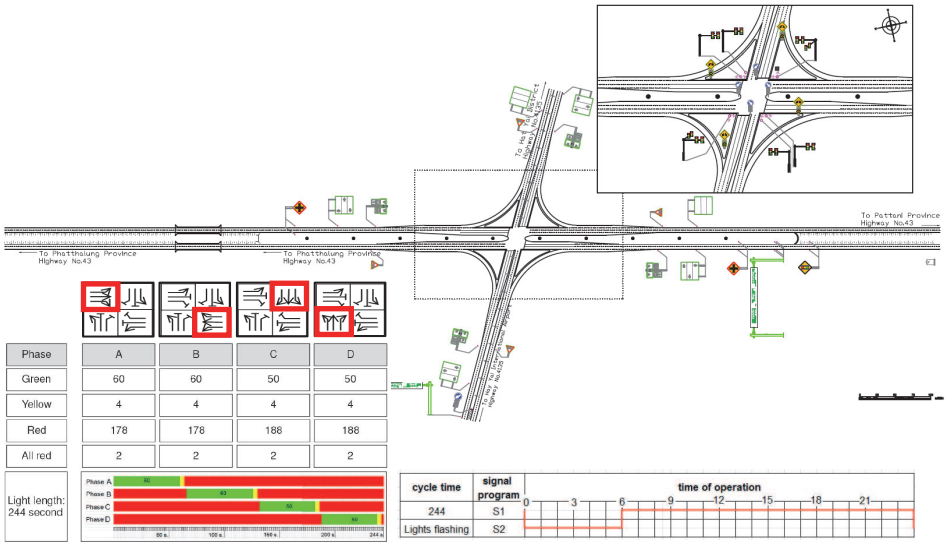

Phase	A	B	C	D
Green	60	60	50	50
Yellow	4	4	4	4
Red	178	178	188	188
All red	2	2	2	2

Light length: 244 second

Figure 3. Physical data of highway route no 43 and highway route no 4135 (before construction) and the signal control program

3. Methodology

This study will point out the traffic problems during the construction work between the construction zone and road users since the first to the last day of this project.

3.1. Stages of construction

During the stages of construction, there were 3 main steps for protecting the road users travelling through this intersection (shown in the figure 4). The project owner planned and installed traffic signs, flashing beacons and other informational signs.

In Zone 1 the river bridge was constructed, the road was extended to 3 lanes and the pillar for a special bridge was constructed on the road island. Concrete blocks and traffic cones were installed for dividing road users from the work zone, but sometimes it was divided explicitly, but sometimes it was not installed to protect and temporary U-turn was constructed by soil material near the river bridge.

In Zone 2 the pillar of the special bridge was constructed, this process was implemented simultaneously with zone 1 and the management process was similar to that of zone 1.

Zone 3 was the last area to work on, after all pillars of the special bridge were constructed in zone 1 and 2. The traffic signals were operating like the old signals (fixed time type, 4 phases, 2 programs a day, but changed the cycle time of the first program from 244 to 254 seconds, it was operating from 06:00 am to 12:00 pm and the second program (flashing amber), was used from 00:00 am to 06:00 am.

24 accidents occurred in the zone no 1 and zone no 2 and all accidents were registered.

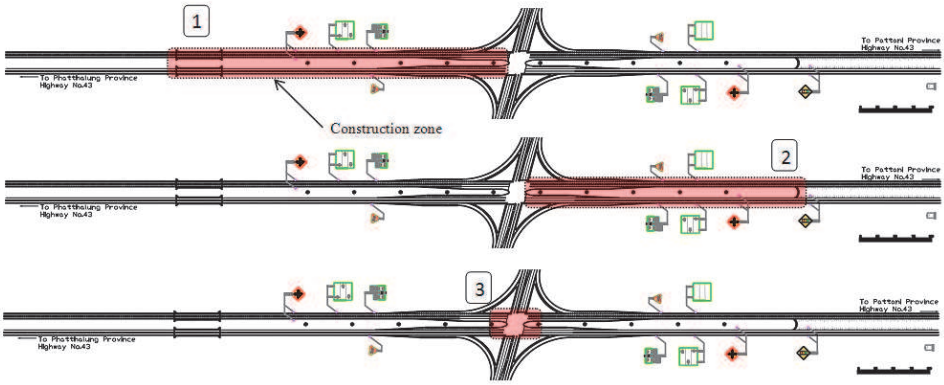

Figure 4. Stage during construction management

3.2 Road Safety Audit

Road Safety Audit under construction stage covers the following items [9];

- Traffic Management,

- ❖ Traffic signs and road markings,
- ❖ Traffic signals,
- ❖ Pedestrians and bicycles,
- ❖ Road surface, and
- ❖ Other issues.

Field audit was conducted during 3 periods: day-time, night-time and raining. The following issues were found during on-site audits:

- ❖ Traffic Managements

The picture of traffic management issues are shown in Figure 5

- The temporary traffic signs were installed at inappropriate locations,
- Did not have the staff to protect 2 zones,
- Auditor found only one of the speed limit signs (50 km/h); it was installed on the HW route 43 before entry to intersection 300 meters,
- Concrete blocks did not cover the construction zone, they did not protect the road users and construction zones, on the contrary, they raised problems for the road users because of their different sizes and, installed at inappropriate locations,
- Street lights according to the guideline of road lane direction were not turned on every night, and
- Road sections and construction zones were not divided clearly, so vehicles could enter and cross construction zones.

- ❖ Traffic signs and Road markings

The pictures of traffic signs and road marking issues are shown in Figure 6

- The installation of temporary traffic signs was not stable, not enough and insufficient,
- Traffic signs were not reflective at night and some traffic signs were damaged,
- Background (brown) and text (black) in traffic signs could not be seen clearly,
- There were traffic signs with different characteristics, and
- Road markings at intersection could not be seen clearly.

Figure 5. Traffic management issues

❖ Traffic lights

- The traffic signal control was using 4 phases, it consisted of 2 programs a day; the first program had a cycle of 254 seconds, it was operating from 06:00 am to 12:00 pm. During peak time (7:45-8:00 am) average queue length of the 4 legs were 48 vehicles (PCU). The second program was flashing amber, it was used from 00:00 am to 06:00 am.

Figure 6. Traffic signs and road marking issues

❖ Pedestrians and bicycles

The pictures of pedestrians and bicycle issues are shown in Figure 7

- There were no stopping lines for motorcycles and bicycles at the intersection,
- There were scraps on the shoulder of the road, the bicycle cannot bike on this area, and
- There were loose aggregates that reduce skid resistance around this construction zone.

❖ Road Surface

The pictures of road surface issues are shown in Figure 7

- Road surface was not smooth and bumpy,
- There was water covering the surface of road after rain, and
- Mud mound, soil, and raw aggregates were found on the sidewalk and on the shoulder.

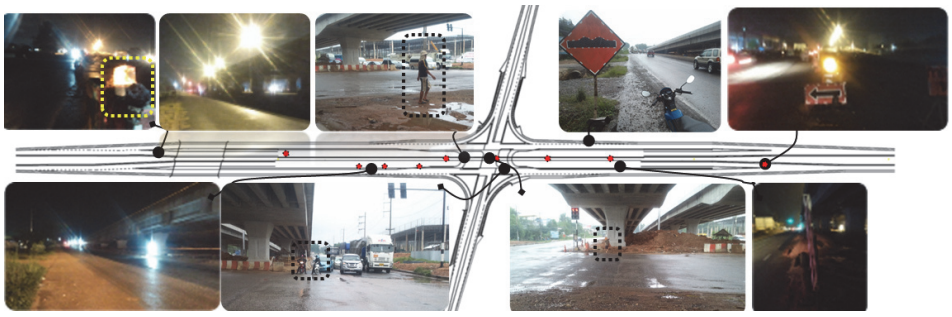

Figure 7. Pedestrians, bicycles and road surface issues

❖ Other issues

The pictures of other issues are shown in Figure 8

- There were no energy absorbing devices at the edge of the river bridge,
- There were no guardrails or concrete blocks between the road surface and roadside area to prevent the vehicles from falling down the road, and
- There were fixed rigid objects near the road surface.

Figure 8. Other issues

3.3. Accident statistics

As for accident statistics during construction work, this study collected data from the Department of Highways (DOH) and from the project owner. During the 929 days of construction, 52 accidents were found, of which 25 were sufficiently documented. Data cover such as spot of accidents, collision diagram, number of casualties, property damage only and cause of the accident.

4. Results and discussions

This intersection was improved by an investment costing about 250 million THB. The intersection was audited according to the road safety manual. In accidents statistic the top three causes of accidents were rear-end in the same lane (6 cases), hit with fixed solid objects (3 cases) and vehicle hits vehicle at intersection (3 cases) respectively. Vehicle types of the top three of the accidents are first one is car (13 vehicles), second is pick up (11 vehicles) and third is trailer (8 vehicles) respectively. On 15th April 2012 the new flyover was opened, under the flyover it is still the old junction controlled by traffic signals.

All of the 25 accidents where the data on the spot of accident and time of the accident are consistent with the time of management of each zone are shown in Figure 10. Accident costs were calculated as follows;

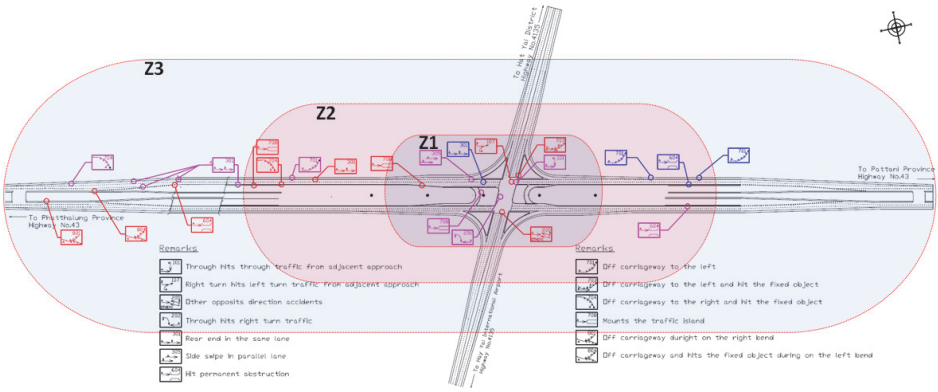

Accident: 25 times/ 929 days (Z1: 9, Z2: 9, Z3: 7)

Time of Accident				Number of Casualty			Property Damage Only
Dry		Wet		Injury	Serious	Died	
Day	Night	Day	Night				
8	11	6	-	20	6	6	1,353,900

Legend

Dry/Day Time

Wet/Day Time

Dry/Night Time

Wet/Night Time

Figure 10. Spot of accident at intersection area and collision diagram

5. Accident costs (AC)

Used to describe the combined effect of number and severity of the accidents [8]

Annual average accident cost ACa [€/year]:

$$ACa(F+SI+LI+PDO) = \frac{A(F)\times MCA(F) + A(SI)\times MCA(SI) + A(LI)\times MCA(LI) + A(PDO)\times MCA(POD)}{t} \quad (1)$$

where: A is number of accidents (acci),

MCA is the mean cost per accident (€/acci) as shown in table 1, and

t is the period of time under review (year).

$$ACa(F+SI+LI+PDO) = \frac{(6\times 5{,}178{,}000) + (6\times 151{,}500) + (20\times 29{,}750) + 1{,}353{,}900}{(929/365)} = 13{,}329{,}336\ Baht$$

Table 1. The mean cost per accident for various severities [5]

Severity	Thailand (Million Baht)	Bangkok (Million Baht)	Other Provinces (Million Baht)
Fatality	5.062 – 5.956	10.561 - 12.413	4.757 - 5.599
Disability	5.114 - 6.910	11.611 - 13.934	5.608 - 6.729
Serious Injury	0.158 - 0.164	0.328 - 0.337	0.148 - 0.155
Slight Injury	0.0386 - 0.0389	0.1731 - 0.1733	0.0297 - 0.0298
Property Damage Only	0.052	0.164	0.039

6. Conclusion

According to Road Safety Audits under construction stage, the issues of on-site audits can be summarized as follows;

- The number of "temporary traffic signs" was not enough, no maintenance during construction, installed at improper locations, not reflective at night and made by hand (different styles and dimensions),
- "Concrete Blocks" not covered the construction zone, they did not protect the road users and construction zones, on the opposite, they caused problems for the road users because of their different sizes and inappropriate locations,
- "Street-lights" were not installed consecutively and not turned on every night,
- "Road surfaces" were not smooth but bumpy, the mud mound on the shoulder of the road made always a problem when raining, and
- There were no guard rails or concrete blocks between the road surface and roadside area to prevent the vehicles from falling down the road, although there were fixed rigid objects near the road.

Accident statistics during construction work is a reflection of construction management; there were 52 accidents (this 52 accidents were collected by 3 agencies) of 929 days. Because the sufficiency of accident data from 3 agencies is different, this study only used accidents data from Department of Highway (25 accidents). The cost of these 25 accidents occurred is equivalent to 13,329,336 THB in 2011.

7. Recommendations

In terms of Road Safety, the recommendations of this study are the followings;

- The "temporary traffic signs" should use standard signs, installed at appropriate and sufficient locations "Road surface" should not have pothole and soil aggregates on the road surface.
- "Street-lights" should be installed consecutively and turned on every night
- "Concrete Blocks" should be installed at appropriate locations, they should clearly show which are road user, roadside and construction zones. They should be installed covering the project construction area without gaps.
- Traffic signal control during construction and open road should follow traffic volumes of each leg and period of the day, and

- Field works should have traffic engineering staff for controlling or checking the possibility of accidents.

References

[1] *Accident rates of 10 countries in Asia*, Asian Development Bank, 2008
[2] *Road Safety Audit*, Austroads Project No. RSS.SS.C.008, Austroads Incorporated, Sydney, NSW, Australia. 2002
[3] *Accident Statistical Report of HAIMS 2011*, http://haims.doh.co.th, visited at 04/04/2013
[4] *Traffic Accident on National Highways in 2011*, Bureau of Highways Safety, Ministry of Transport, Thailand, 2011
[5] *Accident cost rate in Thailand of 2011*, Bureau of Highways Safety, Ministry of Transport, Thailand, 2012
[6] *Definition of Road Safety Audit*, Federal Highway Administration, Washington DC, USA, 2011
[7] Proctor, S.: *Road Safety Audit Guidelines*, The Chartered Institution of Highways & Transportation, www.iht.org, 2002
[8] Gatti, G., Polidori, C., Galvez, I., Mallschützke, K., Jorna, R., de Leur, M.V., Dietze, M., Ebersbach, D., Lippold, C., Schlag, B., Weller, G., Wyczynski, A., Iman, F., Aydin, C.: *Safety Handbook for Secondary Roads*, Final report in EC Sixth Framework Programme, Contract No. 506184, 2005
[9] Taneerananon, P., Tanaboriboon, Y., Srisakda, L.: *Thailand Road Safety Audit Manual*, Department of Civil Engineering, Prince of Songkla University, Thailand, 2009
[10] Vesper, A.: *General Aspects of Road Safety-Transfer of Knowledge*, Bauhaus-Universität Weimar, European Commission, Germany, 2011

Acta
Technica
Jaurinensis

Vol. 7., No.1., pp. 21-32, 2014
DOI: 10.14513/actatechjaur.v7.n1.21
Available online at acta.sze.hu

The Optimal Design of U-Turns on Thai Highways

I. Meel[1], D. Satirasetthavee[2], K. Kanitpong[3], U. Brannolte[4]

[1]EU-Asia Road Safety Centre of Excellence (RoSCoE)
Prince of Songkla University, Hat Yai 90112, Songkla, Thailand
E-mail: ipmeel@yahoo.co.in

[2]Department of Civil Engineering, Faculty of Engineering, Naresuan University
E-mail: dussadee_s@outlook.com

[3]School of Engineering and Technology, Asian Institute of Technology
Pathumthani, Thailand, E-mail: kanitpon@ait.ac.th

[4]Department of Transport Planning and Traffic Engineering, Faculty of Civil Engineering, Bauhaus-University Weimar, Marienstrasse 13C, 99423, Weimar, Germany, E-mail: ulrich.brannolte@uni-weimar.de

Abstract: The purpose of this study is to evaluate optimal layout design of U-turns on basis of road safety for highways of Thailand. In Thailand, U-turns are one of major segments of highways after intersections, contributing to rural highway crashes. Different layout designs of U-turn and variation in its elements are influencing factors for drivers' expectance and causing confusion in drivers. Therefore, the evaluation of layout designs of U-turn of rural highways is important to reduce future crash rates. For this research, initially the 'accident based investigation' was considered, the accident cost rates for different layout designs was planned to be evaluated. But due to underreporting of accident data in various agencies in Thailand, the 'accident based investigation' could not produce reliable results, so 'event based investigation' is considered for further study. For 'event based investigation' study the 'traffic conflict technique' is planned to use.

Keywords: U-turn, road-safety, traffic conflict technique

1. Introduction

1.1. Background

Road safety has received considerable attention all around the world. In order to get a better insight into the safety effects of present highway designs, the partner universities of the international scientific network "RoSCoE: EU-Asia road safety centre of excellence" have established to conduct research works on different segments of rural

highways, such as intersections, U-turns, cross sections, rail-road crossings and grade separated junctions.

Other than intersections, highways can divided in U-turns (median opening), tangent sections and curved sections. U-turns on divided Thai highways are provided to avoid direct right turn from highway to minor roads, to avoid direct right turn from minor road to highways (for left hand traffic), to reduce travel time for emergency services, efficient law enforcement and for highway maintenance purposes. U-turns are classified based on geometric layout.

1.2. Need for the present study

Economic growth in Thailand has brought about an expanding network of roads and an increasing number of the driving public. The growing number of vehicles on the roads, in turn, has contributed to significant increases of road crashes annually. Road crashes have been a major cause of death and injury in Thailand. Traffic accidents are associated economic losses and social consequences. The economic costs include medical services, productivity losses, property damage, emergency services, insurance administration, premature funeral costs, vocational rehabilitation, legal expenses, etc. Annual economic losses in Thailand due to traffic crashes are account about 2 to 3 percent of the Gross Domestic Product (GDP) [1], [5]. Similar statistic of economic losses due to traffic crashes were estimated for Australia [4].

1.3. Approach for the present study

Accident cost rates can be related to the costs of possible improvement measures, so the road administration is able to identify the road sections where safety improvement measures are expected to have the best efficiency [2]. At the beginning, the aim of this research was to evaluate the optimal design of U-turn on divided rural highway in Thailand with respect to accident based investigation (based on accident cost rates). Accident can be categorized on basis of heaviest consequences (severity). Based on calculated accident cost rate for accident categories and classified U-turn, the optimal design could be evaluated. To evaluate accident cost rates, the reliability and quality of data are most important factors to achieve reliable result for an accident based research. There are limitations associated with research based on accidents, accidents are rare events and are therefore associated with the random variation inherent in small numbers, also not all accidents are reported and the level of reporting is unevenly distributed [3]. The Traffic Conflict Technique (TCT) can be considered as a surrogate or complementary methods in place of accident analysis.

A pilot study was conducted to investigate availability and assess quality of accident data for Department of Highways and Royal Thai Police; it has been found that road accident data are underreported in these agencies. Due to underreporting of accident data, it was not possible to continue this research with ‘accident based investigation’, so it is considered to continue study with ‘event based investigation’ on the basis of ‘traffic conflict techniques’.

Traffic is interaction – all events in traffic contain some kind of interaction but of course to varying extent. There is interaction between road users and there is interaction

between the road user and the road environment. Traffic conflict is defined as "A Conflict is an observational situation in which two or more road users approach each other in space and time to such an extent that a collision is imminent if their movements remain unchanged" [7]. A safety pyramid suggested by Hyden [7], as shown in Figure 1 [12].

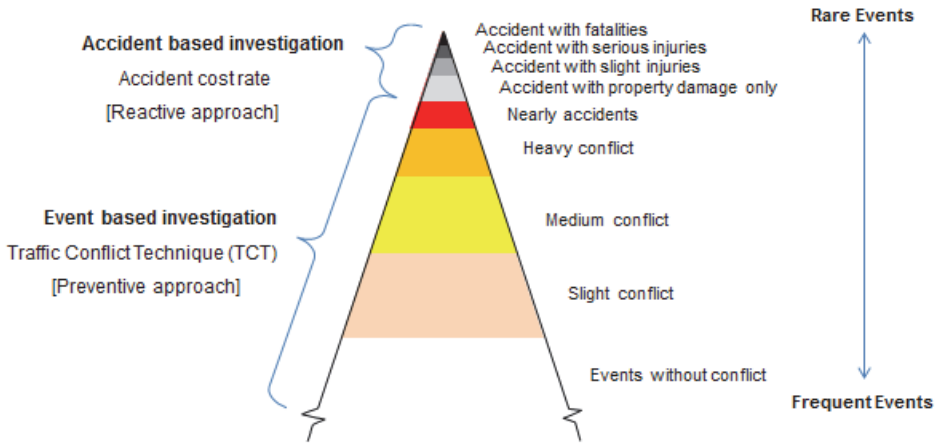

Figure 1. Traffic events with respect to time duration

The effect of various elements of U-turn on road safety can be evaluated with respect to rate of severity of conflicts. The expected outcome of this research will be selection of most appropriate geometric layout of U-turn to enhance highway safety and reduce economic losses to country causes by traffic crashes.

To study road safety aspects on U-turn, its layout designs elements (auxiliary lanes and loon), access control, approach speed, turning vehicle percentage and heavy vehicle percentage are major parameters considered for this research.

1.4. Objectives of the study

The main objectives of the present study are:

1. To assess possibility to evaluate 'accident cost rate' of different 'accident category' on various U-turn layout design practices on rural highways of Thailand,
2. To analyse availability and quality of accident data recorded in various agencies (Department of Highways and Royal Thai Police) for rural highways in Thailand,
3. To evaluate the effect variation of U-turn elements (median opening length, auxiliary lanes, loon etc.) on severity based conflict rate with respect to traffic exposure.
4. To assess most appropriate layout design of U-turn for divided highways of Thailand with respect to traffic exposure and traffic conflict events (Traffic Conflict Technique).

2. Pilot study for accident based investigations

2.1. Aim of the pilot study

A pilot study was conducted to assess the availability and quality of accident data with accident reporting agencies (Department of Highways and Royal Thai Police) in Thailand.

2.2. Scale of the pilot study

Total 35 U-turns locations around Hat Yai were identified for pilot study. Accident data information was collected from 8 responsible Royal Thai Police stations for identified U-turns. Accident data from Department of Highways were also collected and analysed.

2.3. Outcome of the pilot study

There is a serious underreporting with the Department of Highways (DoH) data because DoH only reports accidents if there is damage to property of DoH.

The Royal Thai Police accident reports are unstructured; these reports don't have data of exact location identification of accidents, so it was not possible to identify accidents in these reports for selected U-turns for Pilot study. Also accident reports are prepared in descriptive format (in Thai language) and are manually written (no softcopy available), a number of reports were written in poor handwriting. Some police stations didn't permit to take photo or photo-copy of accident reports. So accident data of Royal Thai Police are not suitable for this study.

An earlier study also indicated about incomplete accident data, no data sharing between agencies in Thailand, the Department of Highways having about 60% underreporting as comparing to Royal Thai Police [8]. Due to these limitations it was not possible to carry on this research study based on accident based investigations.

3. Event based investigation

3.1. Traffic conflict technique and limitations

Traffic conflict techniques are considered as surrogate approach to accident based investigations [9]. The basic hypothesis is that there is a close relationship between conflicts and accidents [3]. Broadly traffic conflict technique classified as 'subjective approach' and 'objective approach' [10]. Subjective methods include considerable judgment of evasive action of road user by the conflict observer. Objective method use Time-space criteria such as Post Encroachment Time (PET) and Time to Collision (TTC). Objective approach requires sophisticated video recording locations and video analysis (image processing) software/ equipment. For this study, there are unavailability of structures near to identified U-turns to fix camera to capture a bird's-eye view (elevated view), as selected U-turns are in non-built up areas and rows of trees along the highway hinder to capture movement of vehicles from transverse direction. Due to these constraints it is planned to conduct further research based on subjective approach of traffic conflict technique.

Table 1 and table 2 are showing requirements and features of subjective and objective approaches of Traffic Conflict Techniques.

Table 1. Requirements TCT approaches

Subjective Approach	Objective Approach
Require trained technical observers	Require sophisticated positions of video cameras for recording and image processing computer programs
Require shorter time period for investigation	Require longer time period for investigation

Table 2. Features of TCT approaches

Subjective Approach	Objective Approach
Surrogate to objective approach	Surrogate to accident based investigation

3.2. Elements, Classification and Zones of U-turns

3.2.1. Elements of U-turns

U-turns are combinations of various elements such as (1) through lanes, (2) deceleration lane, (3) median opening width, (4) acceleration lane, (5) median width at opening, (6) outer widening / loon and (7) directional island as show in Figure 2.

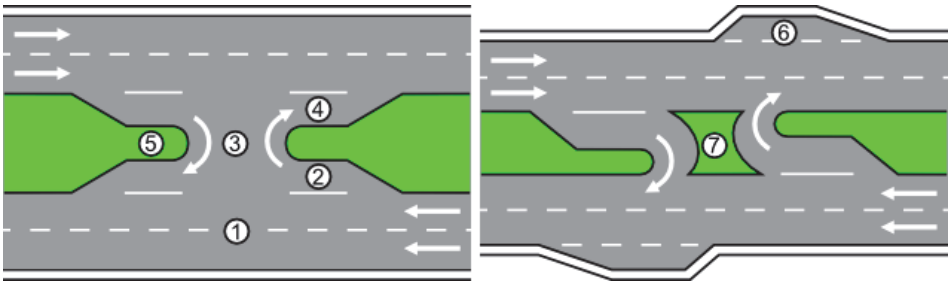

Figure 2. Elements of U-turns

3.2.2. Classification of U-turns

In Thailand various geometric design practices of U-turns are adopted. On the basis of combination of various elements, U-turns in Thailand are classified as following (Figures 3 to 6).

- *UT-1:* Conventional without auxiliary lanes,
- *UT-2:* Conventional with deceleration lanes,
- *UT-3:* Conventional with auxiliary lanes (acceleration and deceleration),
- *UT-4:* Directional with auxiliary lanes (acceleration and deceleration),
- *UT-5:* Conventional with deceleration lane and triangle shape outer widening,
- *UT-6:* Conventional with auxiliary lanes (acceleration. and deceleration) & triangle shape outer widening,
- *UT-7:* Conventional with deceleration lane and outer widening for upstream and downstream, and
- *UT-8:* Conventional with deceleration lane and loon.

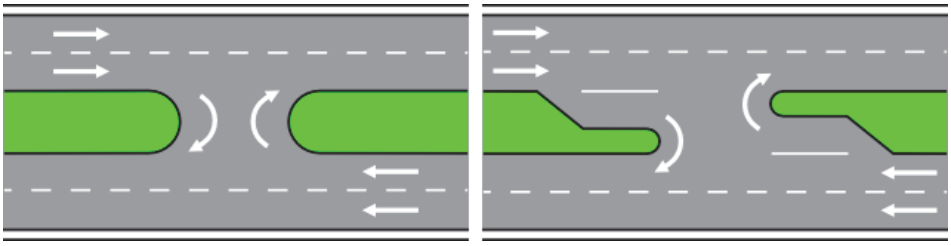

(a) UT-1 *(b) UT-2*

Figure 3. U-turns in Thailand

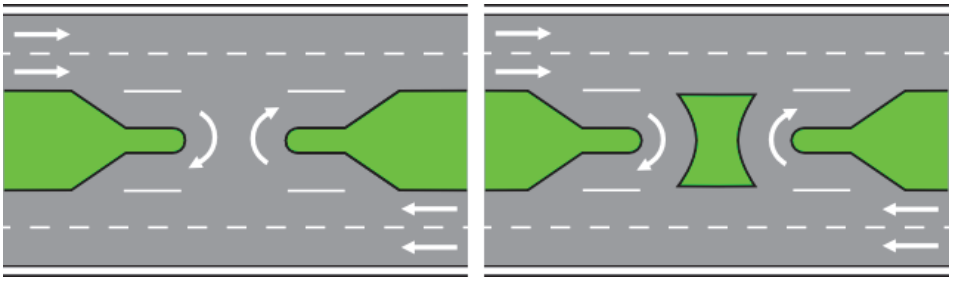

(a) UT-3 *(b) UT-4*

Figure 4. U-turns in Thailand

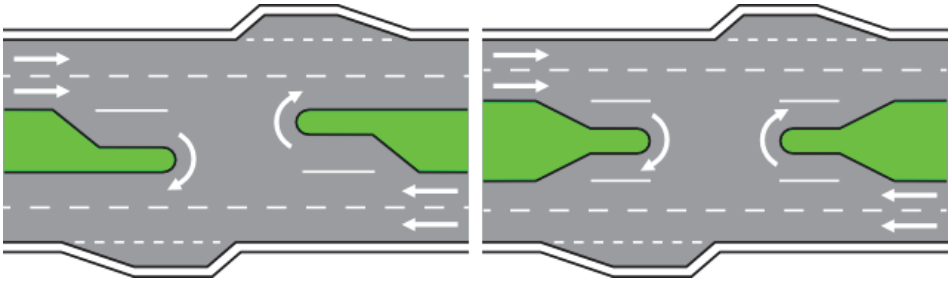

(a) UT-1 *(b) UT-2*

Figure 5. U-turns in Thailand

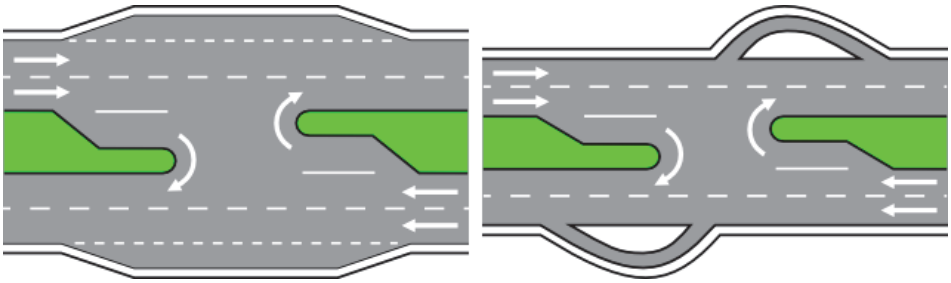

(a) UT-7 *(b) UT-8*

Figure 6. U-turns in Thailand

A similar classification based on U-turn elements was published in an earlier study [6]. Also, it was found that a directional island improves safety at U-turn and Provision of loons along four-lane arterials to accommodate U-turn maneuvers by trucks should be considered while designing [6]. Consistency needs to be maintained with relation to the design of loons and placement of crossovers along narrow medians [11].

3.2.3. U-turn zones

For a U-turn manoeuvre, a road user has to follow three actions, first he has to decelerate and divert from through traffic, second he has to make a turning manoeuvre, and third he has to accelerate and merge in through traffic. For this study, U-turns are divided in three zones as following (Figures 7 and 8).

- *Zone 1:* Upstream zone (for deceleration and diverging),
- *Zone 2:* Turning zone (for turning movement) and
- *Zone 3:* Downstream zone (for acceleration and merging).

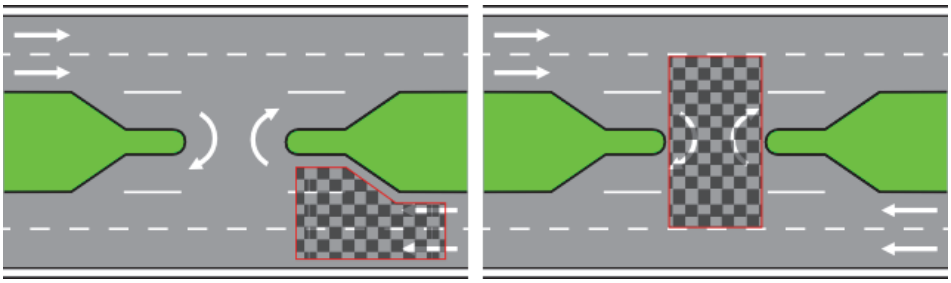

(a) Zone 1 *(b) Zone 2*

Figure 7. U-turn zones

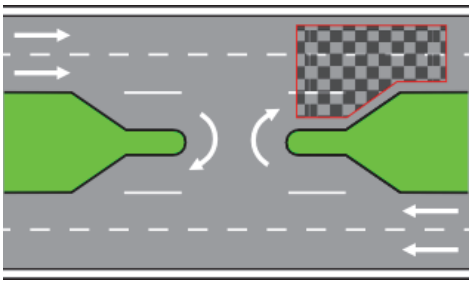

Figure 8. U-turn Zone 3

The number of through lanes and the length of deceleration lane are the variable elements for the upstream zone. In the turning zone the variable elements are median width, width of median opening and presence of Directional Island. For downstream zone the variable elements are the number of through lanes, length of acceleration lane adjacent to median and, layout design and width of outer widening or loon.

3.3. Traffic interactions events

Four types of Traffic Interaction Events are considered for this study.

- *Traffic Interaction without interference:* A situation in which two or more road users approach each other in space and time without interfering each other's speed and manoeuvres.
- *Traffic Interaction with interference:* A situation in which two or more road users approach each other in space and time with interfering each other's speed and/or manoeuvres up to an accepted level (i.e. without any evasive action by any road user).
- *Traffic Conflict (Interaction with heavily interference):* A situation in which two or more road users approach each other in space and time to such an extent where one or both drivers take evasive action to avoid a collision.
- *Traffic Accident:* A situation in which two or more road users approach each other in space and time to such an extent where their vehicles collide even evasive action is taken by one or both drivers.

3.4. Classification of conflicts for U-turns

Based on the three zones, the different possible conflicts are classified as follows.

3.4.1. For Upstream Zone

1. *UC-1 (U-turn and/or Through, Same-Direction):* Occurs when the first vehicle slows to make a U-turn, thus placing a second vehicle in danger of a rear-end or sideswipe collision.
2. *UC-2 (U-turn and Through, Same-Direction, Secondary Conflict):* Occurs when a second (through) vehicle makes a manoeuvre to avoid the first vehicle (U-turn), placing a third vehicle in danger of a collision.
3. *UC-3 (Deceleration lane overflow):* Occurs when U-turn vehicles storage overflow the deceleration lane and block a through lane.
4. *UC-4 (Other conflict type):* Conflict that cannot be assigned to the types 1 – 3.

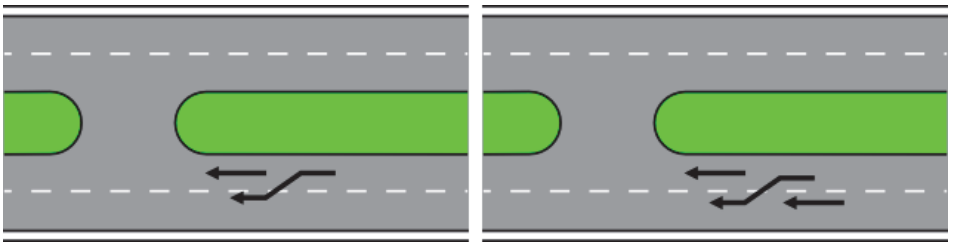

(a) UC-1 *(b) UC-2*

Figure 9. Upstream zones

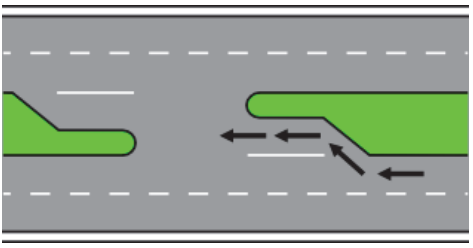

Figure 10. Upstream Zone UC-3

3.4.2. For Turning Zone

1. *TC-1 (U-turn, Same-Direction Conflict):* Occurs when the first vehicle slows/stops while U-turning, thus placing a second following vehicle in danger of a rear-end collision.
2. *TC-2 (U-turn, Opposite-Direction Conflict):* Occurs when vehicles from opposite directions make U-turn such that placing in danger both vehicles of head-on or sideswipe collision.
3. *TC-3 (Opposing U-turn and Through Conflict):* Occurs when an opposing stream vehicle makes a U-turn, placing a second vehicle in danger of a head-on or broadside collision. Here the second vehicle has the right-of-way.
4. *TC-4 (U-turn manoeuvre not from adjacent lane to median, same direction Conflict):* Occurs when the first vehicle, from other then adjacent lane to median makes a U-turn, thus placing a following second vehicle in danger of a rear-end or a sideswipe collision.
5. *TC-5 (Other conflict type):* Conflict that cannot be assigned to the types 1 – 4.

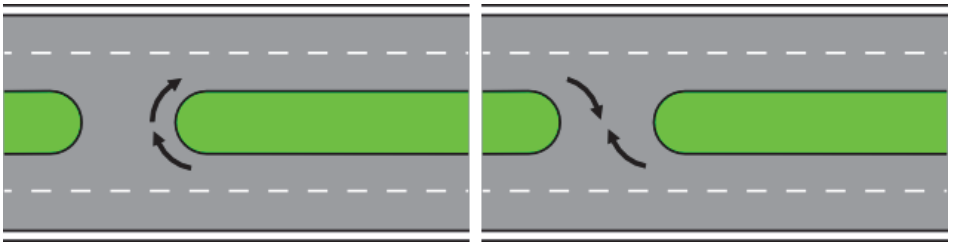

(a) TC-1 *(b) TC-2*

Figure 11. Turning zones

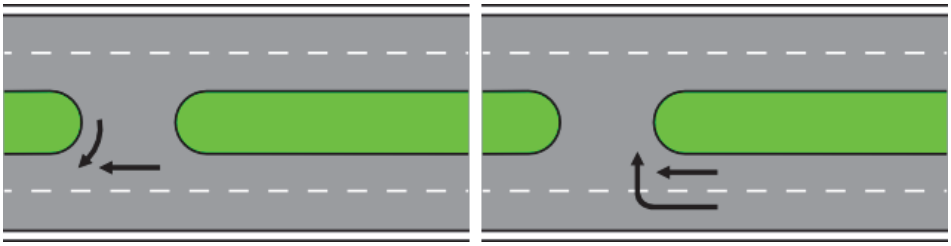

(a) TC-3 *(b) TC-4*

Figure 12. Turning zones

3.4.3. For Downstream Zone

1. *DC-1 (Lane change Conflict):* Occurs when the first vehicle changes lane from auxiliary (acceleration) lane to a through lane, thus placing a through second vehicle in danger of a rear-end or a sideswipe collision.
2. *DC-2 (Secondary Conflict):* Occurs when a second (through) vehicle makes a manoeuvre to avoid the first vehicle (lane changes from acceleration to through), placing a third vehicle in danger of a collision.
3. *DC-3 (Other conflict type):* Conflict that cannot be assigned to the types 1 – 2.

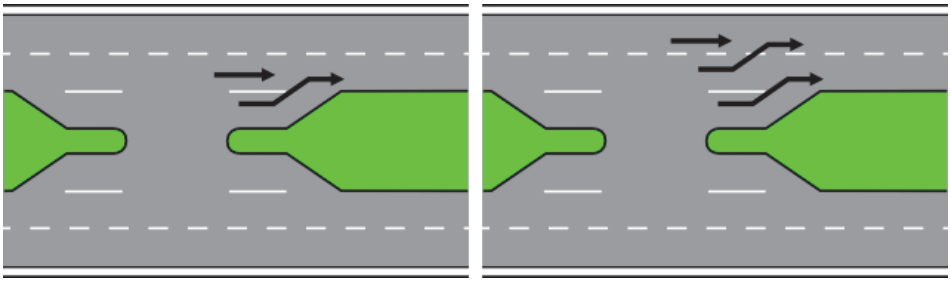

(a) DC-1 *(b) DC-2*

Figure 13. Downstream zones

3.5. Severity of traffic conflict events and indicators

Three types of conflict severities are considered for this study.

1. *Slight traffic conflict event:* A situation where one or more road user use "sudden brake" to avoid collision at a traffic conflict situation.
2. *Moderate traffic conflict event:* A situation where one or more road user "apply sudden brake and stop" to avoid collision at a traffic conflict situation.
3. *Severe traffic conflict event:* A situation where one or more road user use "hard brake" resulting braking sound or skid marks on the road surface to avoid collision at a traffic conflict situation.

3.6. Data collection

For 8 types of classified U-turns, it was decided to collect data on 2 U-turns of each type for 2 peak hours and 2 non-peak hours for both sides of traffic streams. For this study the following data are planned to be collected.

3.6.1. Traffic exposure

- Through traffic volume,
- U-turning vehicle volume,
- Traffic composition (percentage of heavy vehicles with respect to the total number of vehicles),
- Approach speed,

3.6.2. Geometric layout data of U-turns

For this research purpose, the following geometric layout data of U-turns will be collected:

- Number of through lanes,
- Length of deceleration lanes,
- Width of median opening,
- Length of acceleration lanes,
- Median width at U-turn,
- Dimensions of outer widening or loon, and
- Type and dimensions of directional island

3.6.3. Traffic conflict data

For this research purpose, based on severity of conflict, the following conflict data will be collected and video recorded:

- *Slight traffic conflict:* “sudden brake” action,
- *Moderate traffic conflict:* "sudden brake and stop” action,
- *Severe traffic conflict:* “hard brake” causing braking sound or skid marks.

3.7. Data analysis and expected results

Traffic exposure data, conflict data and geometric data of U-turns will be analysed to assess the safest U-turn layout designs for various traffic conditions. The expected outcome of data analysis is as following:

- A relationship between severities based conflict rates with various U-turns elements (auxiliary lanes, directional island etc.).
- A relationship between severities based conflict rates with percentage of turning vehicles.
- A relationship between severities based conflict rates with traffic composition.

4. Conclusions

The outcome of the pilot survey indicates that accident data of Royal Thai Police and Thai Department of Highways are underreported and not reliable for accident based investigations. So it was not practicable to continue this research work on the basis of accident based approach, therefore it was decided to use another surrogate approach of 'event based investigation'. Traffic conflict technique (TCT) is considered for further investigation.

References

[1] Luathep, P. , Tanaboriboon, Y.: *Determination of Economic Losses due to Road Crashes in Thailand,* Journal of the Eastern Asia Society for Transportation Studies, vol. 6, pp. 3413-3425, 2005

[2] Steinbrecher, J., Schubert, T.: *Safety of rural roads in Germany*, 12th WCTR, July 11-15, Lisbon, Portugal, 2010

[3] Svensson, A.: *A Method for Analysing the Traffic Process in a Safety Perspective.* Bulletin 166, Department of Traffic Planning and Engineering, Lund University, Sweden, 1998

[4] Connelly, L.B., Supangan, R.: *The economic costs of road traffic crashes: Australia, states and territories,* Accident Analysis & Prevention, vol. 38, pp. 1087–1093, 2006

[5] Thongchim, P., Taneerananon, P., Luathep, P., Prapongsena, P.: *Traffic accident costing for Thailand*, Journal of the Eastern Asia Society for Transportation Studies, vol. 7, pp. 2891-2906, 2007

[6] Potts, I., Harwood, D., Gluck, J., Levinson, H.: *Safety of U-turns at Unsignalized Median Openings on Urban and Suburban Arterials*, National Cooperative Highway Research Program Report 524, 2005

[7] Amundsen, F.H., Hydén, C. (ed.): *Proceedings: First workshop on traffic conflicts.* TØI Oslo/LTH Lund, ISBN 82-7133-195-7, 1977

[8] Srirat, P.: *Under-Reporting of road casualty accident data: a case study of highways in Nakhon Ratchasima,* Thailand, Master Thesis, Asian Institute of Technology, School of Civil Engineering, Thailand, 2008

[9] Tarko, A., Davis, G., Saunier, N., Sayed, T., Washington, S.: *Surrogate Measures of Safety ANB20(3),* Subcommittee on Surrogate Measures of Safety ANB20 Committee on Safety Data Evaluation and Analysis Contributors, White Paper, 2009

[10] Shinar, D.: *The Traffic Conflict Technique: A Subjective vs. Objective Approach,* Journal of Safety Research, vol. 15, pp. 153–157, 1984

[11] Sisiopiku, V., Aylsworth-Bonzelet, L.: *Application of Loons at Directional Crossovers*, Presented at the 82nd annual meeting of Transportation Research Board, Washington, D.C., 2003

[12] Chin, H. C., Quek, S. T.: *Measurement of Traffic Conflicts*, Safety Science, vol. 26, no. 3, pp. 169-185, 1997

Acta
Technica
Jaurinensis

Vol. 7., No.1., pp. 33-45, 2014
DOI: 10.14513/actatechjaur.v7.n1.9
Available online at acta.sze.hu

Analysis of Road Accident Hazardous Locations in Bangkhen Police Station, Thailand

A. Leelakajonjit, U. Brannolte, K. Kanitpong, P. Iamtrakul

EU-Asia Road Safety Centre of Excellence (RoSCoE)
Prince of Songkla University
Hat Yai, 90112 Thailand
E-mail: amornchai.le@police.go.th, ulrich.brannolte@uni-weimar.de, kanitpon@ait.ac.th, apawinee@hotmail.com

Abstract: A road safety management system needs high quality of accident data to support decision making about accident countermeasures and treatments. As the present road safety management system in most Thai police stations do not use accident data support for hazardous location analysis, this study proposed a better method to identify black spots in Thai police stations. The Bangkhen police station in Bangkok, Thailand was selected as a study area. And, accident data during 2009 – 2011 were collected in this police station. The results from hazardous location analysis found three black spots with a safety potential 538,082 Euro.

Keywords: road accident, hazardous location, black spot, Thailand

1. Introduction

1.1. Road safety situation background

Road traffic accident is an important cause to make Thai citizen death over 10,000 people almost every year [8]. Although the statistics in 2010 show decreasing of fatality number from 10,439 to 7,284, Thai death rate is still high at 11.40 per 100,000 population and 2.56 per 10,000 registered vehicles. These death numbers are like that there is a war in Thailand.

Thailand has various road accident databases both at official organizations such as Royal Thai Police (RTP), Department of Highways (DoH), Ministry of Public Health, and Department of Disaster Prevention and Mitigation and non-government organizations such as insurant companies, rescue team volunteers and accident research centres of various universities. Each organization develops its database for specific purpose. So, each database has different data structure and quality.

Thailand National Statistical Office surveyed deaths in Thailand 383 thousand are male and 211 thousand are female [6]. Causes of death are classified to 5 majors group of death are non-epidemics, epidemics, accident, decrepit, and others. The majority of

deaths are non-epidemics 51.4 percentages, decrepit is 25.4 percentages, epidemics 12.7 percentages, accident 7.9 percentages, and others 2.6 percentages.

How useful of accident analysis in preventing the future occurrence of accidents is a fundamental question to people interested in road safety [1]. Normally, the road accident report forms are often 2 – 4 pages long or more, which require filling-in at the accident sites, mostly by the pen and paper. During road accident situation, road users affected by the traffic disruption and prohibit the police officers from making detailed and accurate records of all relevant data. Furthermore, the police cannot be regarded as professionals for all information, such as vehicle defects, drivers' state and conditions, and environmental deficiencies [10].

1.2. Problem statement

In Thai police stations, police need data to support their road safety works but some of them never analysed the collected data in their station. Some police stations identify hazardous location by their experience and feeling. It will be much better if they analyse accident data for identifying hazardous locations. This study would like to propose a better method to identify the significant hazardous locations.

2. Objectives and scope of the study

2.1. Objective of the study

This study tries to identify hazardous locations in a police station following these objectives.

- To develop accident database for Thai police stations.
- To improve road hazard identification system for Thailand by developing black spot definition

2.2. Scope of the study

This study focuses on road safety management system in Thai police stations. Accident database improvement is limited by these conditions.

(a) The road accident data come from a selected police station.

(b) The accidents happened in 2009 – 2011 only.

(c) The accident data were written in police daily reports.

(d) The accident locations were relocated in Geographic Information System from general descriptions.

3. Literature review

Majority of works in this study are involved with a road safety management system. FHWA gave an explanation that Safety Management System (SMS) gives decision makers and those who manage and maintain local roadways the tools to systematically

identify, prioritize, correct, and evaluate the performance of their transportation safety investments [4].

3.1. Black spot definition

"Black Spot" (BS) is a name of hazardous location on the map. Almost all road safety organizations use black spot to present the hazardous locations because black colour refers to poor or bad safety conditions in each location. However, the methodology to identify black spots is variety depend on each country or area supporting factors.

The Institute of Transport Economics, Norway [3] published "State-of-the-art approaches to road accident black spot management and safety analysis of road networks" consists of summarized black spot definitions as following three groups:

1. Numerical definitions
   a. Accident number
   b. Accident rate
   c. Accident rate and number
2. Statistical definitions
   a. Critical value of accident number
   b. Critical value of accident rate
3. Model-based definitions
   a. Empirical Bayes
   b. Dispersion value

3.2. Black spot definition review

Elvik R. summarized [3] black spot definitions in eight European countries: Austria, Denmark, Flanders of Belgium, Germany, Hungary, Norway, Portugal, and Switzerland.

3.2.1. Definition of black spot in Austria

Black spot identification bases on following condition: There are three or more similar injury accidents within 3 years and a relative coefficient R_k at least 0.8.

$$R_k = \frac{U}{0.5+7\times10^{-5}\times AADT} \tag{1}$$

where:

AADT = Annual Average Daily Traffic (vehicles/24 hours)

U = Number of injury accidents within 3 years.

3.2.2. Definition of black spot in Denmark

Black spots are considered by comparing with normal number of accidents for a location based on the Poisson distribution. The minimum number of accidents for a site to be considered as black spot is four accidents within five years.

3.2.3. Definition of black spot in Flanders of Belgium

Black spots are identified from score of priority (S) equal 15 or more. The score of priority can be calculated from following formula:

$$S = LI + 3 \times SI + 5 \times DI \quad (2)$$

where:

LI = total number of slight injuries
SI = total number of serious injuries
DI = total number of deadly injuries

Size of a sliding window for black spot identification is 100 meters.

3.2.4. Definition of black spot in Germany

Black spots are identified as black if five accidents of similar type have been record within one year at a 100-meter location. For three year period, five or more injury accidents have been recorded or three or more serious injury accidents have been recorded.

3.2.5. Definition of black spot in Hungary

In outside build-up area, a black spot is defined as four injury accidents have been recorded during three years within 1,000 meters. For inside build-up area, a black spot is defined as at least four injury accidents have been record during three years on a 100-meter road section.

3.2.6. Definition of black spot in Norway

There are two types of road hazard locations in Norway. First, a black spot is identified as at least four injury accidents have been recorded within 100 meters during five years. And, a black section is identified as at least 10 injury accidents have been recorded within 1,000-meter road section during five years.

3.2.7. Definition of black spot in Portugal

There are two black spot definitions in Portugal. First definition, black spot is 200-meter road section with at least five accidents and severity index greater than 20 during one year. The severity index can be calculated by the following formula

$$SI = 100 \times FAL + 10 \times SI + SL \quad (3)$$

where:

SI = Severity Index
FAL = total number of fatalities
SI = total number of serious injuries
LI = total number of slight injuries

The second definition, an accident prediction model is applied from five year reference period in order to estimate the expected number of accidents. Then, the worst 20 intersections in each road class are selected for detailed accident analysis.

3.2.8. Definition of black spot in Switzerland

Black spots are defined base on the accident rate and critical value for the minimum recorded number of accidents during two years as following conditions. For motorways, the critical accident count values are 10 for all accidents, 4 for injury accidents, and 2 for fatal accidents. For rural roads, the critical values are 8 for all accidents, 4 for injury accidents, and 2 for fatal accidents. For intersections in urban areas, the critical values are 10 for all accidents, 6 for injury accidents, and 2 for fatal accidents. The black spot length is between 100 to 500 meters based on traffic volume.

4. Methodology

This study was planned starting with review international and local papers about road hazardous location (black spot) identification. As the second step, the police station was selected as study area based on few accident data conditions. Then accident data were collected for three years period. Third step, the collected data were analysed for appropriate black spot definition. Fourth step, an analysis was conducted on the effectiveness of road traffic enforcement on road safety. Fifth step, some black spot identification methods were selected and applied with collected data in order to produce black spot map for comparison.

5. Data collection

This study collected road accident data following the study framework. The collected data from the selected police station were stored in the software developed. Finally, accident data were grouped as accident locations for black spot identification purpose.

5.1. Selection of study area

This study selected three police stations to check required data in the pre-data collection process. The police stations were selected from the provinces with the highest number of fatalities in each region in 2011. The numbers of accident involved persons ordering by number of fatalities in 2011 are in Table 1. Nakhorn Ratchasrima province was selected from north east region. Bangkok was selected from central region. Songkla province was selected from south region. The police stations were pre-data collected are Nakhorn Ratchasrima police station in Nkhorn Ratchasrima province north east region, Bang Khen police station in Bangkok central region, and Hat Yai police station in Songkla province south region.

Result of pre-data collection in three police stations found the problems to collect accident data in Nakhorn Ratchasrima police station and Hat Yai police station. So, Bang Khen police station was selected as study area in this study. Bang Khen police station has an area of 40 sq. kilometres, about 350 intersections, 430,000 population, 33 education places, 84 resident communities, 4 ordinary markets, and 5 super markets.

Table 1. Number of Accident Statistics in 2011 [9]

Order	Province	Fatal Case		Injury Case			Total Acc. No.	Total Involved Persons
		Acc. No.	Fatality No.	Acc. No.	Serious Injuries	Slight Injuries		
1	Bangkok	373	393	21,323	932	23,802	21,696	25,127
2	Nakorn Ratchasrima	343	369	7,600	332	8,596	7,943	9,297
3	Chonburi	274	286	9,774	439	10,657	10,048	11,382
4	Chengrai	219	241	4,795	267	5,160	5,014	5,668
5	Udonthani	190	219	4,123	346	4,680	4,313	5,245
6	Chengmai	195	208	9,906	478	10,848	10,101	11,534
7	Konkang	187	201	3,222	146	3,619	3,409	3,966
8	Burirum	182	193	3,739	553	3,981	3,921	4,727
9	Rayong	180	193	2,802	209	2,932	2,982	3,334
10	Phetchaburi	172	187	4,449	106	5,348	4,621	5,641
11	Songkla	158	182	5,105	617	5,425	5,263	6,224
12	Nakorn Sawan	167	181	5,138	99	6,036	5,305	6,316
13	Ubon Ratchathani	165	178	6,520	222	7,519	6,685	7,919
14	Ayuthaya	163	175	2,177	111	2,463	2,340	2,749
15	Nahorn Srithammarat	160	167	5,369	164	6,119	5,529	6,450

5.2. Data collection procedure

There are three steps for data collection in this study. First, the police daily reports in 2009 - 2011 were categorized into criminal cases and road accident cases. Second, the road accident daily reports were scanned page by page to digital files because it is not allowed taking them out of the police station. Third, the scanned files were read and input to developed accident database. This step needs to locate the accident locations on the map from descriptive details. Finally, the collected data were ready to be analysed. The data collection procedure is in Figure 1.

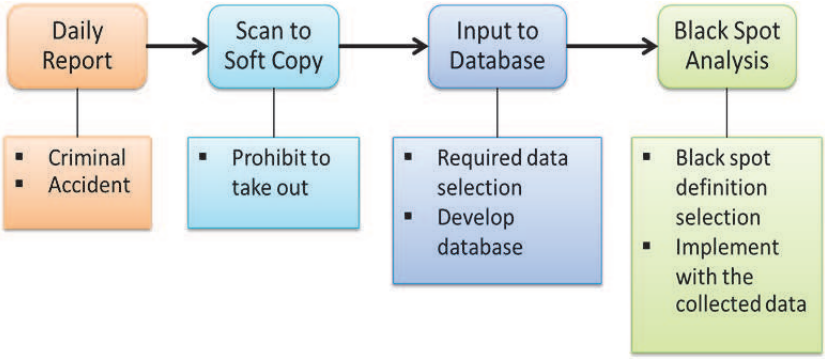

Figure 1. The data collection procedure

5.3. Software development

As one of the objectives of this study is to improve accident database, a Road Accident Management System (RAMS) was developed as a model of accident database and used for inputting collected data. This software is also able to group and count accident in the close locations as groups and present accident data in map-based data too. The Figure 2 shows RAMS accident presentation.

Figure 2. Accident data presentation in RAMS [12]

The collected accident data were categorized by accident severity into fatal accident, serious injury, slight injury, and property damage only (PDO). Accident type of collected data are driving accident, turn off accident, turn in/crossing, crossing over, result from parking, longitudinal accident, and other accident. All the collected data elements for each road accident are 20 variables as in Figure 3.

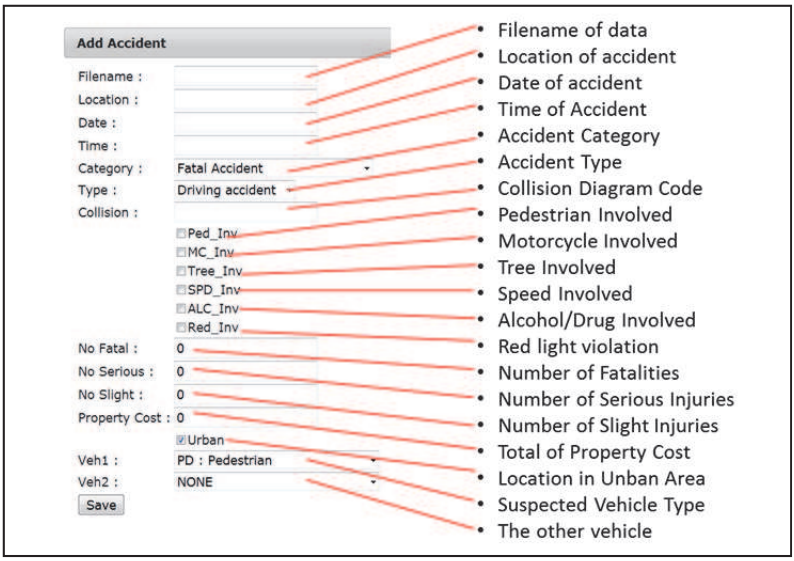

Figure 3. Collected data elements in RAMS

6. Results of 1st Pilot Study

6.1. Scope of 1st pilot study

In the 1st pilot study, 40 kilometre square of Bang Khen police station responsible area was narrowed down to an about 9.5 kilometre square study area of 1st pilot study. The 1st pilot study area has about 214 intersections. The two main roads are Ram Intra and Phahonyothin road. A map of this area is in Figure 4.

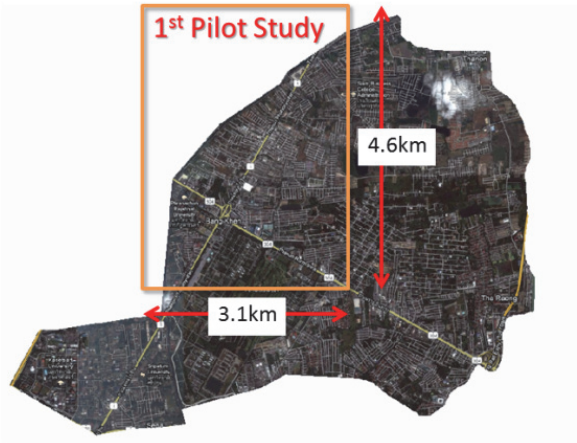

Figure 4. Map of 1st pilot study area

6.2. Collected data

In the 1st pilot study, there are 569 accident happened in 2009 – 2011. These accidents can be grouped into 69 locations including some independent locations. The Figure 5 shows collected accident data in RAMS and VISUM Safety. VISUM Safety was developed by PTV [7]. It provides tools for black spot analysis and accident prediction calculation.

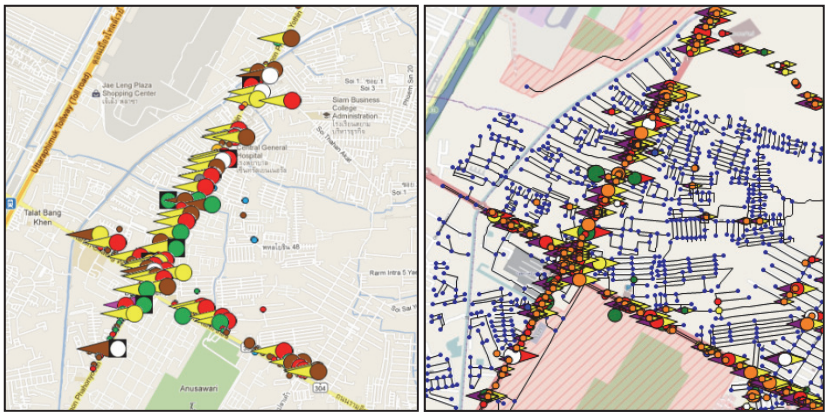

Figure 5. Collected accident locations in RAMS(left) and in VISUM Safety (right)

In 1st pilot study, there are 2 fatalities, 67 serious injuries, and 186 slight injuries. While there are 358 accidents have no injuries. The number of injuries in each accident severity is in Table 2.

Table 2. Number of cases and injuries grouping by accident severity

Severity	Number of cases	Total injuries
Fatal Accident	2	2
Serious injury	55	67
Slight injury	154	186
PDO	358	-
Total	569	255

6.3. Accident cost

6.3.1. Thai Accident Cost in 2012

Taneerananon P. studied [11] cost of accident and reported accident cost for each accident victim severity as in Table 3.

As the monetary value is changed depending on inflation rate, the cost of accident severity in 2012 can be calculated by adapting with inflation rate for each year from Bank of Thailand (BOT). The Thailand inflation rates were shown in Table 4.

Table 3. Cost of accident severity in Thailand [11]

Severity	Min (Baht)	Max (Baht)
Fatality(FAL)	3,959,387	4,658,004
Disability (DIS)	4,503,479	5,404,175
Serious Injury (SI)	123,245	128,836
Slight Injury (SL)	30,289	30,461
Property Damage Only (PDO)	40,220	40,220

Table 4. Inflation rate of Thailand in 2007 – 2011 [2]

Year	Inflation rate
2007	2.3
2008	5.5
2009	-0.9
2010	3.3
2011	3.8

This study uses accident cost from the result of adapting inflation rates as in Table 5 for accident cost calculation.

Table 5. Accident cost of accident severity in 2012

Severity	Accident Cost (Baht)
Fatality(FAL)	5,341,943
Disability (DIS)	6,197,675
Serious Injury (SI)	147,753
Slight Injury (SL)	34,934
Property Damage Only (PDO)	46,126

6.3.2. Average Accident Cost

As some accidents have multiple severities of injuries, the average accident cost for each accident severity category is needed for accident cost estimation. From the collected data in 1st pilot study, the average accident costs are in Table 6.

Table 6. Average Accident Cost in 1st pilot study area (Baht)

Severity	1	2	…	569	Σ	Total cost	Count of Category	Average cost
FAL	xx	xx	xx	xx	2	10,683,887	2	5,341,943
SI	xx	xx	xx	xx	69	10,194,965	57	178,859
SL	xx	xx	xx	xx	197	6,881,923	162	42,481
PDO	xx	xx	xx	xx	569	26,245,434	348	75,418

6.4. Development of black spot definition

The average accident cost for each accident severity of collected accidents in the 1st pilot study can be presented by cumulative accident costs for each accident location as in the Figure 6.

Furthermore, black spots should be selected from hazardous locations with a reasonable number. If it is too many, it cannot emphasize the severity in black spot locations. If it too low, it cannot improve the road safety in the area. This study selected the black spots from ranking the accident costs in each location by the cumulative accident cost figures and found two interesting conditions. First, at 5.14% of the road network (11 locations) occupied 64.84% of all accident cost in the 1st pilot study. All of the 11 locations probably cannot be treated because of budget limitation of Bang Khen district. Second condition, at 1.40% of the road network (3 locations) occupied 39.85% of all accident cost. The number of 3 black spot is more possible to be treated by the road authority. This condition became to be an origin of black spot definition for the 1st pilot study.

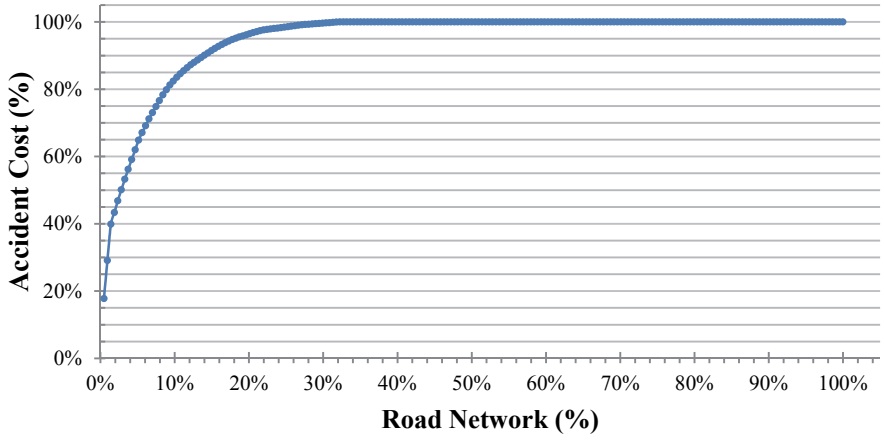

Figure 6. The cumulative accident cost for each accident location in 1st pilot study

The accident figures at the three black spots are 1) 1 fatal accident, 1 serious injury accident, 3 slight injury accidents, 2) 1 fatal accident, 1 serious injury accident, 3) 15

serious injury accidents, 17 slight injury accidents. The other accident locations have no fatal accidents, the number of serious injury accidents is less than 6, and number of slight injury accidents is less than 17. So, the numbers of 1 fatal accident, 6 serious injury accidents, and 17 slight injury accidents were selected to be the black spot definition for the 1st pilot study. The three black spots are shown in Figure 7.

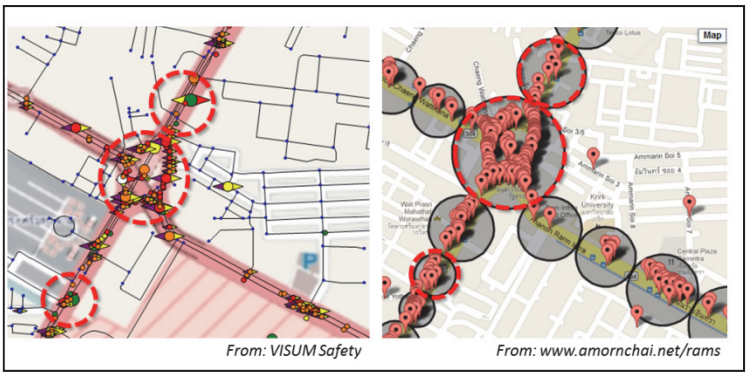

Figure 7. Three black spots from 1st pilot study

6.5. Safety potential

The safety potential can be calculated from the difference of the actual accident cost and expected accident cost for a best practice design [5]. In the 1st pilot study, the actual accident cost is 54,006,208 Baht and the expected accident cost for a best treatment is 32,482,930 Baht. So, the expected safety potential from the black spot definition in the 1st pilot study is 21,523,278 Baht or 538,082 Euro.

7. Conclusion and Recommendations

7.1. Conclusions

- The accident number black spot definition is applicable for Thai police stations.
- The road accident database for police data collection is required for road safety management system development in Thailand.
- The model software of the accident database named Road Accident Management System (RAMS) is successfully developed in this study.
- The result of the 1st pilot study data collection in Bang Khen station presents the obvious black spots with 21,523,278 Baht (538,082 Euro) safety potential.
- The accident database can support road safety enforcement in many allegations.

7.2. Recommendations

- A road accident database should be implemented in Thai police stations.
- The black spots should be identified by the accident number method.
- The local communities should worry about their safety and implement the proposed black spot management system.

References

[1] Loo, B.P.Y.: *Validating crash locations for quantitative spatial analysis,* Accident Analysis & Prevention*,* vol. 38, no. 5, pp. 879-886, 2006

[2] *Inflation Rate in Thai Monetary Market*, Bank of Thailand, 2012

[3] Sørensen, M., Elvik, R.: *State-of-the-art approaches to road accident black spot management and safety analysis of road network,* Final report in EC Sixth Framework Programme, Contract N. 506184, 2007

[4] *Implementing Local Agency Safety Management*, Federal Highway Administration, U.S. Department of Transportation, 2012

[5] Ganneau, F., Lemke, K.: *Network Safety Management – from Case Study to Application,* 23e congrès mondial de la route Paris 2007: Le choix du développement durable, *pp. 1-12, September 17-21,* 2007

[6] *Summary of Hospital Service Usage of Death Patient in Thailand,* National Statistical Office, Thailand, 2006

[7] *PTV VISUM Safety User Guide,* 2012

[8] *Road Accident Statistic,* Royal Thai Police, 2012

[9] RVP: *Accident Statistics in 2011,* Road Accident Victims Protection Company Limited, 2012

[10] Shinar, D., Treat, J.R.: *Tri-level Study: Modification Task 3: Validity Assessment of Police-Reported Accident Data,* U.S. Department of Transportation, National Highway Traffic Safety Administration, Washington, DC, 1979

[11] Taneerananon, P.: *The Study of Traffic Accident Cost in Thailand,* Department of Highways, Thailand, 2007

[12] *Development of a Road Safety Management Systems for Thailand on the Basis of Improved Accident Database,* www.amornchai.net/rams/, visited at 04/04/2013

Acta
Technica
Jaurinensis

Vol. 7., No. 1., pp. 46-61, 2014
DOI: 10.14513/actatechjaur.v7.n1.256
Available online at acta.sze.hu

Attenuation of the Model Error in Observer-Based State-Feedback Regulators

L. Keviczky, Cs. Bányász

Széchenyi István University, Győr
Computer and Automation Research Institute and Control Engineering Research Group, Hungarian Academy of Sciences
H-1111 Budapest, Kende u 13-17, Hungary
E-mail: keviczky@sztaki.hu, banyasz@sztaki.hu

Abstract: An equivalent transfer function representation (TFR) is introduced to study the state-feedback/observer (SFO) topologies of control systems. This approach is used to explain why an observer can radically reduce even large model errors. Then the same principle is combined with Youla-parametrization (YP) introducing a new class of regulators.

Keywords: observer, state-feedback, model error, Youla-parametrization

1. Introduction

It is a well-known methodology to use the state variable representations (SVR) of linear time invariant (LTI) single input - single output (SISO) systems. The SVR proved to be excellent tool to implement both LQR (Linear system - Quadratic criterion - Regulator) control and pole placement design. The practical applicability required to introduce the observers, which make this methodology widely applied even for large scale and higher dimension plants [1]. The thousands of theoretical considerations mostly concentrate on the irregularities and special structures in the SVR appearing. Much less publications deal with the model error properties of these systems.

It is possible to find a proper way to discuss and investigate the limitations if someone replaces the SVR by their TFR. The paper first summarizes the classical state-feedback (SF), state-feedback/observer (SFO) topologies then introduces the TF equivalent forms. Then the model error properties are discussed and it is shown why the SFO method reduces these errors comparing to a trivial parallel model approach. Finally this principle is extended for Youla-parametrized controllers.

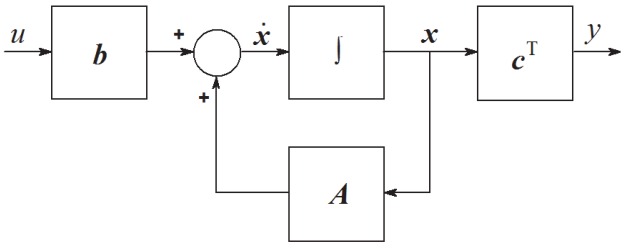

Figure 1. Block diagram of the SVR of a SISO dynamic LTI system

2. State feedback (SF)

Consider a SISO continuous time (t) LTI dynamic plant described by the SVR

$$\frac{\mathrm{d}\boldsymbol{x}}{\mathrm{d}t} = \dot{\boldsymbol{x}} = \boldsymbol{A}\boldsymbol{x} + \boldsymbol{b}u \tag{1}$$

$$y = \boldsymbol{c}^T\boldsymbol{x}$$

The corresponding block diagram of the process is shown in Fig. 1. Here u, y and $\boldsymbol{x}$ are the input, output and state variables of the process to be controlled and T stands for transposition.

The TFR of the open-loop system can be calculated by

$$P = \frac{\mathrm{B}}{\mathrm{A}} = \boldsymbol{c}^{\mathrm{T}}\left(s\boldsymbol{I} - \boldsymbol{A}\right)^{-1}\boldsymbol{b} \tag{2}$$

where $\boldsymbol{I}$ is the unit matrix and

$$B(s) = s^n + b_1 s^{n-1} + \cdots + b_{n-1}s + b_n \tag{3}$$

$$A(s) = s^n + a_1 s^{n-1} + \cdots + a_{n-1}s + a_n \tag{4}$$

are the numerator and denominator polynomials, respectively. If the feedback is restricted to a linear SF, then the classical solution can be written as

$$u = k_{\mathrm{r}}\, r - \boldsymbol{k}^{\mathrm{T}}\boldsymbol{x} \tag{5}$$

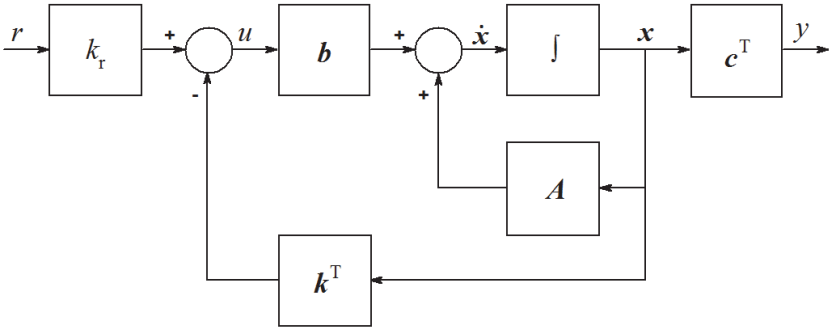

Figure 2. Block diagram of the SF of a SISO LTI system

The resulting closed-loop system is shown in Fig. 2, where r is the reference signal, k_r is a calibrating constant and $\boldsymbol{k}^{\mathrm{T}}$ is the linear SF vector. It is easy to check that the complementary sensitivity function (CSF) from the reference signal r to the output y is

$$T_{\mathrm{ry}}(s)=k_{\mathrm{r}}\boldsymbol{c}^{\mathrm{T}}\left(s\boldsymbol{I}-\boldsymbol{A}+\boldsymbol{b}\boldsymbol{k}^{\mathrm{T}}\right)^{-1}\boldsymbol{b}=\frac{k_{\mathrm{r}}P}{1+\boldsymbol{k}^{\mathrm{T}}\left(s\boldsymbol{I}-\boldsymbol{A}\right)^{-1}\boldsymbol{b}} \tag{6}$$

where k_r is obtained by requiring that the static gain of T_{ry} should be equal to one

$$k_{\mathrm{r}}=\frac{\boldsymbol{k}^{\mathrm{T}}\boldsymbol{A}^{-1}\boldsymbol{b}-1}{\boldsymbol{c}^{\mathrm{T}}\boldsymbol{A}^{-1}\boldsymbol{b}} \tag{7}$$

The calibrating factor k_r is necessary because the closed-loop using SF is not an integrating one.

The usual classical design goal is to determine the feedback gain $\boldsymbol{k}^{\mathrm{T}}$ so that the closed-loop system has the characteristic polynomial

$$R(s)=s^n+r_1s^{n-1}+\cdots+r_{n-1}s+r_n \tag{8}$$

The solution formally means making the characteristic polynomial of the closed-loop equal to the desired polynomial ("placed poles")

$$\det\left(s\boldsymbol{I}-\boldsymbol{A}+\boldsymbol{b}\boldsymbol{k}^{\mathrm{T}}\right)=\mathrm{R}(s) \tag{9}$$

The solution always exists if P is controllable. If the TFR of the process is known then one can easily form a controllable canonical form with

$$\boldsymbol{A}_{\mathrm{c}}=\begin{bmatrix}-a_1 & -a_2 & \cdots & -a_{n-1} & -a_n\\ 1 & 0 & \cdots & 0 & 0\\ 0 & 1 & & 0 & 0\\ \vdots & \vdots & & \vdots & \vdots\\ 0 & 0 & 0 & 1 & 0\end{bmatrix}\ ;\ \boldsymbol{c}_{\mathrm{c}}^{\mathrm{T}}=\left[b_1,b_2,\cdots,b_n\right]\ ;\ \boldsymbol{b}_{\mathrm{c}}=\left[1,0,\cdots,0\right]^{\mathrm{T}} \tag{10}$$

and the feedback gain is obtained from

$$\boldsymbol{k}_{\mathrm{c}}^{\mathrm{T}}=\left[r_1-a_1,r_2-a_2,\cdots,r_n-a_n\right] \tag{11}$$

furthermore the calibration factor is calculated by

$$k_{\mathrm{r}}=\frac{a_n+\left(r_n-a_n\right)}{b_n}=\frac{r_n}{b_n} \tag{12}$$

The SVR of the closed-loop system is described by

$$\begin{aligned}\frac{\mathrm{d}\boldsymbol{x}}{\mathrm{d}t}&=\left(\boldsymbol{A}-\boldsymbol{b}\boldsymbol{k}^{\mathrm{T}}\right)\boldsymbol{x}+k_{\mathrm{r}}\boldsymbol{b}r\\ y&=\boldsymbol{c}^{\mathrm{T}}\boldsymbol{x}\end{aligned} \tag{13}$$

It is easy to see from equation (13) that $T_{ry}(s)$ is now

$$T_{\mathrm{ry}}(s)=\frac{k_{\mathrm{r}}\,\mathrm{B}(s)}{\mathrm{R}(s)} \tag{14}$$

i.e., besides reaching the desired pole-placement the SF leaves the open-loop zeros untouched. If the TFR is not known and we must use a general SVR then the controller gain is obtained as [2]

$$\boldsymbol{k}^{\mathrm{T}}=\boldsymbol{k}_{\mathrm{c}}^{\mathrm{T}}\,\boldsymbol{M}_{\mathrm{c}}^{\mathrm{c}}\,\boldsymbol{M}_{\mathrm{c}}^{-1} \tag{15}$$

where $\boldsymbol{M}_{\mathrm{c}}$ is the controllability matrix

$$\boldsymbol{M}_{\mathrm{c}}=\left[\boldsymbol{b},\boldsymbol{A}\boldsymbol{b},\cdots,\boldsymbol{A}^{n-1}\boldsymbol{b}\right] \tag{16}$$

and $\boldsymbol{M}_{c}^{c}$ is the controllability (Vandermunde) matrix of the controllable canonical form

$$\boldsymbol{M}_{\mathrm{c}}^{\mathrm{c}}=\begin{bmatrix}1 & a_1 & a_2 & \cdots & a_{n-1}\\ 0 & 1 & a_1 & \cdots & a_{n-2}\\ \vdots & \vdots & \vdots & & \vdots\\ 0 & 0 & 0 & \cdots & a_1\\ 0 & 0 & 0 & \cdots & 1\end{bmatrix}^{-1} \tag{17}$$

(Note that there are several other methods available for calculating the optimal controller gain.)

If we want to express the operation of the SF by equivalent scheme using TFR forms Fig. 3 can be used, where the feedback regulator $R_f=K_k$ is obtained from the basic equation of the closed-loop

$$T_{\mathrm{ry}}(s)=\frac{k_{\mathrm{r}}\,\mathrm{B}(s)}{\mathrm{R}(s)}=\frac{k_{\mathrm{r}}\,\mathrm{B}(s)}{\mathrm{A}(s)+\mathrm{K}(s)}=\frac{k_{\mathrm{r}}\,P}{1+K_k\,P} \tag{18}$$

which clearly shows, that the open-loop poles remain unchanged and the closed-loop poles will be the required ones. Here it is obtained that

$$R_{\mathrm{f}}=K_k(s)=\frac{\mathrm{K}(s)}{\mathrm{B}(s)}=\frac{\mathrm{R}(s)-\mathrm{A}(s)}{\mathrm{B}(s)}=\frac{\boldsymbol{k}^{\mathrm{T}}\left(s\boldsymbol{I}-\boldsymbol{A}\right)^{-1}\boldsymbol{b}}{\boldsymbol{c}^{\mathrm{T}}\left(s\boldsymbol{I}-\boldsymbol{A}\right)^{-1}\boldsymbol{b}} \tag{19}$$

and the calibration factor again

$$k_{\mathrm{r}}=\frac{\boldsymbol{k}^{\mathrm{T}}\boldsymbol{A}^{-1}\boldsymbol{b}-1}{\boldsymbol{c}^{\mathrm{T}}\boldsymbol{A}^{-1}\boldsymbol{b}}=\frac{1+K_k(0)P(0)}{P(0)} \tag{20}$$

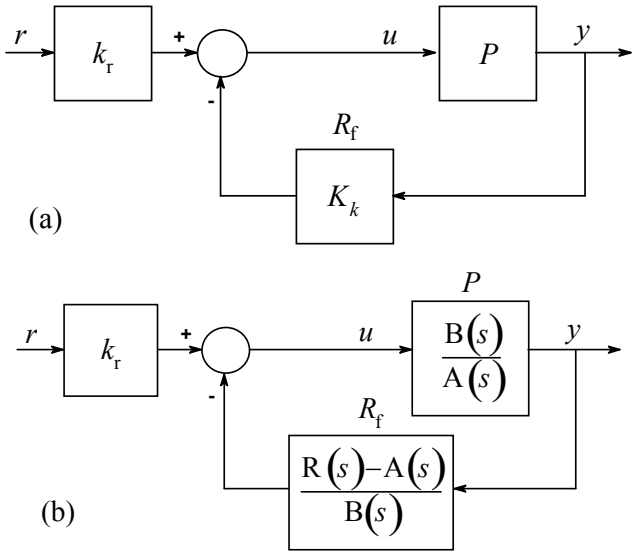

Figure 3. Equivalent schemes of SF using TFR forms

It is a not very frequently discussed question using SF whether the stability of the process polynomials in *P* are required for the closed-loop stability or not. Figure 3b shows the real operation of the SF. The polynomial *R(s)-A(s)* in the feedback path stabilizes the *1/A(s)* denominator of the process, even if it is an unstable one, and places the required poles via the design polynomial *R(s)*. The numerator *B(s)* of the plant is outside of this process and remains unchanged. Observe that this regulation can be interpreted and realized only if SF is used. Figure 3a shows another interpretation of the controller using only TFR's. This equivalent scheme, however, can be realized by the indicated transfer functions, only if the process *P* itself is inverse stable (IS), i.e., if B(s) is a stable polynomial. So note that $K_k(s)$ is realizable for IS process and can be used for stabilization if the process is unstable.

The final conclusion is that the SF stabilizes all observable plants, however, the zeros of the process remain unchanged. Further compensation is necessary if we want to handle these zeros. Note that it is very rare that all state variables are measurable in case of a real plant.

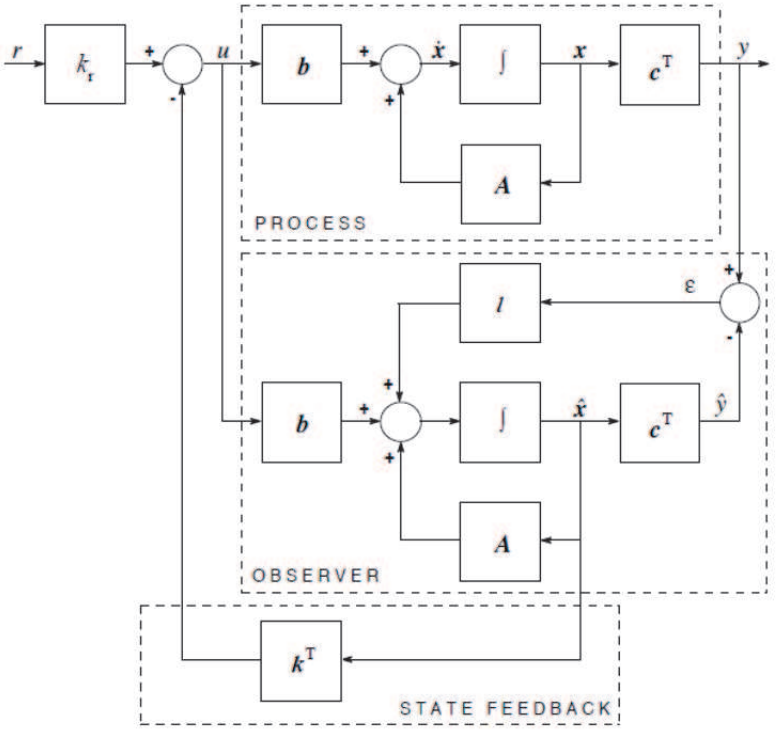

Figure 4. The general basic SFO scheme

3. Observer-Based State-Feedback

The practical applicability of the SF theory was introduced by the development of the observers capable to calculate the unmeasured state variables. The most general SF/observer (SFO) topology is shown in Fig. 4.

In the general basic SFO scheme the controller consists of two parts: one observer and one SF. The observer calculates the estimated state variable $\hat{\boldsymbol{x}}$ and the estimated process output $\hat{y}$. The feedback gain $\boldsymbol{k}^{\mathrm{T}}$ is computed, as if all state variables could be measured, using $\hat{\boldsymbol{x}}$, so

$$u = k_{\mathrm{r}}\, r - \boldsymbol{k}^{\mathrm{T}}\, \hat{\boldsymbol{x}} \tag{21}$$

The observer modifies the internal model of the process by introducing a proportional feedback $\boldsymbol{k}$ from the error $\varepsilon = y - \hat{y}$. It is long and not easy derivation to prove that the CSF from the reference signal r to the output y is

$$T_{\mathrm{ry}}(s) = \frac{k_{\mathrm{r}}\, \boldsymbol{c}^{\mathrm{T}} \left(s\boldsymbol{I} - \boldsymbol{A}\right)^{-1} \boldsymbol{b}}{1 + \boldsymbol{k}^{\mathrm{T}} \left(s\boldsymbol{I} - \boldsymbol{A}\right)^{-1} \boldsymbol{b}} = \frac{k_{\mathrm{r}}\, P}{1 + \boldsymbol{k}^{\mathrm{T}} \left(s\boldsymbol{I} - \boldsymbol{A}\right)^{-1} \boldsymbol{b}} = k_{\mathrm{r}}\, \mathrm{B}(s) / \mathrm{R}(s) \tag{22}$$

thus surprisingly exactly the same as it was for the simple SF case (see equation (6) and [3] for a nice short derivation). This means that the tracking properties of the SFO do not depend on the selected observer gain $\boldsymbol{l}$. (Note that this is only for the exact knowledge of the process parameters in the observer.) This means that the calculation of the calibration factor is also the same. It is possible to compute an equivalent feedback regulator in this case, too

$$R_{\mathrm{f}} = \boldsymbol{k}^{\mathrm{T}}\left(s\boldsymbol{I} - \boldsymbol{A} + \boldsymbol{b}\boldsymbol{k}^{\mathrm{T}} + \boldsymbol{l}\boldsymbol{c}^{\mathrm{T}}\right)^{-1}\boldsymbol{l} = \frac{\boldsymbol{k}^{\mathrm{T}}\left(s\boldsymbol{I} - \boldsymbol{A} + \boldsymbol{b}\boldsymbol{k}^{\mathrm{T}}\right)^{-1}\boldsymbol{l}}{1 + \boldsymbol{c}^{\mathrm{T}}\left(s\boldsymbol{I} - \boldsymbol{A} + \boldsymbol{b}\boldsymbol{k}^{\mathrm{T}}\right)^{-1}\boldsymbol{l}} \tag{23}$$

which has a much more complex structure than what was in (19).

Introducing the state error

$$\tilde{\boldsymbol{x}} = \boldsymbol{x} - \hat{\boldsymbol{x}} \tag{24}$$

the dynamics of the observer is basically determined by the state error equation

$$\frac{\mathrm{d}\tilde{\boldsymbol{x}}}{\mathrm{d}t} = \left(\boldsymbol{A} - \boldsymbol{k}\boldsymbol{c}^{\mathrm{T}}\right)\hat{\boldsymbol{x}} \tag{25}$$

which formally very similar to (13) with no excitation. The usual classical design goal for the observer is to determine the observer feedback gain $\boldsymbol{k}$ so that the dynamic system (25) has the characteristic polynomial

$$Q(s) = s^n + q_1 s^{n-1} + \cdots + q_{n-1}s + q_n \tag{26}$$

The solution formally means making the characteristic polynomial equal to the desired polynomial

$$\det\left(s\boldsymbol{I} - \boldsymbol{A} + \boldsymbol{l}\boldsymbol{c}^{\mathrm{T}}\right) = \mathrm{Q}(s) \tag{27}$$

The solution always exists if P is observable. If the TFR of the process is known then one can easily form an observable canonical form with

$$\boldsymbol{A}_{\mathrm{o}} = \begin{bmatrix} -a_1 & 1 & 0 & \cdots & 0 \\ -a_2 & 0 & 1 & \cdots & 0 \\ \vdots & \vdots & \vdots & & \vdots \\ -a_{n-1} & 0 & 0 & \cdots & 1 \\ -a_n & 0 & 0 & \cdots & 0 \end{bmatrix} \; ; \; \boldsymbol{c}_{\mathrm{o}}^{\mathrm{T}} = \left[1, 0, \cdots, 0\right] \; ; \; \boldsymbol{b}_{\mathrm{o}} = \left[b_1, b_2, \cdots, b_n\right]^{\mathrm{T}} \tag{28}$$

and the feedback gain is obtained from

$$\boldsymbol{l}_{\mathrm{o}} = \left[q_1 - a_1, q_2 - a_2, \cdots, q_n - a_n\right]^{\mathrm{T}} \tag{29}$$

If the TFR is not known and we must use a general SVR then the observer gain is obtained as [2]

$$\boldsymbol{l} = \boldsymbol{M}_{\mathrm{o}}^{-1}\, \boldsymbol{M}_{\mathrm{o}}^{\mathrm{o}}\, \boldsymbol{l}_{\mathrm{o}} \tag{30}$$

where $\boldsymbol{M}_o$ is the observability matrix

$$\boldsymbol{M}_{\mathrm{o}} = \left[\boldsymbol{c}^{\mathrm{T}}, \boldsymbol{c}^{\mathrm{T}}\boldsymbol{A}, \cdots, \boldsymbol{c}^{\mathrm{T}}\boldsymbol{A}^{n-1}\right]^{\mathrm{T}} \tag{31}$$

and $\boldsymbol{M}_o^o$ is the observability (Vandermunde) matrix of the observable canonical form

$$\boldsymbol{M}_{\mathrm{o}}^{\mathrm{o}} = \begin{bmatrix} 1 & 0 & \cdots & 0 & 0 \\ a_1 & 1 & \cdots & 0 & 0 \\ a_2 & a_1 & \cdots & 0 & 0 \\ \vdots & \vdots & & 1 & 0 \\ a_{n-1} & a_{n-2} & \cdots & a_1 & 1 \end{bmatrix}^{-1} \tag{32}$$

(Note that there are several methods available for calculating the optimal observer gain.)

There exists an obvious duality between finding the SF and the observer applying the following equivalence: $\boldsymbol{A} \leftrightarrow \boldsymbol{A}^T$, $\boldsymbol{b} \leftrightarrow \boldsymbol{c}^T$, $\boldsymbol{k} \leftrightarrow \boldsymbol{l}^T$ and $\boldsymbol{M}_c^c \leftrightarrow (\boldsymbol{M}_o^o)^T$.

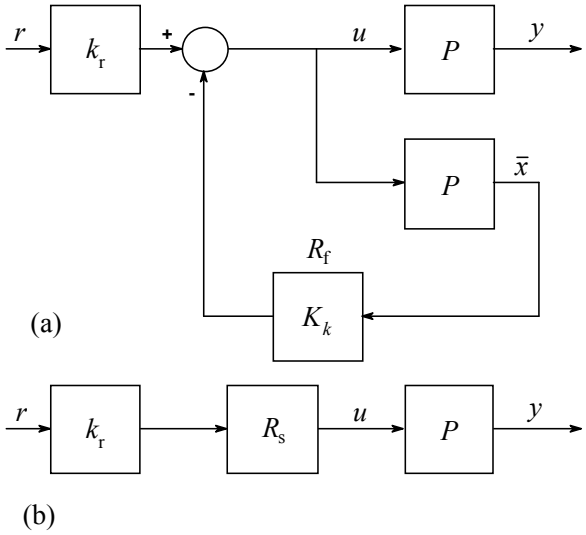

Figure 5. Equivalent schemes of SF using TFR forms

The SVR of the entire SFO closed-loop system is described by

$$\frac{\mathrm{d}}{\mathrm{d}t}\begin{bmatrix} \boldsymbol{x} \\ \tilde{\boldsymbol{x}} \end{bmatrix} = \begin{bmatrix} \boldsymbol{A} - \boldsymbol{b}\boldsymbol{k}^{\mathrm{T}} & \boldsymbol{b}\boldsymbol{k}^{\mathrm{T}} \\ \boldsymbol{0} & \boldsymbol{A} - \boldsymbol{l}\boldsymbol{c}^{\mathrm{T}} \end{bmatrix}\begin{bmatrix} \boldsymbol{x} \\ \tilde{\boldsymbol{x}} \end{bmatrix} + \begin{bmatrix} k_{\mathrm{r}}\boldsymbol{b} \\ \boldsymbol{0} \end{bmatrix} r$$

$$e = y - \hat{y} = \boldsymbol{c}^{\mathrm{T}}\tilde{\boldsymbol{x}} \tag{33}$$

Since the matrix on the right-hand side is block diagonal the characteristic equation of the closed loop system is

$$\det\left(s\boldsymbol{I}-\boldsymbol{A}+\boldsymbol{b}\boldsymbol{k}^{\mathrm{T}}\right)\det\left(s\boldsymbol{I}-\boldsymbol{A}+\boldsymbol{l}\boldsymbol{c}^{\mathrm{T}}\right)=\mathrm{R}(s)\mathrm{Q}(s) \tag{34}$$

This polynomial is the product of two terms: one which is used for the *SF* design and the other which is used for the observer design. In spite of (34) it is interesting to observe that Q(s) does not appear in the $T_{ry}(s)$ given by (22). The explanation of this phenomenon can be given by the investigation of the internal topology of the equivalent *TFR* forms of the *SFO* scheme.

4. Equivalent TFR Forms of the SFO Scheme

Introducing Figs. 3a-b the technique using equivalent *TFR* forms of *SF* has been discussed above. To get a more general procedure consider Figs. 3a-b again in the forms presented in Figs. 5a-b. It follows from Fig. 5 that the serial compensator R_s can be calculated by

$$R_{\mathrm{S}}=\frac{1}{1+R_{\mathrm{S}}P}=\frac{1}{1+K_kP}=\frac{\mathrm{A}(s)}{\mathrm{A}(s)+\mathrm{K}(s)}=\frac{\mathrm{A}(s)}{\mathrm{R}(s)} \tag{35}$$

Observe that this serial compensator cannot be applied for unstable processes because of the full pole cancellation in R_s, in spite the fact that k_rR_sP ensures the same overall transfer function T_{ry}. Finding the equivalent *TFR* form an auxiliary internal signal $\bar{x}$ is introduced and used (which is not equal to $\boldsymbol{x}$) indicating that finally both the *SF* and the observer use a *SISO* filter realizing their effect. The difference is that they use internal state variable vectors ($\boldsymbol{x},\hat{\boldsymbol{x}},\tilde{\boldsymbol{x}}$ etc.) instead of scalar ones. It is always possible to find input/output equivalence between these representations. Using this approach the general basic *SFO* scheme in Fig. 4 can be redrawn into another topology shown in Fig. 6.

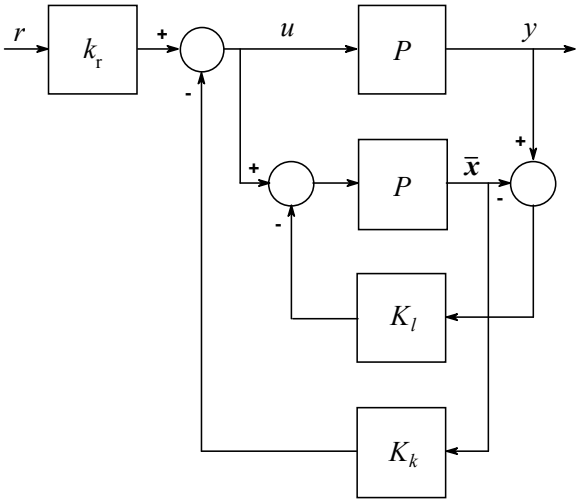

Figure 6. Equivalent topology of the general basic SFO scheme using TFR forms

After some long, but straightforward block manipulations the equivalent *SFO* scheme can be transformed into another unity feedback closed-loop form given in Fig. 7.

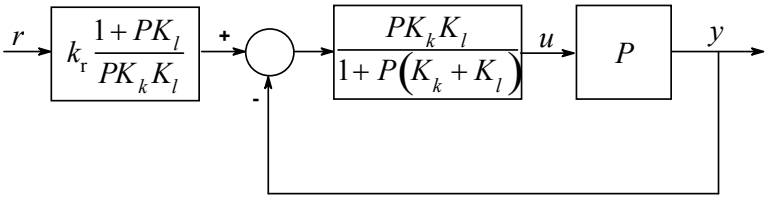

Figure 7. Reduced equivalent topology of the general basic SFO scheme

Here reasonably and in accordance with the previous discussions the following *TFR* forms are selected:

$$K_k(s)=\frac{\mathrm{K}(s)}{\mathrm{B}(s)} \qquad K_l(s)=\frac{\mathrm{L}(s)}{\mathrm{B}(s)} \tag{36}$$

where the pole-placement design goals for both the *SF* and the observer dynamics require

$$\mathrm{K}(s)=\mathrm{R}(s)-\mathrm{A}(s) \qquad \mathrm{L}(s)=\mathrm{Q}(s)-\mathrm{A}(s) \tag{37}$$

It is interesting to observe that the transfer function of the closed-loop in Fig. 7 has a very special structure

$$\frac{P^2K_kK_l}{1+P(K_k+K_l)+P^2K_kK_l}=\frac{PK_k}{1+PK_k}\frac{PK_l}{1+PK_l}=\frac{\mathrm{K}}{\mathrm{R}}\frac{\mathrm{L}}{\mathrm{Q}} \tag{38}$$

which is formally two simpler closed-loop cascaded, which dynamically completely corresponds to the characteristic equation (34). The overall transfer function of the *SFO* system is

$$T_{ry}(s)=k_r\frac{1+PK_l}{PK_kK_l}\frac{PK_k}{1+PK_k}\frac{PK_l}{1+PK_l}=\frac{k_rP}{1+PK_k}=\frac{k_r\mathrm{B}}{\mathrm{R}} \tag{39}$$

which is equal to (22) as expected: the poles introduced by the observer do not appear in the tracking dynamics of the *SFO* system. This behaviour can be well seen in Fig. 8.

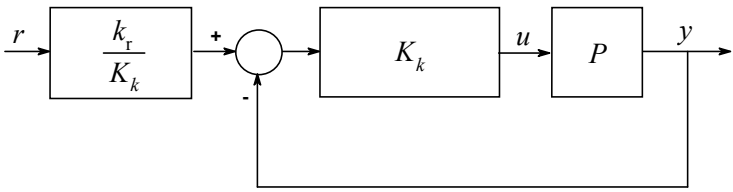

Figure 8. The overall tracking structure of the SFO scheme

5. Model Error Properties

The above widely applied methodology has a common problem, that in all regulator and observer equations the true process P is used instead of the estimated model $\hat{P}$ of the process. A logical notation should be if $\hat{\boldsymbol{A}}, \hat{\boldsymbol{b}}, \hat{\boldsymbol{c}}^T$, belonging to $\hat{P}$ is used instead of $\boldsymbol{A}, \boldsymbol{b}, \boldsymbol{c}^{\mathrm{T}}$, representing P. The equivalent *TFR* form of the *SF* using the model of the process is shown in Fig. 9.

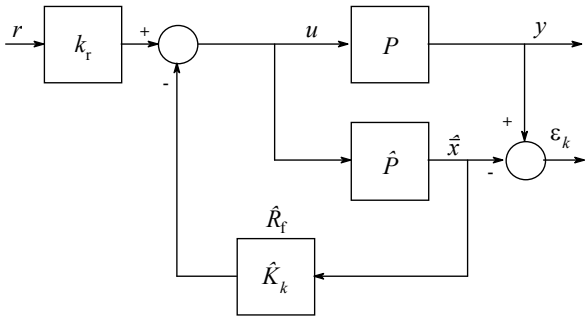

Figure 9. The model based SF scheme and error

In spite of the practical reality of this scheme a major drawback raises with the parallel model *TFR* of the *SF* method, because it cannot stabilize unstable plants. A model-based equivalent serial compensator (35) cannot provide stable operation with pole cancellation. The *SF* is operable if the exact states are available for feedback. So the parallel scheme in Fig. 9 is used only to compute the model error. Using (22) the model-based version of T_{ry} is

$$\hat{T}_{\mathrm{ry}} = \frac{k_{\mathrm{r}} P}{1 + K_k \hat{P}} = \frac{k_{\mathrm{r}} \mathrm{B}}{\mathrm{R}} \frac{\hat{\mathrm{A}}}{\mathrm{A}} = T_{\mathrm{ry}} \frac{\hat{\mathrm{A}}}{\mathrm{A}} \tag{40}$$

and its relative uncertainty

$$\ell_{\mathrm{T}} = \frac{\hat{T}_{\mathrm{ry}} - T_{\mathrm{ry}}}{\hat{T}_{\mathrm{ry}}} = \frac{\hat{\mathrm{A}} - \mathrm{A}}{\mathrm{A}} = \ell_{\mathrm{A}} \tag{41}$$

which shows that $\ell_{\mathrm{T}} = 0$ for $\ell_A = 0$. Introducing the additive $\Delta = P - \hat{P}$ and relative plant model error

$$\ell = \frac{\Delta}{\hat{P}} = \frac{P - \hat{P}}{\hat{P}} \tag{42}$$

the modelling error ε_k in Fig. 9 can be expressed as

$$\varepsilon_k = \frac{k_{\mathrm{r}} \hat{\mathrm{B}}}{\mathrm{R}} \ell r = T_{\mathrm{ry}} \frac{\hat{\mathrm{B}}}{\mathrm{B}} \ell r = \hat{P} \ell u \tag{43}$$

After some long but straightforward computations

$$\varepsilon_l = \frac{\hat{P}}{1+K_l\hat{P}}\ell\, u = \frac{\hat{\mathrm{B}}}{\mathrm{Q}}\ell\, u = \frac{1}{1+K_l\hat{P}}\varepsilon_k \tag{44}$$

is obtained. Equation (44) clearly shows the influence of the *SFO* scheme, because it decreases the modelling error ε_k by $(1+K_l\hat{P})$. Selecting fast observer poles, one can reach quite small "virtual" modelling error ε_l in the major frequency domains of the tracking task.

In spite of the above analysis the *SFO* scheme is widely applied in the practice with model-based *SVR*, so it is interesting how the model-based scheme in Fig. 10 influences the original modelling error ε_k.

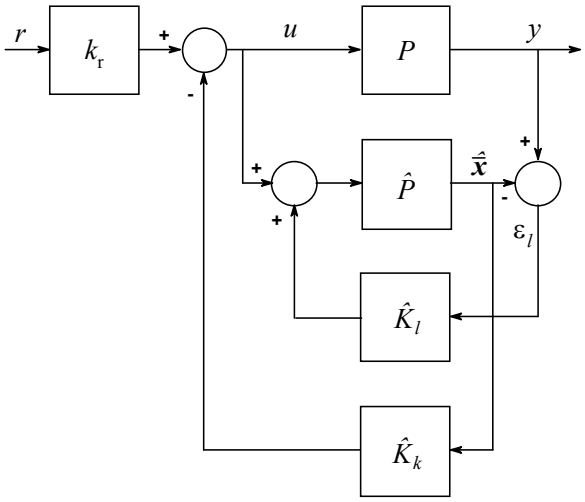

Figure 10. Model based SFO scheme with TFR forms

Besides the radical model error attenuating behaviour of the model-based *SFO* scheme, it has also a very important drawback, namely the nice cascade structure shown in (38) changes to

$$\frac{\hat{P}^2K_kK_l(1+\ell)}{1+\hat{P}(K_k+K_l)+\hat{P}^2K_kK_l(1+\ell)} \tag{45}$$

which form is not factorable. On the basis of Fig. 10 and (45) it is easy to see that the poles of the observer feedback loop remains unchanged using the placement design equation form model-based *SFO* (29). However, in this case the pole placement equation (11) is no longer valid. The only solution is to use the available model of the process, in this case $\hat{A}$, and

$$\hat{\boldsymbol{k}}_{\mathrm{c}}^{\mathrm{T}} = \left[p_1-\hat{a}_1, p_2-\hat{a}_2, \ldots, p_n-\hat{a}_n\right] \tag{46}$$

for the pole placing equation. Because this design ensures the required poles only for small ℓ (see (46), therefore a serious robust stability investigation is necessary first. Next it is important where the actual pole can be located for not zero ℓ, so how big is the performance loss coming from the model based *SFR*. These steps are usually neglected in most of the published papers, books and applications.

6. Observer Based Youla-Regulator

For open-loop stable processes the all realizable stabilizing (*ARS*) regulator is the *Youla-parametrized* one:

$$C = \frac{Q}{1 - QP} \tag{47}$$

where the "parameter" Q ranges over all proper ($Q(\omega = \infty)$ is finite), stable transfer functions [5], [6].

It is important to know that the *Y-parametrized* closed-loop with the *ARS* regulator is equivalent to the well-known form of the so-called *Internal Model Control* (*IMC*) principle [6] based structure shown in Fig. 11.

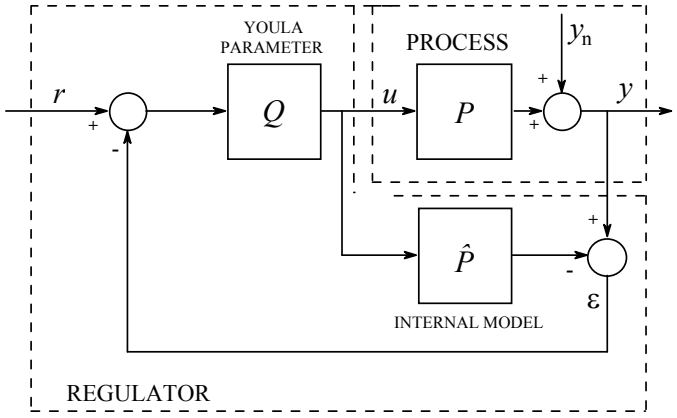

Figure 11. The equivalent IMC structure of an ARS regulator

Q is anyway the transfer function from r to u and the closed-loop transfer function (i.e., *CSF*) for $\hat{P} = P$

$$T_{ry} = \frac{CP}{1 + CP} = QP \tag{48}$$

is linear (and hence convex) in Q.

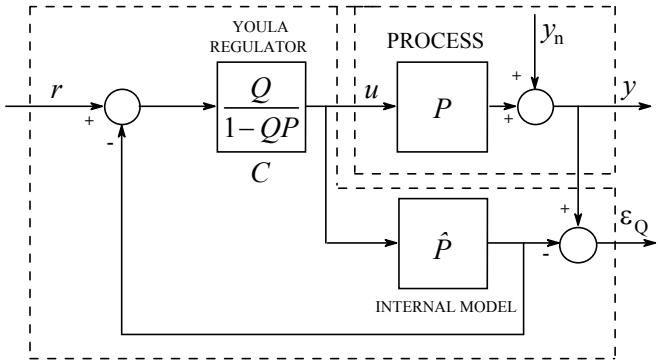

Figure 12. Another equivalent IMC structure

The equivalent *IMC* structure performs the feedback from the model error ε. It is possible to form another formally equivalent scheme (shown in Fig. 12), where the feedback is from the output of the internal model, similarly to the formerly presented *SFO* topology.

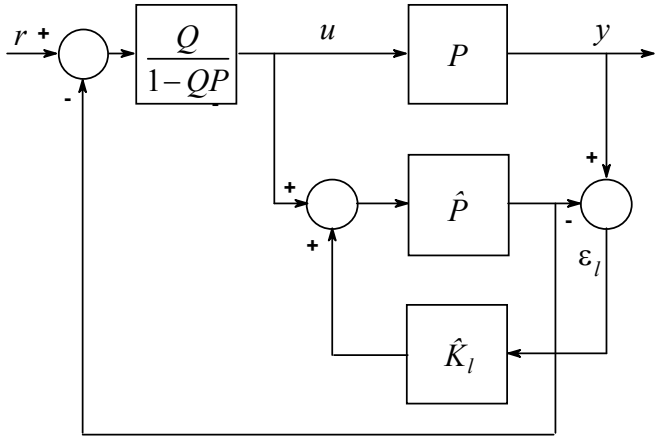

Figure 13. The observer-based Youla-regulator

It is easy to check that the same T_{ry} can be obtained for this structure in case of $\hat{P} = P$. The advantage of the last equivalent scheme is that it is possible to invent an observer-like feedback, similarly to Fig. 10 as Fig. 13 shows. After some long but straightforward computations

$$\varepsilon_l = \frac{1}{1+\hat{K}_l\hat{P}}\left(y - \hat{P}u\right) = \frac{1}{1+\hat{K}_l\hat{P}}\varepsilon_Q \tag{49}$$

is obtained. Equation (49) clearly shows the influence of the *SFO* scheme here, too, because it decreases the modelling error ε_Q by $(1+\hat{K}_l\hat{P})$. Selecting fast observer poles,

one can reach quite small "virtual" modelling error ε_l in the major frequency domains of the tracking task.

It is not difficult to prove by equivalent block manipulations that the simple closed-loop corresponding to the observer-base Youla-regulator has the structure shown in Fig. 14. This means that the introduction of the observer feedback changes the *Youla-parametrized* regulator to

$$C' = \frac{Q}{1 - Q\dfrac{\hat{P}}{1 + \hat{K}_l \hat{P}}} = \frac{Q}{1 - Q\hat{P}'} \tag{50}$$

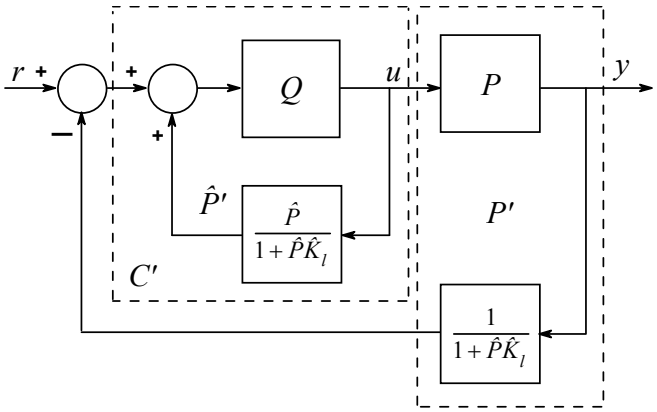

Figure 14 Equivalent closed-loop for the observer-based Youla-regulator

The form of C' shows that the regulator virtually controls a fictitious plant $\hat{P}'$, which is also demonstrated in Fig. 14. Here the fictitious plant is

$$\hat{P}' = \frac{\hat{P}}{1 + \hat{K}_l \hat{P}} \tag{51}$$

7. Conclusions

It was shown that the *SFO* methodology results in such a *TDOF* control system, which leaves the open-loop zeros untouched for the tracking properties and unfortunately the disturbance rejection (regulatory) properties can only be partly designed, because they are not independent of the tracking design.

The *TFR* of these classical methods are introduced to get a simple and useful tool to analyse and explain further behaviours, which are difficult to obtain using *SVR*. Using *TFR* it was shown, if the *SVR* used in the *SFO* scheme is model-based then the original (without observer) model error decreases by the sensitivity function of the observer feedback loop. This model error reducing capability gives the theoretical background of the success of practical model-based *SFO* applications.

Finally the *SFO* method was applied for the Youla *ARS* regulators opening a new class of methods for open-loop stable processes.

Acknowledgement

This work was supported in part by the Control Engineering Research Group of the Hungarian Academy of Science, at the Budapest University of Technology and Economics and by the project TAMOP 4.2.2.A-11/1/KONV-2012-2012, at the Széchenyi István University of Győr.

References

[1] Åström, K.J., Wittenmark, B.: *Computer controlled systems: theory and design*, Prentice-Hall, Englewood Cliffs, NJ, 1984

[2] Åström, K.J.: *Control System Design*, lecture notes, University of California, Santa Barbara, 2002

[3] Kailath, T.: *Linear Systems*, Prentice Hall, Englewood Cliffs, NJ, 1980

[4] Keviczky, L.: *Combined identification and control: another way*. Invited plenary paper, 5th IFAC Symposium on Adaptive Control and Signal Processing, ACASP'95, Budapest, Hungary, pp. 13-30, 1995

[5] Keviczky, L., Bányász, Cs.: *Iterative identification and control design using K-B parametrization*, In: Control of Complex Systems, Eds: Åström, K.J., Albertos, P., Blanke, M., Isidori, A., Schaufelberger W., Sanz, R., Springer, pp. 101-121, 2001

[6] Maciejowski, J.M.: *Multivariable Feedback Design*, Addison Wesley, Boston, 1989

Acta
Technica
Jaurinensis

Vol. 7., No. 1., pp. 62-70, 2014
DOI: 10.14513/actatechjaur.v7.n1.218
Available online at acta.sze.hu

Extractive Spectrophotometric Determination of Samarium with Chlorophosphonazo III

J. Uhrovčík, J. Lesný

University of SS. Cyril and Methodius in Trnava
Department of Ecochemistry and Radioecology
Nám. J. Herdu 2, SK-91701, Trnava, The Slovak Republic
E-mail: jozef.uhrovcik@ucm.sk

Abstract: A rapid and sensitive extractive spectrophotometric method has been developed for the determination of samarium using 0.04% Chlorophosphonazo III in 1 mol L^{-1} hydrochloric acid media after extraction into isoamylalcohol. Absorbance was measured in 1-cm cell and the complex has a sensitive absorption peak at 667 nm. The complex of Sm(III)-Chlorophosphonazo III is formed instantly in organic phase and remains stable at least for 2 hours with constant absorbance under normal laboratory conditions. Validity of Beer's law was verified in range 0–10 µg Sm(III) per 10 mL of the organic phase with an estimated molar absorptivity $\varepsilon_{667} \sim 1.14\ 10^5$ mol^{-1} L^{-1} cm^{-1}. Limit of detection (3-σ approach) reached 0.22 µg Sm(III). Some foreign cations interference in samarium determination has been checked. The method has been applied on spiked sample of mineral water. Obtained results of apparent recovery were found in very good agreement with acceptable range. The percent relative standard deviation for repeatability was less than ±5 % (n = 3).

Keywords: samarium, Chlorophosphonazo III, spectrophotometry, extraction, iso-amylalcohol

1. Introduction

Besides its industrial applications samarium is used first of all in microelectronics as dopant and in optics. Samarium(III) occurs in nature in the Earth's crust in the form of the mineral monazite with different proportions and it is followed by uranium, thorium and other lanthanides. Determination of samarium is a specific analytical problem due to its chemical similarity to the other rare earth metals and uranium. Therefore, high precision and low detection limit are required for samarium determination in most of real samples. Samarium is exclusively determined by inductively coupled plasma with mass spectrometry (ICP-MS) and inductively coupled plasma with atomic emission spectrometry methods [6,12]. However, spectrophotometric determination represents suitable and relatively cheap alternative in comparison with above mentioned methods. The application of organic reagents for spectrophotometric determination of samarium is well known. Chlorophosphonazo III (Fig. 1) belongs to azo-dyes based on

chromotropic acids. It is commercially available and soluble in water and diluted acids. The reagent has ability to form stable chelates and can work in strongly acidic medium eliminating the chances of partial hydrolysis of metal ions to be determined. Its analytical properties were described for the first time by soviet research group led by Alexander Nemodruk [9].

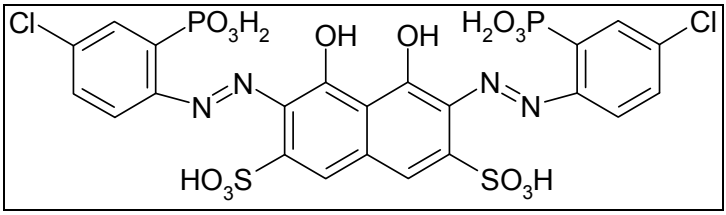

Figure 1. Structure of Chlorophosphonazo III.

Chlorophosphonazo III is a complexing reagent primarily suggested for the spectrophotometric determination of lanthanides [3-5], actinides [1, 11] and alkaline earth metals [10,17]. The utilization of Chlorophosphonazo III as a complexing reagent for spectrophotometric determination of various elements was markedly preferred in the 1960s and 70s. The reagent has valuable advantages such as an excellent time stability of the absorbance and a relatively wide linear range, while the major disadvantage is its rather high price. Chlorophosphonazo III still has a justified place among the complexing agents utilized in trace analysis and the interest in its analytical applications significantly grows in recent years. The first use of Chlorophosphonazo III for extractive spectrophotometric determination of samarium and other lanthanides from media of diluted hydrochloric acid into organic solvent has been published by Taketatsu and co-workers [14]. The extraction of Sm(III)-Chlorophosphonazo III complex led to an increase of selectivity and sensitivity of the relevant determination. Similar effect was observed at extractive spectrophotometric determination of thorium with Chlorophosphonazo III into isoamylalcohol [16]. While the successful applicability of Chlorophosphonazo III for spectrophotometric quantification of samarium in different matrices is indisputable, the number of works dealing with detailed evaluation of particular determinations by means of Chlorophosphonazo III with extraction into organic solvents is surprisingly limited [15]. The presented study is devoted to evaluation of important validation parameters for extractive spectrophotometric determination of samarium using Chlorophosphonazo III with extraction of formed complex into isoamylalcohol.

2. Experimental

2.1. Reagents

All used reagents were of analytical grade and all solutions were prepared in deionised water. Samarium stock solution with concentration 10 µg mL^{-1} was prepared by appropriate dilution of standard solution (Fluka Analytical, Austria) and it was stabilized with addition of concentrated nitric acid (Merck, Germany). The concentration of solution of the Chlorophosphonazo III (Dojindo Laboratories, Japan) was 0.04% (w./v.). The medium of measured solutions has been adjusted by addition of

concentrated hydrochloric acid (Mikrochem, Slovakia). The foreign ions stock solutions were prepared by dilution of their standard solutions (Fluka Analytical, Austria). Isoamylalcohol (Panreac Química, Spain) was used for the extraction of formed Sm(III)-Chlorophosphonazo III complex.

2.2. Apparatus

All absorbance measurements were performed using the Cary WinUV 50 (Varian Inc., Australia) double-beam spectrophotometer equipped with 1-cm quartz cells. Every point of calibration curve was measured for five times and the average values were taken into account in next calculations. Laboratory centrifuge Universal 320R (Hettich, Germany) was used for removing of droplets of water from organic phase. Deionised water with specific conductivity < 0.054 μS cm^{-1} was prepared by means of ultrapure water system Millipore Simplicity 185 (Millipore, Germany).

2.3. Recommended procedure

Place a sample containing 0 – 10 μg of samarium in a 100 mL Squibb-type separatory funnel. Adjust the aqueous phase to 1 mol L^{-1} with appropriate addition of concentrated hydrochloric acid. Add 1.5 mL of aqueous 0.04 % Chlorophosphonazo III solution and mix. Add exactly 10 mL of isoamylalcohol and shake for 2 minutes. Remove aqueous phase and treat the organic phase by centrifugation (4500 rpm, 5 minutes). Measure the absorbance of the clear organic phase at 667 nm against a reagent blank as a reference. Obtain the samarium quantity from a calibration curve by method of external calibration. In case of matrix effect is necessary to apply the method of standard addition. After equilibration, the volume of the organic phase decreased due to the slight solubility of isoamylalcohol in water. In order to avoid the use of volume change correction is advantageous to consider absolute amount of samarium (m_0) instead the molar or mass concentration in all next calculations.

2.4. Real sample analysis

To assess the applicability of the presented method, mineral water sample was analyzed from the brook “Brusnianka” using the recommended procedure. The sample was spiked with different known amounts of samarium.

3. Results and discussion

The most important chemical variables were assessed to obtain the highest sensitivity for the determination of samarium. Sm(III)-Chlorophosphonazo III complex in isoamylalcohol showed two absorption peaks, namely at 616 nm and 667 nm (Fig. 2). Due to the higher value of analytical signal and favourable value of background absorption (dashed line) the latter wavelength was selected.

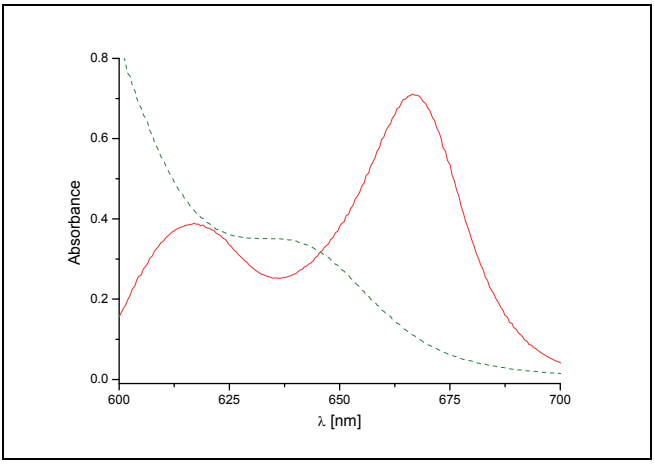

Figure 2. Absorption spectrum of Sm(III)–Chlorophosphonazo III complex against a reagent blank. m_0 Sm(III) = 10 μg; c(HCl) = 1 mol L^{-1}; V(Chlorophosphonazo III) = 1 mL.

3.1. The effect of acidity

As shown in Figure 3, absorbance of samarium complex in the organic phase reached the maximal value at hydrochloric acid concentration of 0.5 mol L^{-1}, but at this concentration of acid remained some Chlorophosphonazo III in aqueous phase. For this reason 1 mol L^{-1} hydrochloric acid was used in further investigations.

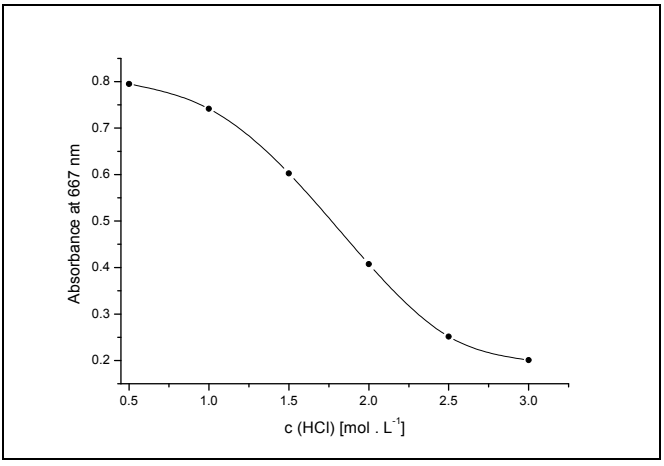

Figure 3. Effect of acidity of aqueous phase on absorbance of organic phase. m_0 Sm(III) = 10 μg; V(Chlorophosphonazo III) = 1 mL.

3.2. The effect of amount Chlorophosphonazo III

In the Fig. 4 is showed that absorbance of organic phase is almost constant when 1.4 mL of complexing agent solution is added into aqueous phase. For convenience, the volume of 1.5 mL of 0.04 % Chlorophosphonazo III solution was used for subsequent measurements.

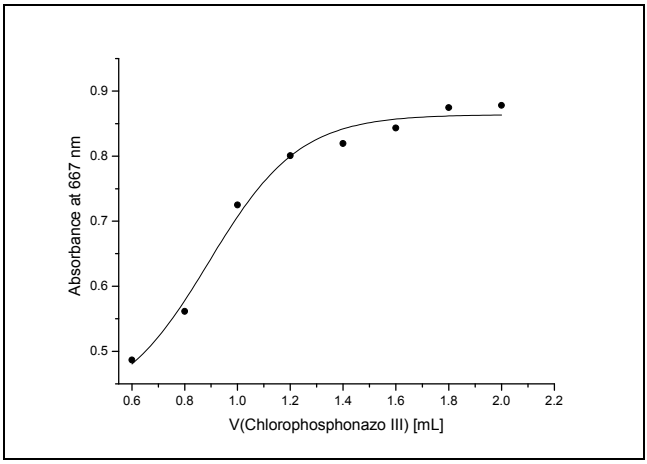

Figure 4. Effect of added volume of Chlorophosphonazo III on the absorbance of organic phase. m_0 Sm(III) = 10 μg; c(HCl) = 1 mol L^{-1}.

3.3. Shaking and recovery

The degree of extraction of Sm(III)-Chlorophosphonazo III into isoamylalcohol was examined by the following experiment: 10 μg of samarium was extracted according to the recommended procedure and samarium remaining in the aqueous phase was examined by adding another Chlorophosphonazo III solution, extracting with 10 mL of the organic solvent and measuring the absorbance of the organic phase. It was confirmed that extraction is quantitative in two steps and the degree of extraction in the first step is ~ 90 %, but this finding is not critical for analytical application of suggested method. Extraction of samarium complex is very rapid. Shaking for 30 seconds was enough to attain equilibrium when the complexing agent was added to the aqueous phase and shaked with addition of isoamylalcohol.

The validity of Beer's law was established from 0 to 10 μg of samarium in organic phase by application of recommended procedure (Figure 5). Calculated equation of regression reached value: $A = 0.77 \pm 0.001\, m_0 + 0.007$ (data in parentheses represent uncertainty of parameters). Coefficient of determination had value $R^2 = 0.9990$. Value of molar absorptivity was estimated from equation of regression $\varepsilon_{667} \sim 1.14\ 10^5$ mol^{-1} L^1 cm^{-1}. It was not revealed presence of any constant systematic error(s) by application of Student *t*-test (significance level $\alpha = 0.05$).

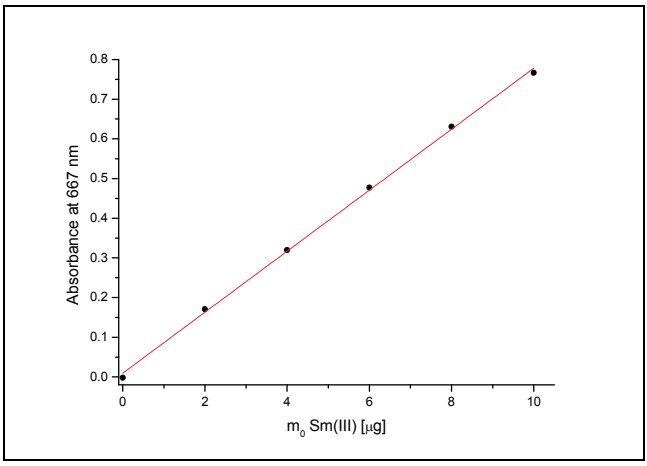

Figure 5 Absorbance of Sm(III)-Chlorophosphonazo III complex as a function of samarium absolute amount against a reagent blank.

The values of limit of detection (LOD) and limit of quantification (LOQ) were calculated by 3-σ and 10-σ approach [2] and ULA2 approach [8] as well. In the case of computation by 3-σ and 10-σ approach residual standard deviation ($s_{y/x}$), standard deviation of *y*-intercept (s_b) and standard deviation of blank (s_{blank}) were applied [7]. Results of calculations are given in Table 1.

Table 1. LOD and LOQ values calculated by using two different approaches.

3-σ and 10-σ approach			***ULA2 approach***	
$\mathbf{s_{blank}}$ †	LOD [μg]	0.22	LOD ($\alpha = 0.05$) [μg]	0.34
	LOQ [μg]	0.72	LOQ ($\alpha = 0.05$) [μg]	1.03
$\mathbf{s_{y/x}}$	LOD [μg]	0.39	LOD ($\alpha = 0.01$) [μg]	0.61
	LOQ [μg]	1.31	LOQ ($\alpha = 0.01$) [μg]	1.82
$\mathbf{s_b}$	LOD [μg]	0.28	†10 blank determinations	
	LOQ [μg]	0.95		

Reference measurement of samarium content in the mineral water sample was carried out by ICP-MS method in accredited laboratory of the State Geological Institute of Dionýz Štúr in Spišská Nová Ves (Slovakia). Reference concentration value of samarium was 3 ng · L^{-1}. So on the basis of this finding, mineral water sample can be considered a suitable model for potential matrix effect study. For this reason the sample of mineral water was spiked with 2; 5 and 7 μg of samarium and then analyzed according to recommended procedure. Results for obtained apparent recovery and repeatability are shown in Table 2.

Table 2. Obtained data for repeatability and trueness of measurement (n=3).

m_0 Sm(III) [μg]	apparent recovery [%]	relative standard deviation [%]
2	100.2	±5.2
5	101.6	±1.8
7	98.8	±1.4

Absence or presence of matrix effect was established by the second independent technique, namely by method of standard addition. On the basis of obtained results it may be concluded that influence of matrix effect on the trueness of determination was not confirmed at this type of sample.

The optical density of measured complexes was found constant at least for 2 hours under normal laboratory conditions within the linear range of the proposed method (temperature 22°C).

The influence of some potentially interfering ions was checked and their impact is summarized in Table 3. Three replicate determinations were carried out for each interfering ion.

Table 3. Effect of chosen cations on samarium determination with Chlorophosphonazo III after extraction into organic solvent. m_0 Sm(III) = 5 μg.

foreign ion	deviation [%]
Ca(II)[(a)] (*1:100*)	+1.4
Fe(III)[(a)] (*1:30*)	+3.4
Eu(III)[(b)] (*10:1*)	+39.9
La(III)[(b)] (*10:1*)	+3.8
Mg(II)[(a)] (*1:100*)	+2.4
Th(IV)[(b)] (*10:1*)	+10.1
U(VI)[(b)] (*1:1*)	+38.5

[(a)]as nitrate [(b)]as chloride

The average value of three replicate Sm(III) Chlorophosphonazo III absorbances (not containing foreign ions) was taken into account as a reference value. Mass ratio between Sm(III) and given interfering ion is listed in the Table 3. The target analyte can be effective separated from most of interfering ions by means of convenient type of cation-exchange resin, for example AG50W-X8 (BioRad, Germany) [13].

4. Conclusions

A rapid and sensitive extractive spectrophotometric method was developed for samarium determination using 0.04% Chlorophosphonazo III in diluted hydrochloric acid. The gained complex exhibited two absorption peaks, namely at 616 nm and 667 nm, respectively, from which the latest one was a set for all subsequent measurements. The relevant complex remained under laboratory conditions stable at least for 2 hours maintaining the constant value of absorbance. Beer's law obeyed in the range from 0 to 10 μg per 10 mL of organic phase. Only U(VI), Th(VI)

and Eu(III) interfered seriously in model solutions and the presence of above mentioned cations led to a significant increase of absorbance. The application of the investigated method for mineral water sample analysis shows favourable results concerning trueness and repeatability. However, its utilization for determination of the target analyte in very complex matrices containing significant quantity of interferences will require implementation of appropriate separation procedures. Due to the fact that the concentration of samarium in most of real matrices is negligible, it is necessary to include the suitable types of preconcentration techniques into analytical cycle.

References

[1] Bykhovtsova, T. T., Tserkovnitskaya, I. A.: *Photometric determination of uranium(VI) by means Chlorophosphonazo III in organic solutions after the extraction separation of uranium by means of trialkylamines*, Zhurnal Analiticheskoi Khimii, vol. 32, no. 5, pp. 745-750, 1977

[2] Currie, L. A.: *Nomenclature in evaluation of analytical methods including detection and quantification capabilities. IUPAC Recommendations*, Pure and Applied Chemistry, vol. 67, no. 10, pp. 1699-1723, 1995
DOI: 10.1351/pac199567101699

[3] Dedkova, V., Shvoeva, O., Savvin, S.: *Sorption-spectrophotometric determination of lanthanum, gadolinium, and ytterbium using chlorophosphonazo III on a PANF-Chel adsorbent*, Journal of Analytical Chemistry, vol. 66, no. 10, pp. 937-940, 2011
DOI: 10.1134/S1061934811080089

[4] Gajduk, O. V., Pantaler, R. P., Blank, A. B.: *Spectrophotometric determination of cerium in the presence of Ca, Sr, and Al*, Zavodskaya Laboratoryia, vol. 73, no.3, pp. 15-18, 2007

[5] Ivanov, V. N., Ermakova, N. V.: *Sorption of Lanthanum, Terbium, and Erbium Complexes of Some Mono- and Bisazoderivatives of Chromotropic Acid in the Presence of Surfactants*, Journal of Analytical Chemistry, vol. 18, no. 3, pp. 217-224, 2003
DOI: 10.1023/A:1022678202473

[6] Li, B., Sun, Y., Yin , J.: *Determination of cerium, neodymium and samarium in biological materials at low levels by isotope dilution inductively coupled plasma mass spectrometry*, Journal of Analytical Atomic Spectrometry, vol. 14, no. 12, pp. 1843-1848, 1999
DOI: 10.1039/A905346H

[7] Miller, J. N., Miller, J. CH.: *Statistics and Chemometrics for Analytical Chemistry*, Ellison Horwood, Chichester, 2005

[8] Mocák, J., Bond, A. M., Mitchell, S., Scollary, G.: *A statistical overview of standard (IUPAC and ACS) and new procedures for determining the limits of detection and quantification: Application to voltammetric and stripping techniques,* Pure and Applied Chemistry, vol. 69, no. 2, pp. 297-328, 1997
DOI: 10.1351/pac199769020297

[9] Nemodruk, A. A., Novikov, Y. P., Lukin, A. M., Kalinina I. D.: *2,7-Bis-(4-Chloro-2-phosphonbenzene-azo)-1,8-dihydroxynapthalene-3,6-disulphonic acid (ChlorophosphonazoIII). A new reagent for the photometric determination of uranium,* Zhurnal Analiticheskoi Khimii*,* vol. 16, pp. 180-184, 1961.

[10] Noda, K., Sato, Y., Miura, T., Katayama, K., Kojima, R.: *Development of novel measurement assay for calcium in serum by the chlorophosphonazo-III vanadate method*, Annals of Clinical Biochemistry, vol., 47, no. 5, pp. 440-446, 2010 DOI: 10.1258/acb.2010.010013

[11] Oguma, K., Suzuki, T., Saito, K.: *Determination of uranium in seawater by flow-injection preconcentration on dodecylamidoxime-impregnated resin and spectrophotometric detection*, Talanta, vol., 84, no. 5, pp. 1209-1214, 2011 DOI: 10.1016/j.talanta.2010.12.020

[12] Paama, L., Pämoja, E., Must, M., Perämäki, P.: *Optimal conditions for europium and samarium determination in cathodoluminophors by inductively coupled plasma atomic emission spectrometry*, Journal of Analytical Atomic Spectrometry, vol. 16, no. 11, pp. 1333-1336, 2001 DOI: 10.1039/B105520H

[13] Strelow, F. W. E.: *Quantitative separation of lanthanides and scandium from barium, strontium and other elements by cation-exchange chromatography in nitric acid*, Analytica Chimica Acta, vol. 20, pp. 249-254, 1980 DOI: 10.1016/S0003-2670(01)84368-3

[14] Taketatsu, T., Kaneko, M., Kono, N.: *Solvent extraction-spectrophotometric determination of rare earths with chlorophosphonazo-III,* Talanta, vol. 21, no. 1, pp. 87-91, 1974 DOI: 10.1016/0039-9140(74)80065-2

[15] Vilímec, J., Jakubec, K.: *Direct spectrophotometric determination of rare earths in organic extracts with chlorophosphonazo III*, Microchemical Journal, vol. 35, no. 3, pp. 325-327, 1987 DOI: 10.1016/0026-265X(87)90118-4

[16] Yamamoto, T.: *Extraction-photometric determination of thorium with chlorophosphonazo-III*, Analytica Chimcia Acta, vol. 63, no. 1, pp. 65-70, 1973 DOI: 10.1016/S0003-2670(01)82174-7

[17] Zenki, M., Masutani, T., Yokoyama, T.: *Repetitive determination of calcium ion and regeneration of a chromogenic reagent using Chlorophosphonazo III and an ion exchanger in a circulatory flow injection system*, Analytical Sciences, vol. 18, no. 10, pp. 1137-1140, 2002 DOI: 10.2116/analsci.18.1137

Acta
Technica
Jaurinensis

Vol. 7., No.1., pp. 71-86, 2014
DOI: 10.14513/actatechjaur.v7.n1.253
Available online at acta.sze.hu

Examination of the effect of sensor properties on the secondary battery model in simulation environment

I. Lakatos[1], P. Kőrös [2], F. Hajdu[3]

[1] Széchenyi István University, Department of Automotive and Railway Engineering
Egyetem tér 1., 9026 Győr, HUNGARY
E-mail: lakatos@sze.hu

[2, 3] Széchenyi István University, Department of Mechatronics and Machine Designes
Egyetem tér 1., 9026 Győr, HUNGARY
E-mail: korosp@sze.hu, hajdfl@sze.hu

Abstract: The aim of the presented method is to develop a simulation environment which is able to handle diagnostic tools of electric vehicles. Steps of forming the simulation environment are described in the article. Implementation of real sensors is not dealt with. The structure of a modular and easily adaptable testing approach is explained.

Keywords: drivetrain, battery, simulation

1. Introduction

Numerous software vendors and research teams work on development of vehicle simulation programmes these days. There are several possibilities for us to use this kind of software at our university. During our research, AVL CRUISE is used for drivetrain simulation while IPG Carmaker is used for calculations in vehicle dynamics. Our own tested and inserted models were prepared in MATLAB and Simulink programming environment.

The vehicle modelled and presented below is the car developed and built in 2013 by SZENERGY Team of our University. (Fig. 1.) This car participated in the Shell Eco Marathon race. The reason why we chose this vehicle as the object of our research is the availability of simulation parameters even from its design phase. At the same time, the model can be validated with the help of the existing vehicle. Whereas the control unit built in the vehicle enables measurements of the data needed for validation.

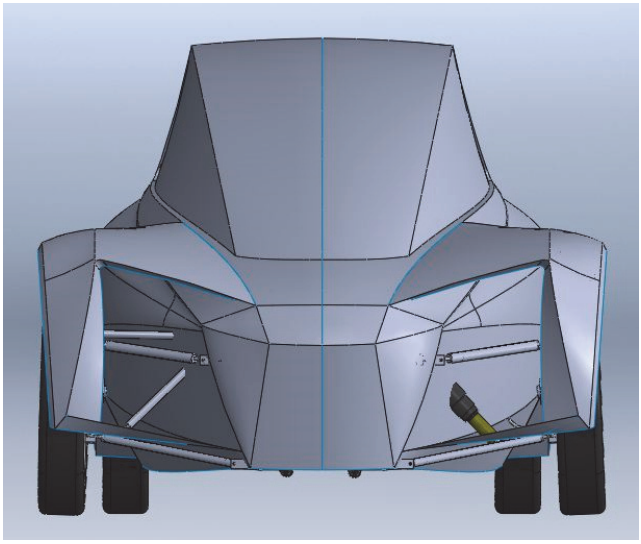

Figure 1. CAD model of the 2013 SZENERGY vehicle

2. Elaboration of the Carmaker model

As the first step, the Carmaker programme model was established based on the CAD models. The AVL Cruise simulation can be attached directly to the Carmaker model. Parameters that cannot be measured easily (like the drag coefficient for instance) were determined by means of a simulation program.

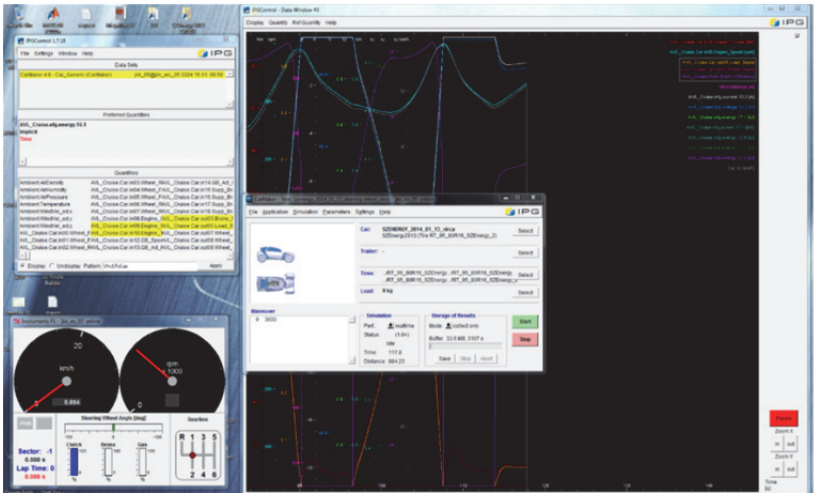

Figure 2. IPG Carmaker simulation program for vehicle dynamics

Characteristics of the PMSM with the given controller were measured on test bench. This was used as a basis for building the drivetrain model.

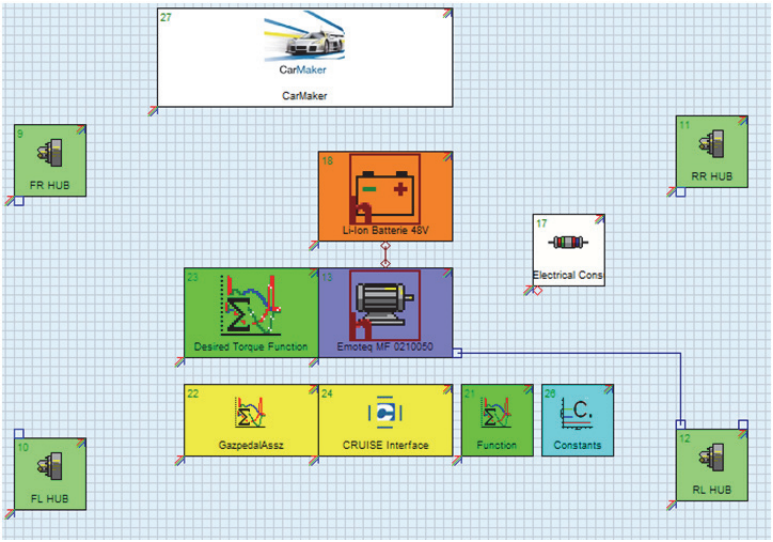

Figure 3. AVL CRUISE drivetrain model

The battery model to be tested was realised as a Simulink model.

3. The battery model established

The chosen model is built according to Chen and Rincón-Mora's [1], and Knauff's [2] method. In reference [3], the selection of the modelling principle and the properties of similar models are described in detail. The main characteristics of the model built by ourselves are the following:

- internal resistance and open circuit voltage (Uoc) are the function of the state of charge (SOC),
- the model is empirical, its parameters are determined by measurements,
- applicable to any battery, only the coefficient values change,
- heating effect, ageing and the number of cycles are not dealt with,
- input characteristics of the model: load current,
- output characteristics of the model: voltage, obtained energy, SOC, efficiency
- parameters: capacitance, number of series and parallel cells, maximum and minimum permissible voltage,
- voltage has to be between the given maximum and minimum values,
- in order to easier handling, the parameters were at first given with the help of a Matlab script which can be easily modified any time.

Differential equations (1) to (2) [2] which describe the operation of the model:

$$\dot{x} = \begin{bmatrix} 0 & 0 & 0 \\ 0 & -(R_{TS}C_{TS})^{-1} & 0 \\ 0 & 0 & (R_{TL}C_{TL})^{-1} \end{bmatrix} x + \begin{bmatrix} -C_{CAP}{}^{-1} \\ -C_{TS}{}^{-1} \\ -C_{TL}{}^{-1} \end{bmatrix} i \quad (1)$$

$$u = g(x_1) + x_2 + x_3 + R_s u \quad (2)$$

Within the equation, R_{ts}, C_{ts}, R_{tl} and C_{tl} are the capacitances and resistances of the transient RC circuits, C_{cap} is the total capacitance of the battery, R_s stands for the internal resistance, g(x) describes the non-linear relationship between *SOC* (state of charge) and open circuit voltage (U_{OC}). State vector *x* is the output voltage of the RC circuits. Input *i* stands for the current entering the battery, output *u* stands for the voltage between the battery terminals. The developed battery model is shown in Fig. 4.

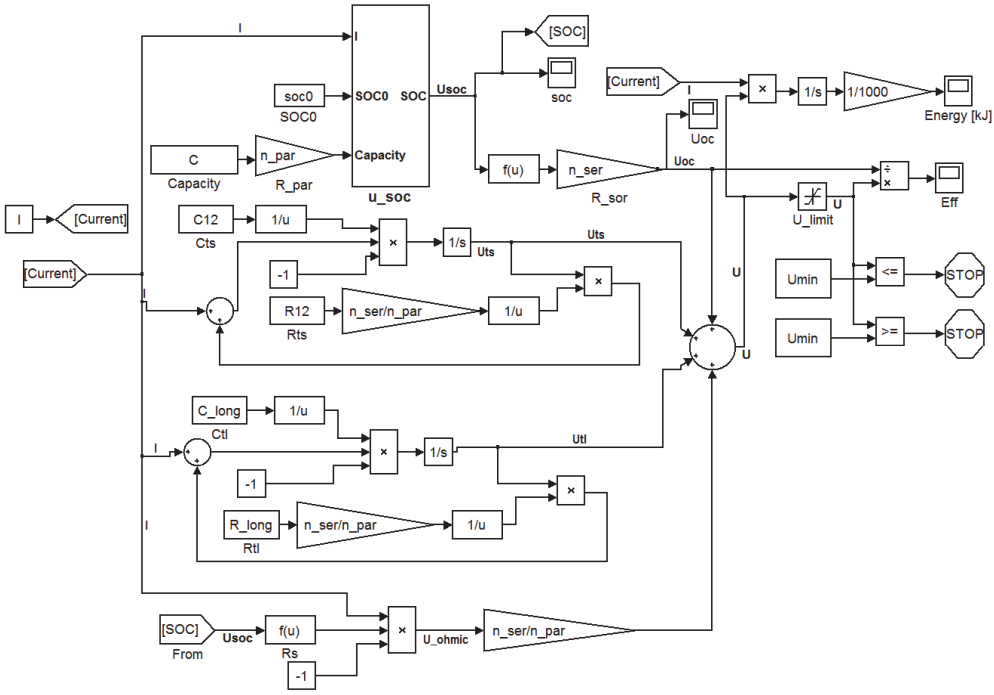

Figure 4. Battery model developed by ourselves

Since each parameter is the function of SOC, a sub-system for SOC modelling was created in order to simplify usability. The output value of the sub-system is a number between 0 and 1. The change of parameters is given as a function of this value, with the help of a function block. The equation (3) [2] which describes how the SOC block works:

$$u_{soc}(t) = u_{soc}(0) - \frac{1}{C_{CAP}} \int_0^t i(\tau) d\tau \tag{3}$$

Block diagram of the SOC sub-system is shown in Figure 5:

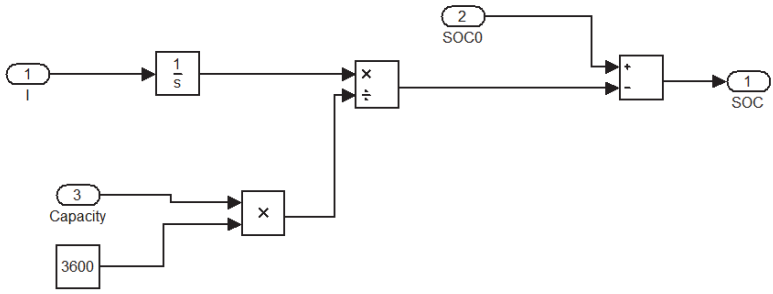

Figure 5. Modelling of SOC

The value of capacitance should be given in Ah and Simulink converts it into Coulomb according to formula (4):

$$C_{CAP}[C] = 3600 C_{CAP}[Ah] \tag{4}$$

Parameters used by the model were taken in the first run from reference [1]. Later on, however, the parameters can be determined for the given battery type by means of own measurements.

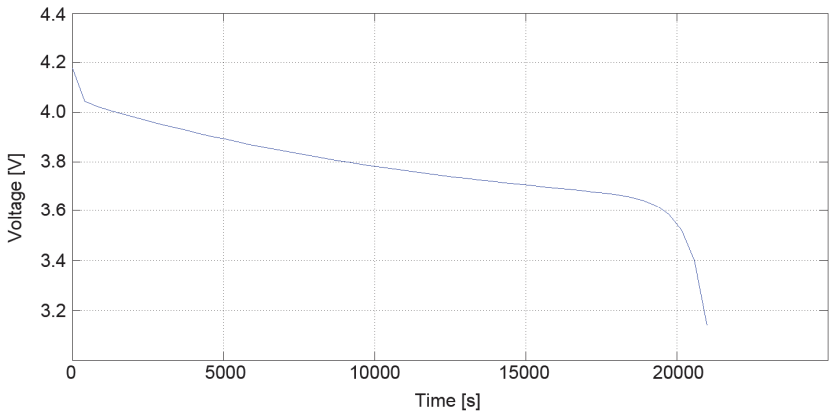

Figure 6. Voltage-time diagram of the initial battery model (discharging with 0.1C current)

3.1. Defining parameters with the help of measurements

In the model, the relationship between Uoc-SOC and resistance-SOC were determined by means of curve fitting based on measurements.

There are several methods available for determining the U_{OC}-SOC diagram [4], [6]. Open circuit voltage-time diagram is shown in Fig. 7.

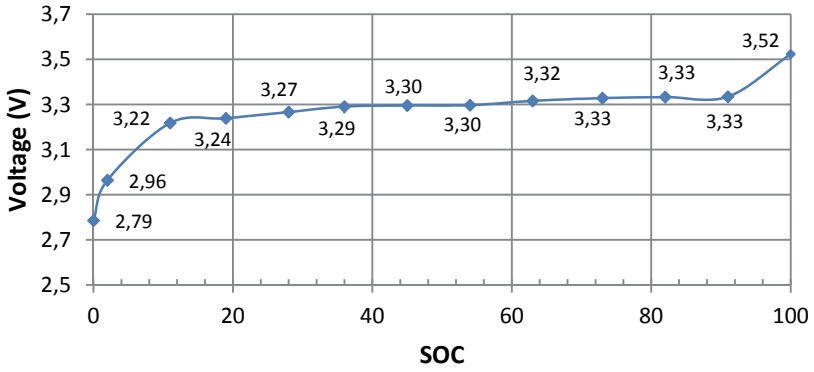

Figure 7. Open circuit voltage- SOC diagram of Thundersky 40 Ah battery (own measurement)

The curve was fitted by means of Matlab Curve Fitting Toolbox. The function used for approximation:

$$V_{OC}(SOC) = \frac{(a+b\cdot SOC+c\cdot SOC^2)}{(d+e\cdot SOC+f\cdot SOC^2)} \tag{5}$$

Approximation was done on one hand with basic Matlab Trust-region algorithm, on the other with Levenberg-Marquart algorithm. Fig. 8. shows that the approximation with Trust-region algorithm is not accurate enough, therefore, Levenberg-Marquart algorithm was selected for use.

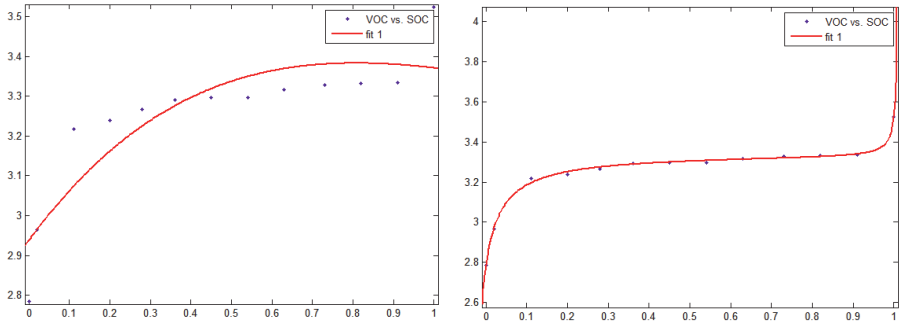

Figure 8. Fitted curve with Trust-region (to the left) and Levenberg-Marquardt (to the right) algorithm

Formula (5) is applicable to any battery type, only the coefficients will change. Therefore, the variables for the simulations were given with the help of Matlab script.

Abu-Sharkh's and Doerffel's measurements were used as the bases for defining the rest of the parameter values [5]. The circuit diagram which we used for determining the parameters can be seen in Fig. 9.

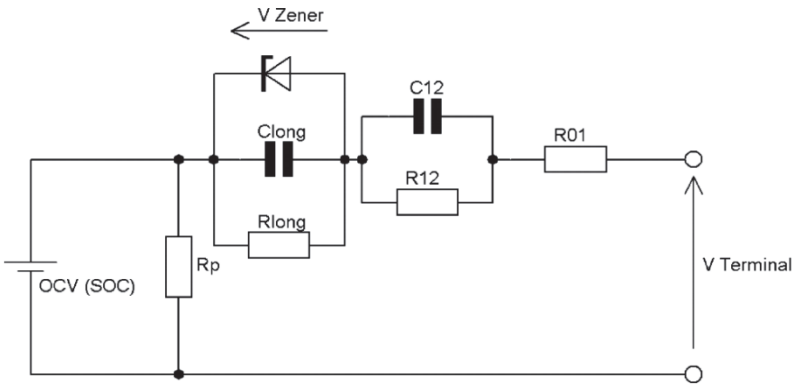

Figure 9 Circuit diagram of the battery model [5]

Symbols in Fig. 9:

- OCV (U_{OC}): open circuit voltage,
- R_p: self discharge resistance,
- R_{01}: ohmic resistance of the cell,
- R_{long}-C_{long} circuit: describes the behaviour of the battery at low currents, like small standby load and equalising currents,
- R_{12}-C_{12} circuit: determines the dynamic behaviour of the battery, for example at sudden high loads (when vehicle accelerates or brakes).

Among the parameters, the value of U_{OC}, R_{01} and R_{12} can be determined by this measurement.

Two charge-discharge cycles should be run during the test:

- The first cycle is needed for bringing the battery into the appropriate condition (conditioning cycle).
- While the second one is for determining the parameters of the battery.

There should be a one hour break between charge and discharge cycles in order to maintain the equilibrium potential. During the second cycle, one minute breaks should be held after each 2mV change. The process of the measurement is shown in Fig. 10.

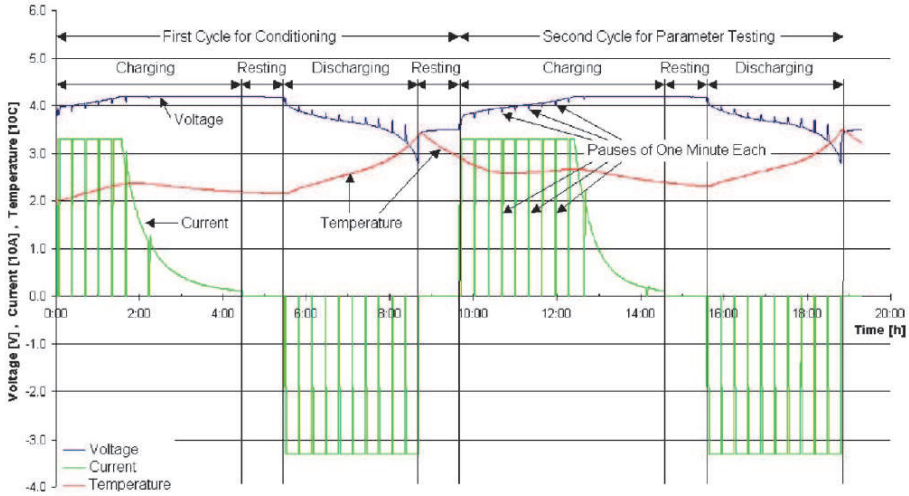

Figure 10. Characteristics of the measurement [5]

As a result of the one minute breaks, the voltage starts to recover. R_{01} and R_{12} values can be calculated from the recovery phenomenon. Voltage data needed for calculation are shown in Fig. 11.

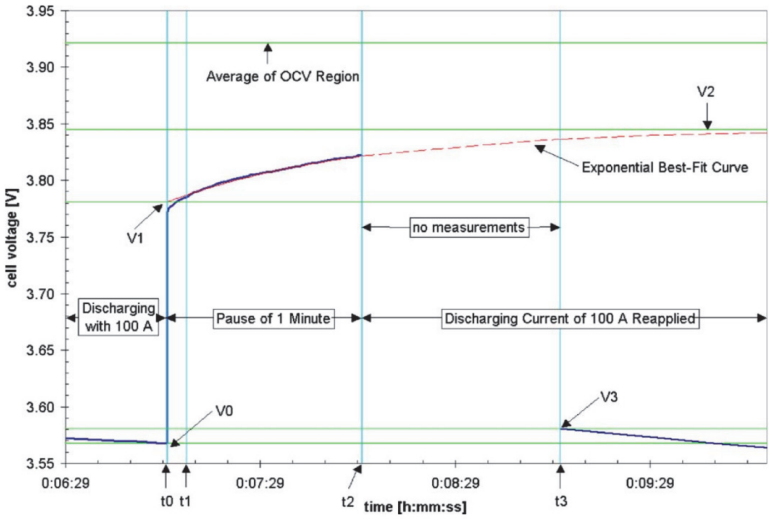

Figure 11.Voltage diagram to estimate the parameters [5]

$$R_{01} = \frac{V_1 - V_0}{|I|},\ R_{12} = \frac{V_2 - V_1}{|I|}$$

Internal resistance (R_{01})-SOC diagram measured by ourselves, shown in Fig. 12.

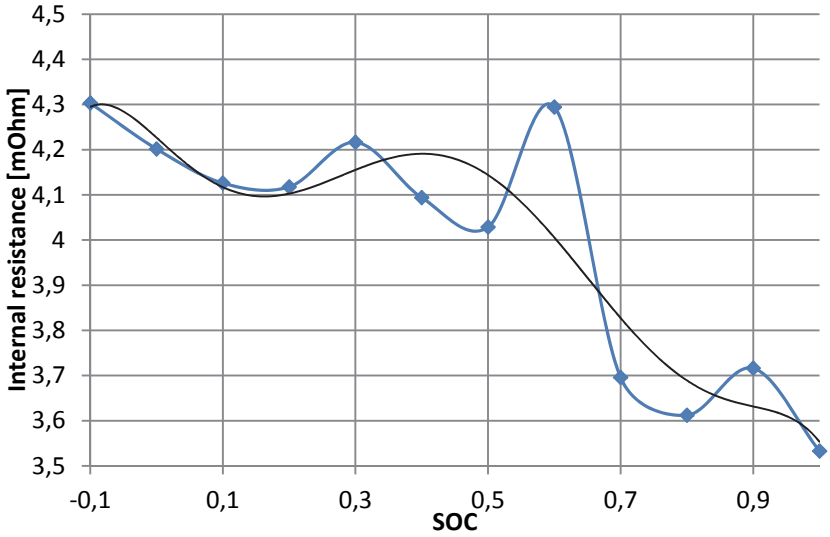

Figure 12. Internal resistance as a function of SOC (own measurement)

Similarly to the U_{OC}-SOC diagram, the function was determined by means of the Matlab Curve Fitting Toolbox. At first, it was approximated by a fifth degree polynomial, but, this caused large fluctuation of the output voltage. In case of third or second degree polynomials there is no fluctuation. The final R_{01} (SOC) function:

$$R_{01} = -0{,}0011SOC^2 + 0.0003SOC + 0{,}0042$$

R_{12} is given as a constant [2], its value: R_{12}=3,87 mΩ.

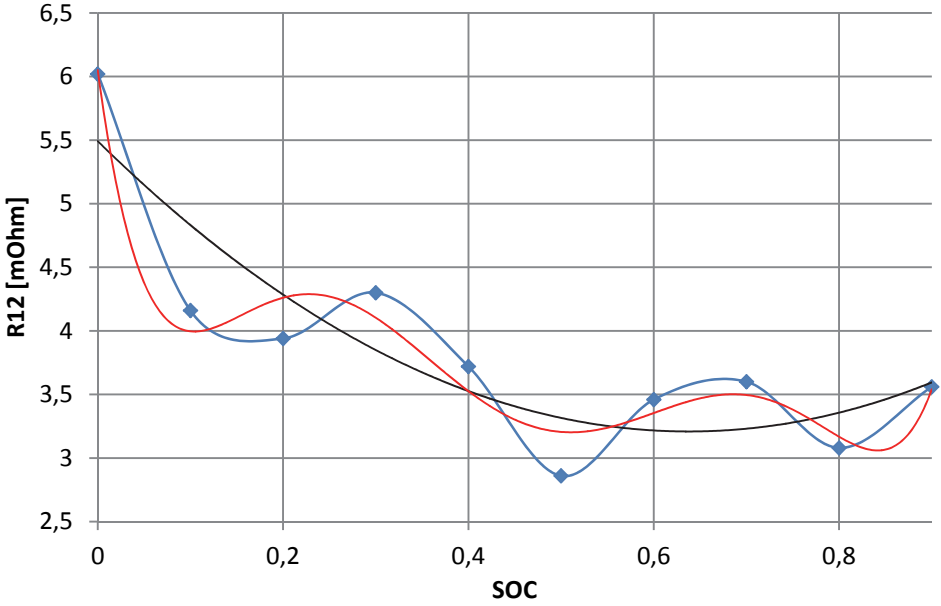

Figure 13. R_{12} as a function of SOC (own measurement)

3.2. Defining parameters in Simulink environment

At first, the value of R_{long} was set to R_{long}=0,027909 Ω based on reference [2]. Then the model was made more accurate with the help of measurement results. The voltage-time graph before and after parameter definition is shown in Fig. 14.

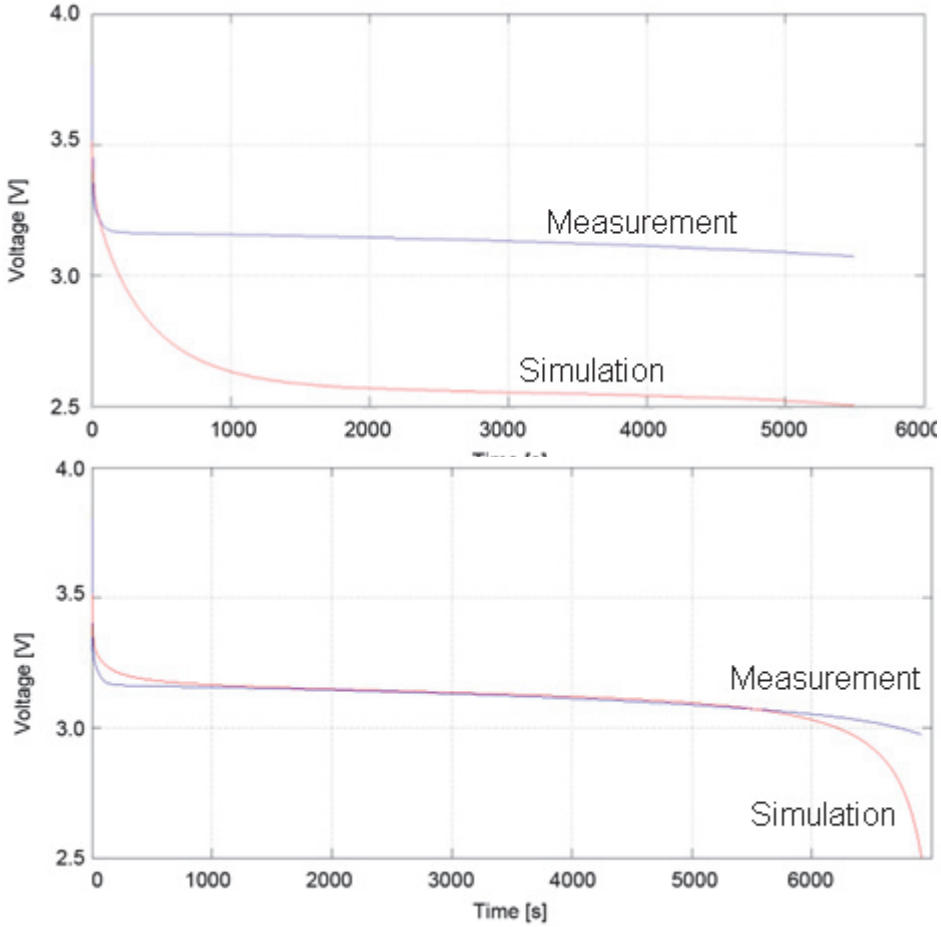

Figure 14. The voltage-time diagram before (to the top) and after (to the bottom) determining the value of R_{long} (blue: measurement result, red: simulation result)

It can be seen in the diagram that the measured graph is well enough approximated by the simulated voltage values.

3.3. Measurements necessary to further improve the battery model

The following measurements are planned with the aim of battery model improvement and validation:

- current off-current on or HPPC (Hybrid Pulse Power Characterization) to determine Voc and the resistance values [8]
- Dynamic Discharge Performance Test to validate the model

4. Measurements already performed to validate the model

4.1. Battery measurement system

The measurement system consists of separate charge and discharge modules. Modular scheme of the battery measuring system is shown in Figure 15.

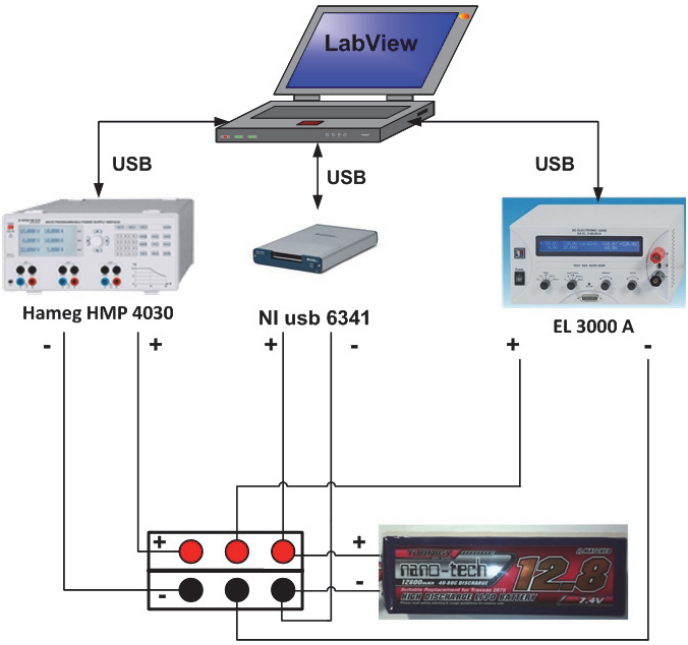

Figure 15. Modular scheme of the battery measuring system

Hameg power supply unit (HMP 4030) was used for the purpose of charging. The unit is controlled via Labview software. Communication between the unit and the computer is done via USB. The program developed in Labview is shown in Fig. 16.

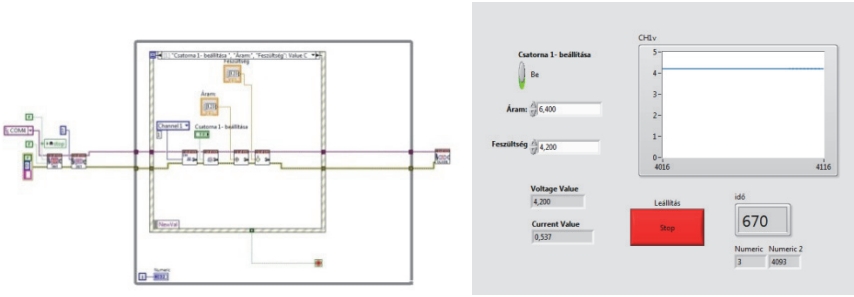

Figure 16. Labview charging program

During charging, it is possible to adjust the voltage and current of the charger with the help of the program. 100% charge of the cell was indicated by its voltage reaching 4.2 V.

Constant current/constant voltage strategy was used for charging (cc/cv: cc – constant current, cv – constant voltage). The battery was charged with constant current in the first phase of the charging process. As soon as SOC approaches 100%, the charge current is decreased by the charger automatically and then switches to constant voltage keeping. Charging ends when charge current decreases below 3% of the preset charge current. In this case, with preset 6.4 A it means 0.192 A.

Dummy load EL 3000 A was used for discharging.

Figure 17. Dummy load EL 3000 A

The dummy load was controlled by means of the original software via USB port of the computer.

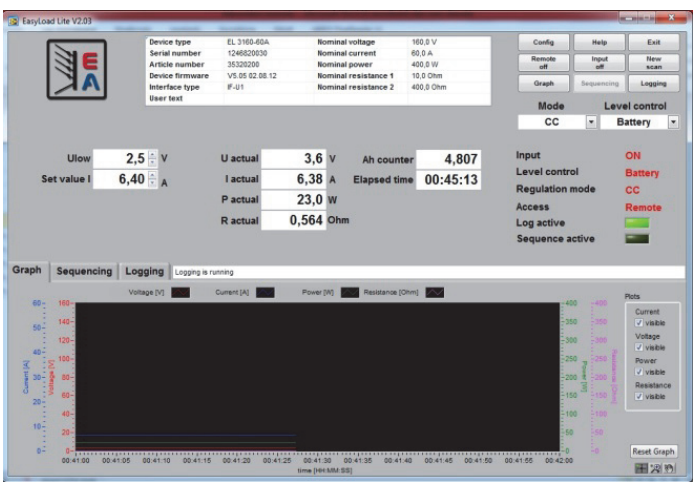

Figure 18. Control software EL 3000

4.1. Testing of the Turnigy nano-tech 12800mAh battery

The Turnigy nano-tech 12800mAh battery was used as testing medium because the very same battery was applied in the new vehicle of the SZENERGY Team. The whole package is built up of two cells connected in line and two parallel.

It was decided that the maximum voltage should be 4.2 V, and the minimum should be 2.5 V. The test was performed on one cell and also on the whole battery package. The cell or the package was charged at first to 100% SOC, than after one hour pause discharge started. Voltage-time and current-time diagrams are shown in Fig. 20-23.

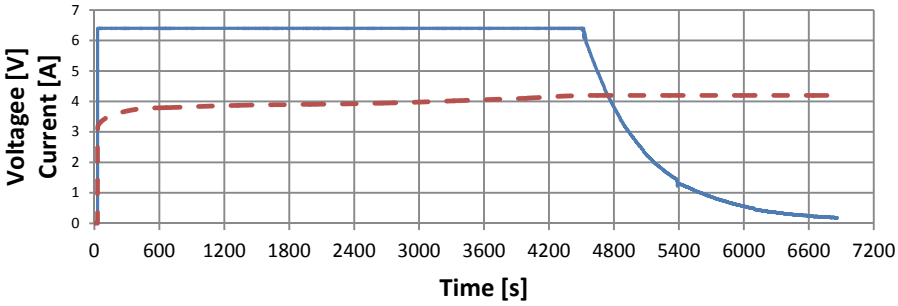

Figure 19. Voltage-time (dashed line) and current-time (solid line) diagrams when charging one cell

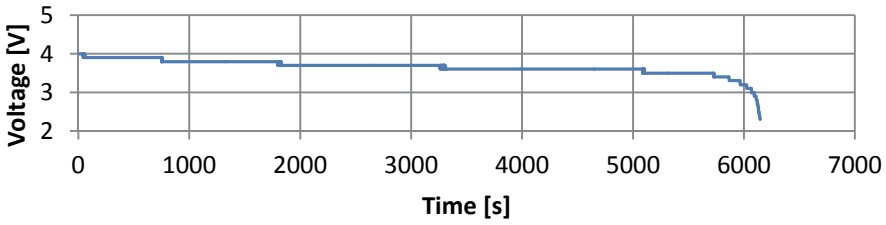

Figure 20. Voltage-time diagram when discharging one cell

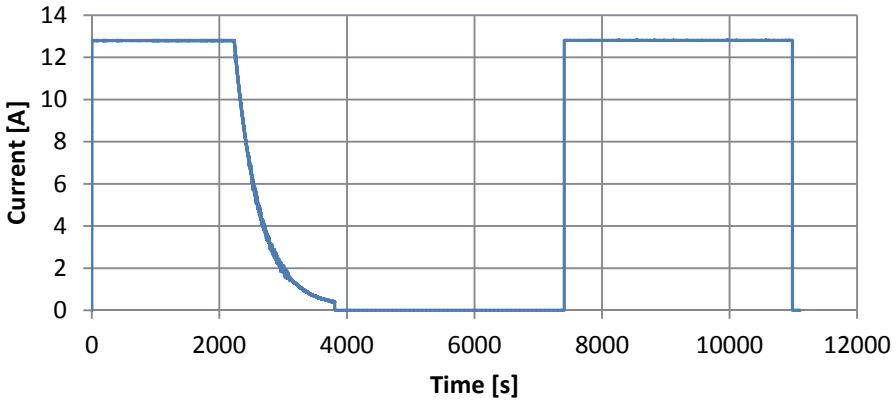

Figure 21. Current-time diagram when charging and discharging one battery package

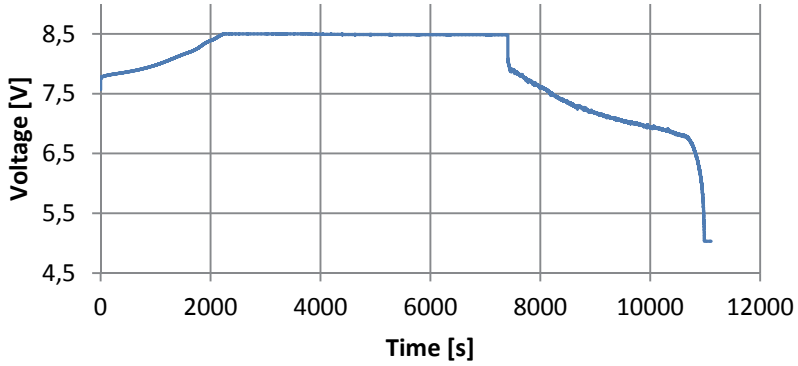

Figure 22. Voltage-time diagram of the package (whole cycle)

Summary

The initial steps of building the simulation model have been taken. Currently, the preparation of the measurements is in progress in order to validate the model. It is planned to demonstrate by means of simulating sensor malfunctions how the quality of the sensors influence the diagnostic models, in this manner, the value in use of the vehicle. The above connection can easily be understood when one thinks of the fact that the current range of the vehicle is determined by the state of charge of its battery.

Acknowledgement

TÁMOP-4.2.4.A/2-11/1-2012-0001 identification number of the National Excellence Program - was the establishment and operation system for domestic students, researchers and staff support as a priority project by the convergence program. The project is funded by the EU, the European Social Fund co-funded.

References

[1] Chen, M., Rincón-Mora, G.A: *Accurate Electrical Battery Model Capable of Predicting Runtime and I–V performance*, IEEE Transactions on energy conversion, vol. 21, no. 2, pp 504-511, 2006

[2] Knauff, M., McLaughlin, J., Dafis, C., Niebur, D., Singh, P., Kwatny, H., Nwankpa, C.: *Simulink Model of a Lithium-Ion Battery for the Hybrid Power System Testbed*, IEEE Electric Ship Technologies Symposium – ESTS, pp. 421-427, Arlington, 2007

[3] Hajdu F., Lakatos I. Phd, Kőrös P.: Lithium battery modelling in Simulink environment (in Hungarian), IFFK, pp.132-140., Budapest, 2013

[4] Rahimi-Eichi, H., Chow, M.Y.*: Adaptive Parameter Identification and State-of-Charge Estimation of Lithium-Ion Batteries*, 38th Annual Conference of the IEEE Industrial Electronics Society, Montreal, 2012

[5] Abu-Sharkh, S., Doerffel, D.: *Rapid test and non-linear model characterisation of solid-state lithium-ion batteries,* Journal of Power Sources vol. 130, no. 1-2., pp.266–274, 2004

[6] Wu, T., Liu, L., Xiao, Q.,Cao, Q., Wang, X.*: Research on SOC Estimation Based on Second-order RC Model,* Journal of Asian Electric Vehicles,Vol. 8, No. 2, pp.1419-1423., 2010

[7] Daowd, M., Omar, N., Verbrugge, B., Van Den Bossche, P., Van Mierlo, J.: *Battery Models Parameter Estimation based on Matlab/Simulink*, The 25th World Battery, Hybrid and Fuel Cell Electric Vehicle Symposium & Exhibition, Shenzhen, 2010

[8] Omar, N., Daowd, M., Hegazy, O., Mulder, G., Timmermans, J.M., Coosemans, T., Van den Bossche, P., Van Mierlo, J.: *Standardization Work for BEV and HEV Applications: Critical Appraisal of Recent Traction Battery Documents*, Energies (19961073) Vol. 5. No. 1, pp. 138-156, 2012

Acta
Technica
Jaurinensis

Vol.7., No.1., pp. 87–105, 2014
DOI: 10.14513/actatechjaur.v7.n1.20
Available online at acta.sze.hu

Repair of Internal and External Circular Failures Using Winding Technology

B. Pere[1], J. Égert[1] and T. Szabó[2]

[1]**Széchenyi István University, Department of Applied Mechanics**
[2]**University of Miskolc, Robert Bosch Department of Mechatronics**

The first part of the paper deals with the FEM computation of deformations, stresses and strain in the surrounding area of internal and external circular artificial failures with a set of given geometrical dimensions in steel pipelines. For the investigation of this problem three groups of mechanical models are applied: multilayered elastic shell, 3D elastic solid and 3D elastic-plastic solid FEM models. The aim of this analysis is to clarify the case in which the pipeline fails. When a pipe fails and needs repair or reinforcement, this is called critical case.

In the second part of the paper the repaired pipes are investigated. For repairing of the internal and external failures, internal or external multilayered textile composite reinforcements are applied by winding technology. The task is to determine the width of the reinforcement and the number of layers needed for repair.

The different mechanical models (multilayered elastic shell, 3D elastic solid and 3D elasto-plastic solid) are compared on the basis of numerical results. The critical cases are determined and the questions of repair are answered also numerically.

Keywords: *Steel pipeline, artificial circular damage, textile composite reinforcement, FEM analysis, elastic shell and 3D elastic-plastic modelling*

1. Introduction

Oil and gas pipelines often have internal and external circular failures. The internal failures usually originate from welding on location, and the external failures result from any other violent external effect, for instance due to agricultural equipment working above the pipeline.

The first task is to predict the risk caused by these circular failures. In the first step one needs to clarify the deformations, stresses and strains around the damaged part of the pipe. On the basis of such analysis one can find critical cases in which repairs are needed.

The second task is to fix or to repair the damaged pipe. In this paper an internal or external multilayered textile composite reinforcement are applied at the location of the failures. The multilayered textile composite reinforcement is made by winding technology. During the design of this composite reinforcement the width and the number of layers of the winding should be determined. The failures are considered to be fixed when stresses are below the critical values both in the steel pipe and in the composite reinforcement.

The numerical aspects of both tasks are discussed in this paper. In the first step two kinds of circular damaged pipe-parts using the finite element method and the I-DEAS program code are investigated. The failures may have a high number of varieties therefore two typical artificial failure geometries are chosen. On the basis of the numerical analysis the critical cases have been determined in which repairs are needed. In the second step an internal and/or external composite reinforcement with different widths and numbers of layers are applied for the critical cases. When analyzing critical cases the proper width and number of layers of reinforcement can be found.

2. Geometry of typical artificial failures and reinforcements

Fig. 1. shows the global geometry i.e. the location of the investigated internal and external circular failures.

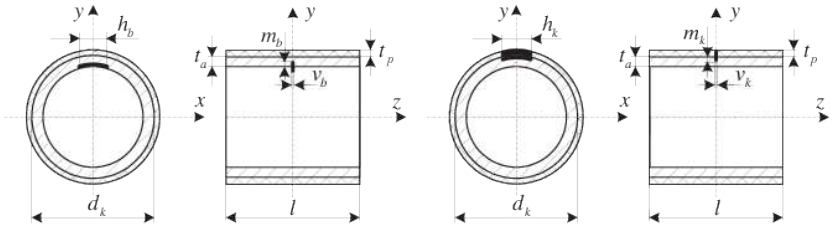

Figure 1. Global geometry of the internal and external circular failures

The steel pipe's external diameter is $d_k = 323{,}9$ mm, its wall thickness is $t_a = 7{,}1$ mm and the length of the investigated pipe part is $l = 2000$ mm. The steel pipe is coated with a $t_p = 3{,}12$ mm thick polyethylene insulation layer against corrosion. The longitudinal dimension of the circular failures are $h_b = h_k = 150$ mm for both internal and external cases, the width is $v_b = 1{,}5$ mm for the internal case and $v_k = 2$ mm for the external case. There are three depth versions $m_b = m_k = 2; 4; 6$ mm investigated.

Fig. 2. shows the local geometry of analyzed internal and external circular failures. The geometry of the artificial failures (Fig. 2.) can be easily reproduced later for the planned experiments.

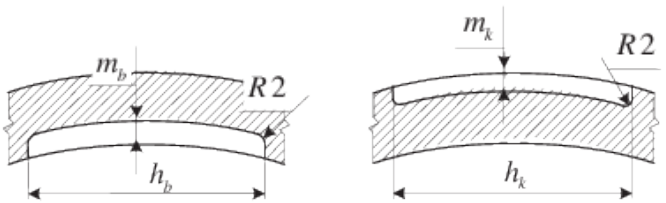

Figure 2. Local geometry of the internal and external circular failures

Internal and external circular failures of pipes can be reinforced theoretically from the outside or the inside as well. Fig. 3. shows the reinforcement possibilities for an internal failure. At the location of the failure the anti-corrosion layer is removed and the reinforcement is winded directly to the steel surface.

The layer thickness of reinforcement in each case is the same $t_k = t_b = 0{,}3$ mm, and three different widths of the winding bands are investigated $s_k = s_b = 50; 100; 200$ mm.

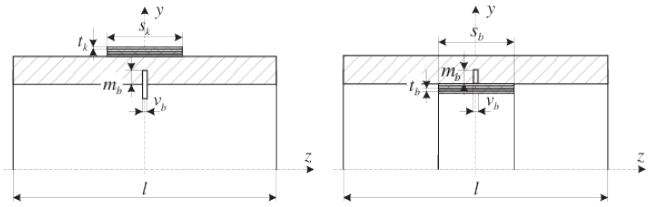

Figure 3. Reinforcement versions for the internal circular damage

3. Mechanical modelling of the materials and working conditions

The pipe is made of steel, the protecting layer against corrosion is polyethylene and the material of the reinforcement is carbon fiber textile reinforced plastics (CFRP). From the mechanical point of view the steel and the polyethylene are modelled as linear elastic materials given by two material constants, the yield strength and ultimate strength. These material parameters in Table 1 are measured by the Department of Mechanical Technology of Miskolc University [7].

In Table 1 E is the modulus of elasticity, ν is the Poisson's ratio, $\mathbf{R_{t0,5}}$ is the yield limit and $\mathbf{R_m}$ is the breaking strength of material.

In linear elastic, isotropic, plane stress problems the following Hooke's law provides the

Material	**E** [MPa]	ν [–]	$\mathbf{R_{t0,5}}$ [MPa]	$\mathbf{R_m}$[MPa]
Steel	205 000	0,3	499	603
Polyethylene	527	0,31	–	12,8

Table 1. Material constants and ultimate stress values

constitutive equations:

$$\varepsilon_1\varepsilon_2\gamma_{12} = 1E - \nu E0 - \nu E1E0002(1+\nu)E\sigma_1\sigma_2\tau_{12}, \tag{1}$$

1 and 2 are directions perpendicular to each other in the tangent plane of the middle surface of the pipe. ε_1,ε_2 and σ_1,σ_2 are strains and normal stresses in direction 1, 2 respectively. γ_{12} and τ_{12} are the in-plane shear strain and the shear stress.

The elasto-plastic computations are carried out by using the stress-strain diagram in Fig. 4. given by the Department of Mechanical Technology of Miskolc University [7].

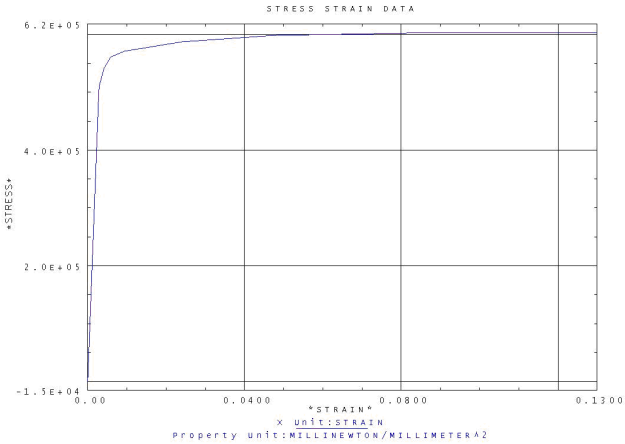

Figure 4. Stress-strain diagram of the steel pipe

For isotropic materials the well known von Mises failure criterium is applied:

$$12\left(1R_{t0,5}\right)^2\left[\left(\sigma_I-\sigma_{II}\right)^2+\left(\sigma_{II}-\sigma_{III}\right)^2+\left(\sigma_I-\sigma_{III}\right)^2\right]\leq 1, \quad \text{or} \tag{2}$$

$$\sigma_{red\,max} \leq R_{t0,5}, \tag{3}$$

where σ_I,σ_{II},σ_{III} are the principal stresses.

According to references [1], [2], the carbon fiber textile reinforced composite can be modelled from the macroscopic point of view by an orthotropic constitutive law:

$$\varepsilon_1\varepsilon_2\gamma_{12} = 1E_1 - \nu_{12}E_20 - \nu_{21}E_11E_20001G_{12}\sigma_1\sigma_2\tau_{12}, \tag{4}$$

In the above equations the indices 1, 2 stand for the principal material direction of CFRP. In the constitutive law E_1,E_2 are orthotropic moduli of elasticity, ν_{12},ν_{21} are Poisson's ratios and G_{12} is the independent in-plane shear modulus. The Poisson's ratios are not independent from each other and due to energy reasons [2] the following relation exists :

$$\frac{\nu_{12}}{E_2} = \frac{\nu_{21}}{E_1}. \tag{5}$$

Macroscopic modelling means that equations are not appropriate to determine stresses and strains in the carbon fibers or in the matrix material, but do well for a larger area with a lot of fibers. Therefore, the above stresses and strains are the average features of an area with a lot of fibers.

For the orthotropic material the Tsai-Wu's failure criterium is applied:

$$\sigma_1^2\sigma_{H1}\sigma_{D1}+\sigma_2^2\sigma_{H2}\sigma_{D2}-\sigma_1\sigma_2\sqrt{\sigma_{H1}\sigma_{D1}\sigma_{H2}\sigma_{D2}}+\tau_{12}^2\tau_{S12}^2+$$
$$+\left(1\sigma_{H1}-1\sigma_{D1}\right)\sigma_1+\left(1\sigma_{H2}-1\sigma_{D2}\right)\sigma_2 \leq 1, \tag{6}$$

or

$$K_{tw} \leq 1, \tag{7}$$

where σ_{H1},σ_{H2} are tensile, σ_{D1},σ_{D2} are compressive and τ_{S12} is shear strengths.

Table 2 contains the measured material constants and ultimate stress values of the applied CFRP measured by the Department of Polymer Engineering of the Budapest University of Technology [8].

The deformations, stresses and strains in the damaged pipe and in the reinforced pipe are determined for two loading cases, i.e. for a normal working condition and for a loading condition, that can be verified by an experiment.

Thickness [mm]	$\mathbf{E_1}$ [MPa]	$\mathbf{E_2}$ [MPa]	ν_{12} [–]	$\mathbf{G_{12}}$ [MPa]
0,3	47 600	45 000	0,036	2 000

$\sigma_{\mathbf{H1}}$ [MPa]	$\sigma_{\mathbf{H2}}$ [MPa]	$\sigma_{\mathbf{D1}}$ [MPa]	$\sigma_{\mathbf{D2}}$ [MPa]	$\sigma_{\mathbf{S12}}$ [MPa]
436	430	310	340	76

Table 2. Material constants and ultimate stress values of CFRP layers

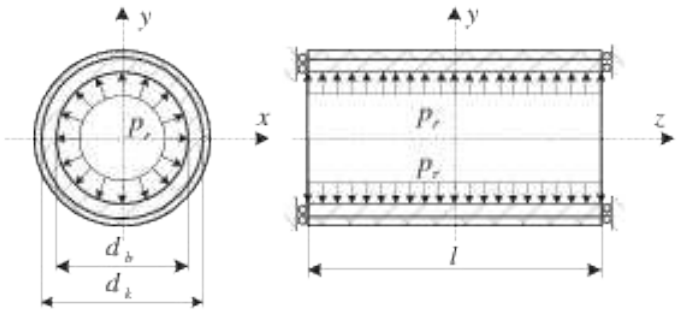

Figure 5. Mechanical model for normal working condition

In normal working conditions the pipeline is embedded in the earth which does not allow the longitudinal displacements of the investigated pipe parts. This is the reason why the mechanical model is clamped at both ends of the pipe part in the normal working loading case. There is a $p_r = 63$ bar internal pressure in both loading cases in the pipe.

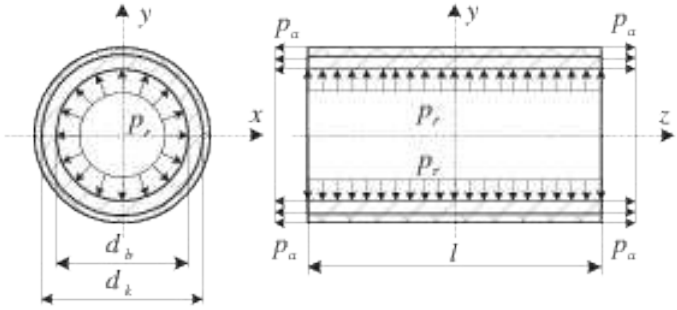

Figure 6. Mechanical model for experimental checking

In the experiments the investigated pipe part is closed at both ends. The internal pressure provides an $p_a = d_b^2 p_r \left(d_k^2 - d_b^2\right)$ additional axial loading because of the closed ends. So the experimental loading case consists of the internal pressure and the axial loading.

4. Finite element approaches and meshes

For computation of deformations, stresses and strains around the circular failures the following three models are applied: multilayered elastic shell, 3D elastic solid and 3D elasto-plastic solid elements. However computations of repaired pipes are carried out only by multilayered elastic shell elements.

By using layered shell elements it is possible to model failures by proper choice of layer thicknesses. Fig. 7. shows two cases for the proper thickness choice. The left one is at a common location of the pipe and the right one is at an internal failure with 4 mm depth. In both cases in Fig. 7. the upper layer represents the insulation and two internal layers for modelling the internal failure are shown in the right picture. Naturally, for the failure area zero values should be given for material constants.

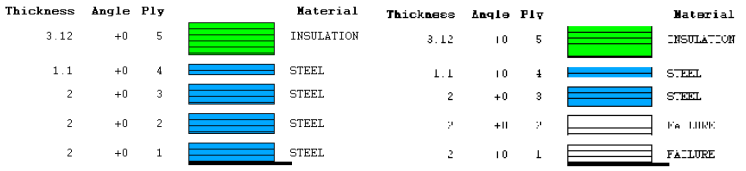

Figure 7. Modelling of failure thickness by multilayered shell elements

Fig. 8. shows two cases for the proper thickness choice of layers at reinforcement. The left and right pictures represent the thicknesses of layers in undamaged and damaged locations, respectively.

Using multilayered shell elements it is only possible to apply a sharp corner approach for failures, so the R2 mm rounding in Fig. 2. is not taken into consideration at shell modelling.

The 3D modelling allows a very accurate approach of real geometry of artificial internal and external failures, even an R2 mm rounding.

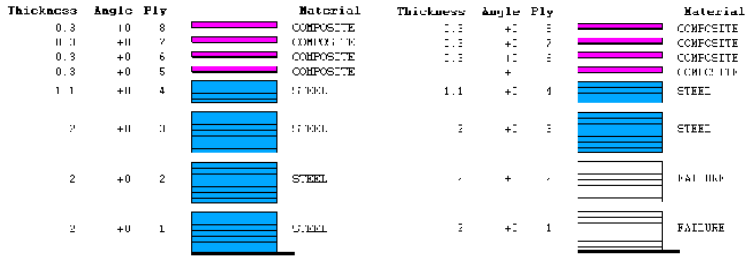

Figure 8. Modelling of reinforcement and failure thickness by shell elements

	Shell model	3D solid model
Number of elements	5 000	17 500
Number of nodes	15 000	36 000

Table 3. Characteristic data for FEM meshes

Table 3 includes the parameters of the applied meshes. The nodes of shell elements have six degrees of freedom and the nodes of 3D solid elements three, so one has to solve in both tasks a linear algebraic equation system with about 90-108 thousand unknowns. The computations for both shell and 3D solid modelling are carried out also with much denser mesh in order to prove that the applied mesh provides accurate results.

When creating finite element meshes the double symmetry is taken into account. Naturally, the mesh is much denser around the failures than at the other areas of the model in the interest of accuracy of computations.

Fig. 9. shows an example for a shell model and a mesh part for a 3D solid model. The $l_m = l/2 = 1000$ mm length of mesh is chosen so that the influence of the boundary conditions at the end of the pipe part and the influence of the circular failure do not disturb each other.

On the basis of computational experience it is enough to apply shorter models with $l_r = l_m/2 = 500$ mm length for the computation of reinforced pipe parts. In these meshes

one has to take into consideration the width of the reinforcing composite band at meshing (Fig. 10.).

5. Numerical results of analysis

5.1. Influence of insulation layer

The analysis of the influence of the external polyethylene insulation is carried out only for internal circular failure. Numerical results prove that the insulation layer has no importance from the mechanical point of view, since the stiffness of the insulation layer is negligible compared to the steel's stiffness. Therefore the insulation layer is neglected in the investigations.

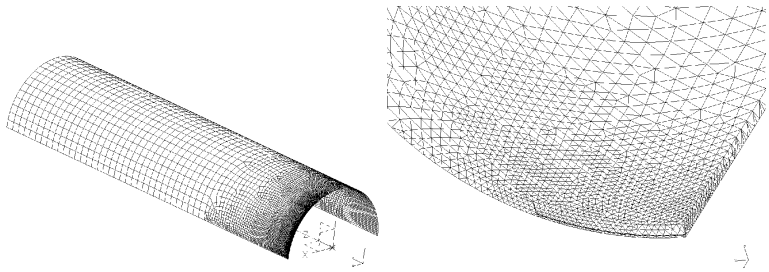

Figure 9. Shell mesh and 3D solid mesh part for circular failure

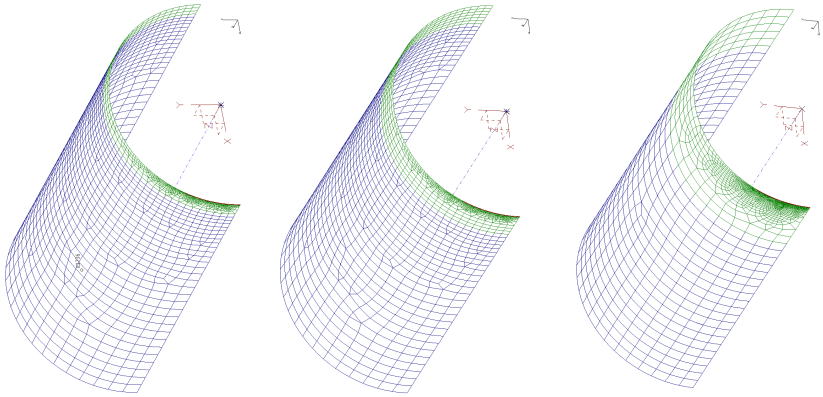

Figure 10. Shell meshes for different reinforcements

5.2. Results of damaged steel pipes

The characteristics of deformations and stress/strain distributions is similar for both loading cases. However the critical values of deformations, stresses and strains are a little higher for the experimental checking than for the normal loading conditions. This is the consequence of the additional axial loading originated from the internal pressure. This axial loading seems to be a little higher than the axial loading originated from the clamped ends of the pipe model at normal working conditions. Therefore, only the results of this hazardous experimental loading case are presented in this paper.

Numerical results show that the deformation of pipes with internal failure depends significantly on the depth of failure. Fig. 11-13. demonstrates these differences on the radial displacement distribution of the middle surface. It is very interesting that the maximum deformation occurs not directly at the failure but beside that. Fig. 14-16 shows

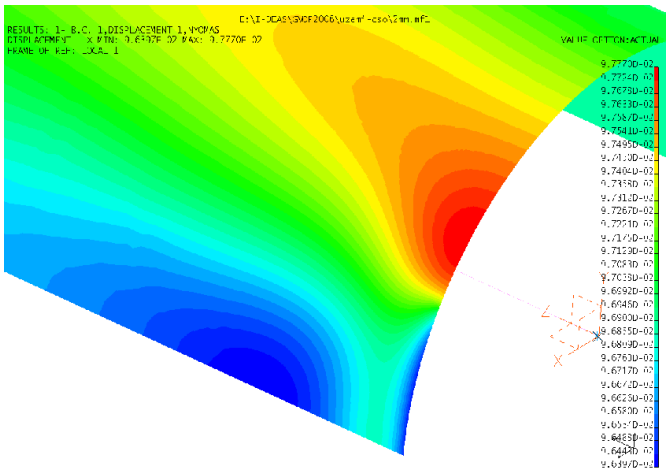

Figure 11. Radial displacements at internal failure with 2 mm depth

the radial displacements in the case of external failure for the three investigated failure depths. In this case the distribution of the deformations do not depend on the depth of external failure. Naturally, the magnitudes of deformation are different. The different distributions of deformations for internal and external failure will play a very important role at the repair.

Table 4 summarizes the critical strain and von Mises reduced stress values for the hazardous experimental loading case at internal failure. Compering the $\varepsilon_{z\,max}$ axial and

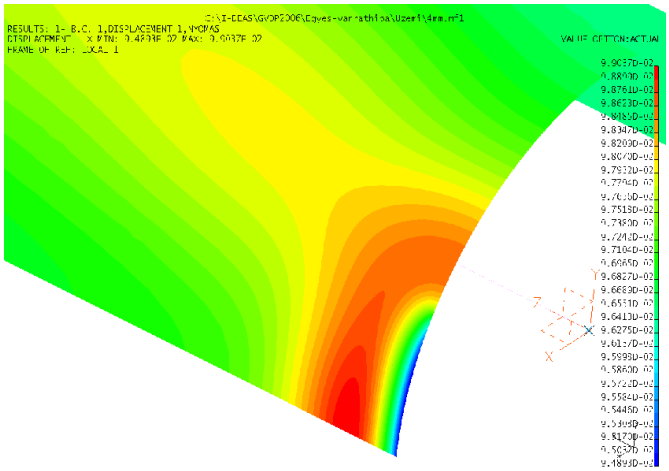

Figure 12. Radial displacements at internal failure with 4 mm depth

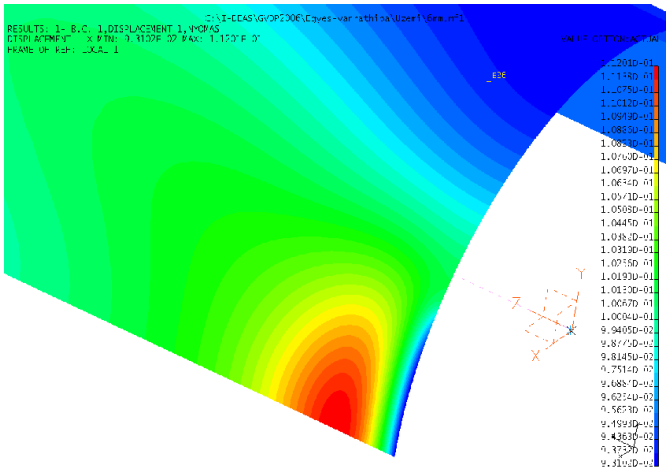

Figure 13. Radial displacements at internal failure with 6 mm depth

$\varepsilon_{\varphi\,max}$ circular strains it is seen that they are in the same order of magnitude at lower depths. However the $\varepsilon_{z\,max}$ axial strains become dominant at increasing failure depth. Therefore one can state that the influence of axial loading is dominant for strains around the circular failure at higher depths.

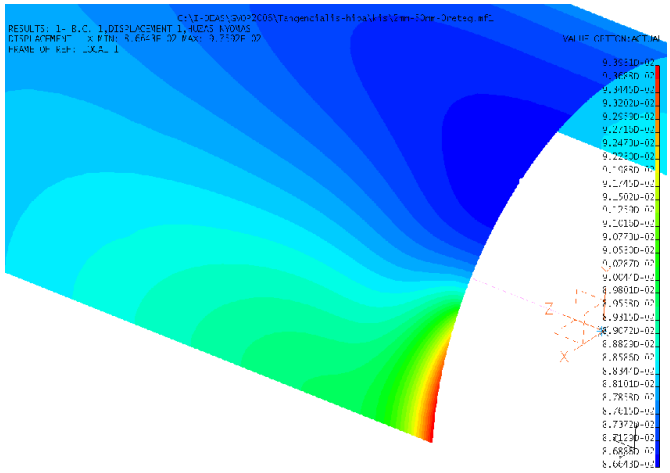

Figure 14. Radial displacements at external failure with 2 mm depth

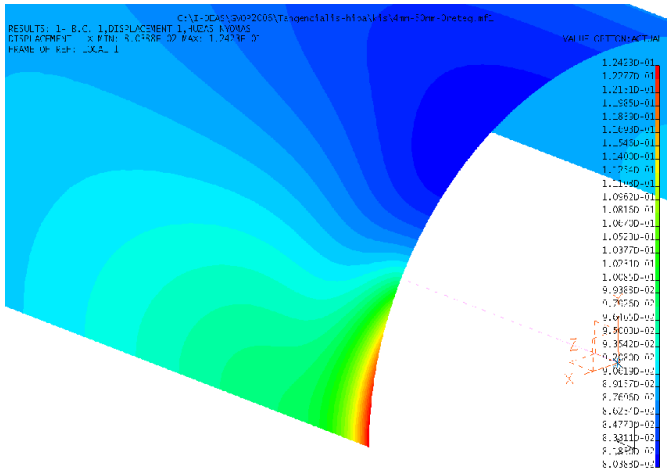

Figure 15. Radial displacements at external failure with 4 mm depth

The maximum reduced stresses computed by different models are close to each other below the yield stress, in cases of 2 and 4 mm deep internal failures. At 4 mm failure depth the maximum reduced stresses reach or are close to the yield stress value. For 6 mm failure depth every model, including the shell model, indicates the fracture of the pipe.

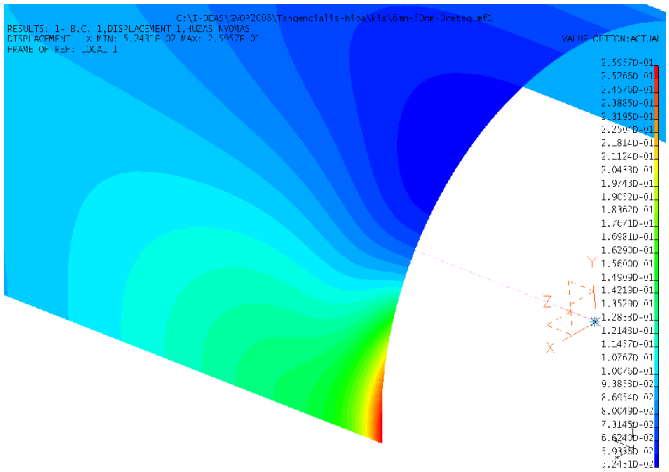

Figure 16. Radial displacements at external failure with 6 mm depth

Therefore the damaged pipe needs repair only at 6 mm failure depth. Table 5 summarizes

Depth [mm]	Quantity [Dimension]	Shell model	3D elastic model	3D elasto-plastic model
2	$\varepsilon_{\varphi\ max}$ [1]	$1{,}2603 \cdot 10^{-3}$	$9{,}3827 \cdot 10^{-4}$	$9{,}3827 \cdot 10^{-4}$
	$\varepsilon_{z\ max}$ [1]	$1{,}0610 \cdot 10^{-3}$	$1{,}2283 \cdot 10^{-3}$	$1{,}2283 \cdot 10^{-3}$
	$\sigma_{red\ max}$ [MPa]	222,37	243,03	243,03
4	$\varepsilon_{\varphi\ max}$ [1]	$2{,}4310 \cdot 10^{-3}$	$8{,}7135 \cdot 10^{-4}$	$8{,}7235 \cdot 10^{-4}$
	$\varepsilon_{z\ max}$ [1]	$7{,}2919 \cdot 10^{-3}$	$2{,}5820 \cdot 10^{-3}$	$2{,}5820 \cdot 10^{-3}$
	$\sigma_{red\ max}$ [MPa]	*502,38*	455,11	455,11
6	$\varepsilon_{\varphi\ max}$ [1]	$2{,}8736 \cdot 10^{-3}$	$9{,}3700 \cdot 10^{-4}$	$9{,}4239 \cdot 10^{-4}$
	$\varepsilon_{z\ max}$ [1]	$3{,}5439 \cdot 10^{-2}$	$6{,}7759 \cdot 10^{-3}$	$7{,}4800 \cdot 10^{-3}$
	$\sigma_{red\ max}$ [MPa]	**898,85**	**1191,4**	**603,0**

Table 4. Critical values - internal failures - experimental loading case

the characteristic critical strain and von Mises reduced stress values for the more hazardous experimental loading case at external failure. These results show very similar behavior from the point of view of strains and stresses for the external damaged pipe than for the internal failure. Also the external damaged pipe needs repair only at 6 mm failure depth. It is curious that though the deformations are different similar strain and stress values have been obtained for the internal and external failures.

Depth [mm]	Quantity [Dimension]	Shell model	3D elastic model	3D elasto-plastic model
2	$\varepsilon_{\varphi\, max}$ [1]	$8{,}9118 \cdot 10^{-4}$	$9{,}8610 \cdot 10^{-4}$	$9{,}8610 \cdot 10^{-4}$
	$\varepsilon_{z\, max}$ [1]	$7{,}2939 \cdot 10^{-4}$	$1{,}1496 \cdot 10^{-3}$	$1{,}1496 \cdot 10^{-3}$
	$\sigma_{red\, max}$ [MPa]	196,39	233,38	233,38
4	$\varepsilon_{\varphi\, max}$ [1]	$1{,}1614 \cdot 10^{-3}$	$1{,}1841 \cdot 10^{-3}$	$1{,}1841 \cdot 10^{-3}$
	$\varepsilon_{z\, max}$ [1]	$2{,}5196 \cdot 10^{-3}$	$2{,}7328 \cdot 10^{-3}$	$2{,}7328 \cdot 10^{-3}$
	$\sigma_{red\, max}$ [MPa]	*531,40*	490,62	490,62
6	$\varepsilon_{\varphi\, max}$ [1]	$1{,}4874 \cdot 10^{-3}$	$1{,}6668 \cdot 10^{-3}$	$1{,}6706 \cdot 10^{-3}$
	$\varepsilon_{z\, max}$ [1]	$4{,}8891 \cdot 10^{-3}$	$5{,}5436 \cdot 10^{-3}$	$7{,}1033 \cdot 10^{-3}$
	$\sigma_{red\, max}$ [MPa]	**1009,7**	**973,58**	**603,0**

Table 5. Critical values - external failures - experimental loading case

All the three applied models indicate the fracture of the pipe for the same failure depth. From here on the simplest multilayered shell model is used in the investigation of repaired cases because it needs less numerical efforts than the others.

5.3. Results of repaired pipes

As it is determined in 5.2 the axial loading becomes dominant at both increasing internal and external circular failure depths. This dominant loading results very different deformations at internal (Fig. 17.) and external (Fig. 18.) failure. The highest radial deformations occur shifted in axial direction nearby the internal failure and exactly in the middle of the external failure.

The phenomenon can be explained by Fig. 19. If there is no failure in the pipe wall the stress resultant over the thickness is only the N_a force. In the undamaged case there is no bending effect in the pipe wall.

However in the case of internal failure the stress resultants provide a N_a force and an additional M_{ti} bending moment. This bending moment opens the internal failure and results maximum radial deformations shifted nearby the failure. in the case of external failure the stress resultants provide a N_a force and an additional M_{to} bending moment. This bending moment also opens the external failure and results maximum radial deformations in the middle of the failure. Both internal and external failures can be fixed from the outside or from the inside. Fig. 20. shows the repair versions for an internal failure. The pipe can be considered as fixed if the $\sigma_{red\, max}$ reduced stresses in the steel wall do not reach the yield stress value (3.3) and the K_{tw} Tsai-Wu failure coefficient in the reinforcement do not reach the value 1 (3.7).

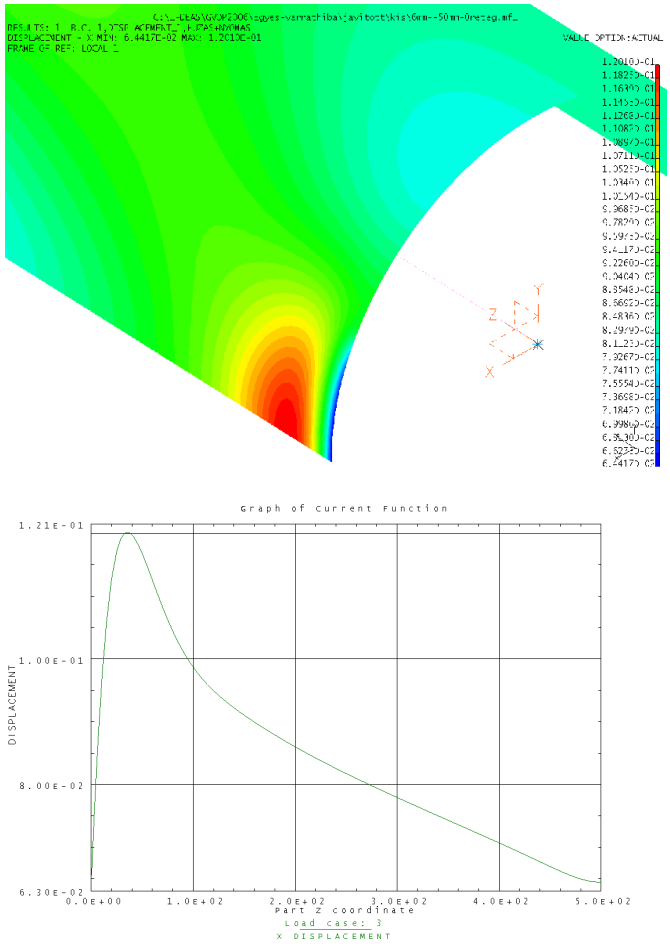

Figure 17. Radial displacements at internal failure with 6 mm depth

Computations are carried out for repaired internal failure by 50, 100 and 200 mm bandwidth of CFRP layers. The numerical results proved that the bandwidth in this range practically does not influence the behavior of repaired case.

Table 6. summarizes the numerical results for a 6 mm deep internal failure with 50 mm bandwidth reinforcement, in the left two columns for external reinforcement and in the right two columns for internal reinforcement. It can be seen from Table 6. that an internal

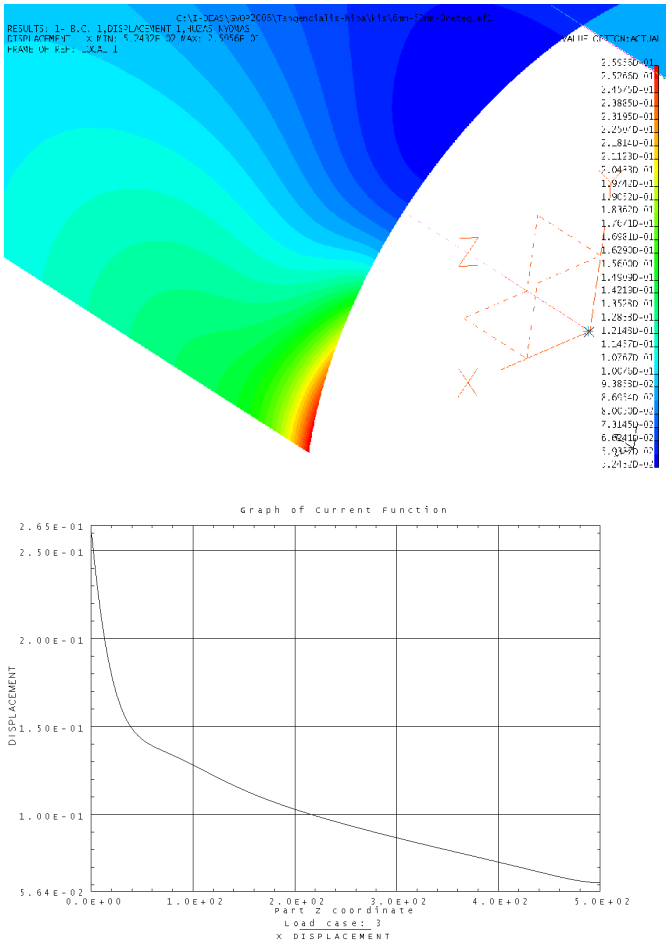

Figure 18. Radial displacements at external failure with 6 mm depth

circular failure can be repaired better by internal reinforcement than by external one. Both goals for failure criteria (3.3) and (3.87) can already be fulfilled by 8 layers of internal winding. The external reinforcement with a low number of layers makes the situation worse and the pipe can only be fixed with a very high number of layers.

This phenomenon can be explained by Fig. 20. With a lower number of external layers the e eccentricity is increased by the reinforcement which makes the M_{ti} local bending

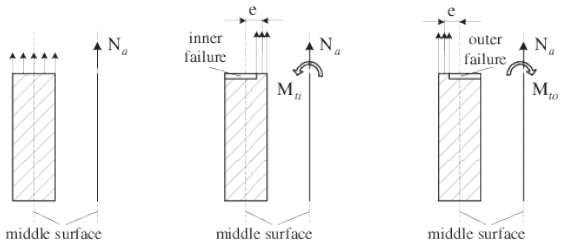

Figure 19. Force and moment resultants at internal and external failure

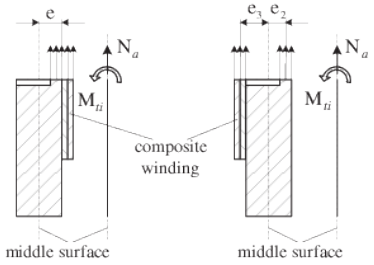

Figure 20. Repairing the internal failure by composite winding

moment higher but a high enough number of layers can compensate this action. However the internal reinforcement creates an opposite bending moment by e_3 eccentricity which can balance the original bending moment.

Table 7. summarizes the numerical results for a 6 mm deep external failure with 50 mm bandwidth reinforcement, in the left two columns for external reinforcement and in the right two columns for internal reinforcement. When repairing external circular failure the situation is the opposite to the previous case. It is seen from Table 7 that an external circular failure can be repaired better by external reinforcement than by internal one. Also in this case both failure criteria can already be fulfilled by 8 layers of external winding. The internal reinforcement with a low number of layers makes the situation worse and the pipe can be fixed only with a very high number of layers. The argument for this phenomenon is the same as given at internal failures.

6. Conclusions

The conclusions of the numerical investigation are the following:

Number of layers/ thickness [mm]	$\sigma_{\mathrm{red\,max}}^{\mathrm{external}}$ [MPa]	$\mathbf{K}_{\mathbf{tw}}^{\mathbf{external}}$ [–]	$\sigma_{\mathrm{red\,max}}^{\mathrm{internal}}$ [MPa]	$\mathbf{K}_{\mathbf{tw}}^{\mathbf{internal}}$ [–]
0/0	908	–	908	–
4/1,2	1046,0	0,6137	600,2	0,0641
8/2,4	984,4	0,7704	499,1	-0,0187
12/3,6	804,6	0,4633	–	–
16/4,8	674,1	0,2729	–	–
20/6,0	586,0	0,1909	–	–
24/7,2	523,0	0,1188	–	–
28/8,4	475,5	0,0862	–	–

Table 6. Reduced stresses and failure coefficients for internal failure with 6 mm depth

Number of layers/ thickness [mm]	$\sigma_{\mathrm{red\,max}}^{\mathrm{external}}$ [MPa]	$\mathbf{K}_{\mathbf{tw}}^{\mathbf{external}}$ [–]	$\sigma_{\mathrm{red\,max}}^{\mathrm{internal}}$ [MPa]	$\mathbf{K}_{\mathbf{tw}}^{\mathbf{internal}}$ [–]
0/0	1009,7	–	1009,7	–
4/1,2	550,2	0,0704	1125,5	0,7026
8/2,4	499,2	0,0111	1017,3	0,8056
12/3,6	–	–	825,1	0,4745
16/4,8	–	–	692,3	0,2791
20/6,0	–	–	602,8	0,1807
24/7,2	–	–	539,4	0,1280
28/8,4	–	–	491,9	0,0974

Table 7. Reduced stresses and failure coefficients for external failure with 6 mm depth

- From the engineering point of view the multilayered shell model is a suitable tool for numerical analysis of pipe failures and for investigation of repaired pipes.
- From the mechanical point of view the the insulation layer is negligible.
- The experimental loading case is more hazardous than the normal working conditions.
- The critical strains and stresses are similar at internal and external circular failures, however the character of deformations is different.
- It is sufficient to use only a few number of CFRP layers for repair of very deep circular failures, if they are applied from the failure side.
- The internal and external failures have to be fixed by internal and external reinforcement, respectively.

- The bandwidth in the investigated range of composite layers does not play an important role at the repair of circular failure.

Acknowledgment

The authors wish to acknowledge the assistance given by the Hungarian Agency for Research Fund Management and Research Exploitation (GVOP-3.1.1.-2004-05-0215/3.0) and by the Hungarian Scientific Research Fund (T 049126 and T 048359) for supporting the research.

References

[1] Reddy, J. N.: *Mechanics of laminated composite plates and shells, Theory and Analysis*, CRC Press (2004).

[2] Matthews, F. L., Davies, G. A. O., Hitchings, D., Soutis, C.: *Finite element modelling of composite materials and structures*, Woodhead Publishing Ltd, Camgridge (2000).

[3] BATHE, K. J.: *Finite Element Procedures*, Prentice Hall International Editions (1996).

[4] *I-DEAS User' Guide*, UGS PLM Solutions Inc. (2004).

[5] Égert, J., Pere, B., Molnár-Égert, É.: *Csövek varrathibái textil kompozitos javításának szilárdságtani vonatkozásai (Mechanical aspects of reinforcements of pipeline welding failures by fabrics)*. EMT Műszaki Szemle (EMT Technical Rewiev), (2008), pp 125–131. (in Hungarian)

[6] Pere, B., Égert, J.: *Finite Element modelling opportunities of artificial welding failures and external damage of pipelines*. Proc. microCAD 2008 Int. Sci. Conf. 20-21 March 2008., Section F: Applied Mechanics, pp 39–44.

[7] Lukács, J., Nagy, Gy. and Török, I.: *Kísérleti csőszakaszok vizsgálata (Investigation of test pipe parts)* Polimer mátrixú kompozittal erősített hibrid csövek integritása - konferencia kiadvány (Integrity of hybride pipes reinforced by polymere matrix composite - Conf. Proc.) Miskolc-Egyetemváros, (2008), pp 174–193. (in Hungarian)

[8] Czél, G.: *Polimer kompozit csőanyagok sajátos anyagvizsgálati módszerei (Special material test methods for polymere composite pipe materials)* Polimer mátrixú kompozittal erősített hibrid csövek integritása - konferencia kiadvány (Integrity of hybride pipes reinforced by polymere matrix composite - Conf. Proc.) Miskolc-Egyetemváros, (2008), pp 17–24. (in Hungarian)